Scuola Internazionale Superiore Studi Avanzati (SISSA)

Neurobiology Area

The non-octarepeat copper-binding site of the prion protein and its potential role in prion conversion

Supervisor

Prof. Giuseppe Legname

PhD candidate

Thanh Hoa Tran

A thesis submitted for the degree of
Doctor of Philosophy
in Functional and Structural Genomics
February 2016

Acknowledgements

Foremost, I would like to express my sincere gratitude to my supervisor Prof. Giuseppe Legname whom I appreciate for the vast knowledge and skills and for giving me the great opportunity to work in his lab. Without his continuous assistance, his useful advices, his patience and encouragement, I would not have accomplished my Ph.D. research and dissertation.

A very special thanks go out to Prof. Juan-María Torres (Centro de Investigación en Sanidad Animal, Spain), Prof. Paola D'Angelo (University of Rome "La Sapienza", Italy) and Dr. Fabio Moda (Istituto Neurologico Carlo Besta, Italy) for all the fruitful collaborations.

In addition, I want to express my deepest thanks to all the members of the Prion Biology lab, Suzana, Paola, Giulia, Joanna, Elena, Xuan Nguyen, Andrea... for helping and supporting me during all these years, for your friendship and the time we spent together.

I am grateful to Dr. Gabriele Giachin for his invaluable help on my work, for teaching writing a scientific paper, correcting and giving valuable advices on my writing. I must also acknowledge Kate Pischke for proofreading the English in this thesis. Thanks also go out to Mai Thao, Le Nhat, Minh Do for their helpful guidance at the beginning of my Ph.D. life, for sharing the time here in peaceful Trieste.

I would also like to extend my thanks for the invaluable support from Tullio, Jessica, Micaela, Massimo, Federica, Andrea, Sandra and all SISSA staff, especially the Students' Secretariat, Riccardo and Federica.

I have a very special thanks to Lina Nguyen for standing by my side over last three years, taking care of me and supporting me without holding back.

Finally, I wish to thank my family for their endless love, support and encouragement through my entire life.

Abstract

Transmissible spongiform encephalopathy (TSE) or prion diseases are fatal neurodegenerative disorders caused by a change in conformation of the prion protein from the normal cellular form (PrP^{C}) to a misfolded form (PrP^{Sc}). Prion protein has long been known as a copper binding protein. Although the functional implication of copper binding to PrP is not yet clear, it is believed that copper is an important cofactor in prion disease. Therefore, the aim of this work is to determine the potential role of copper in prion conversion. Copper can effectively bind to PrP^{C} via histidine residues in the octapeptide repeats (OR) and the non-OR region located in the disordered N-terminal of the protein. Our hypothesis is that if copper binding plays a role in prion disease, removal of histidine residues in N-terminal domain may affect the prion conversion process. To examine this, we created a series of mutant murine PrP (MoPrP) molecules by replacing histidine residue at OR and non-OR region by tyrosine. These constructs were transfected into ScN2a cells and the efficiencies of prion conversion were evaluated. The results showed that replacing histidine by tyrosine at non-OR region led to an increasing of PrP^{Sc} conversion. When copper was removed by cuprizone, the construct with tyrosine at non-OR site (MoPrP H95Y) did not alter the level of PrP^{Sc} which meanwhile increased in case of the MoPrP wild-type (WT). To test these mutants *in vitro*, we produced recombinant protein, did the fibrilization assay and compared the lag phase. The result clearly showed that these constructs with tyrosine (H95Y, H110Y, H95Y/H110Y) need a shorter time to aggregate making fibrils faster than WT MoPrP. In particular, $N2aPrP^{-/-}$ cells expressing non-OR mutations PrP spontaneously cause prion formation that can be detected by ASA or PMCA. Moreover, transgenic mice overexpressing MoPrP H95Y showed clinical signs and died at ~100 days with PK-resistant PrP in their brain. Based on these data, we can

concluded that the substitution of histidine by tyrosine at non-OR region can enhance PrP^{C}-PrP^{Sc} conversion process, and the non-OR copper binding site may have a critical role in this process.

List of Publications

Le NT, J Narkiewicz, S Aulić, G Salzano, **TH Tran**, D Scaini, F Moda, G Giachin, and G Legname. 2015. "Synthetic prions and other human neurodegenerative proteinopathies". *Virus Research.* 207: 25-37.

Giachin G, PT Mai, **TH Tran**, G Salzano, F Benetti, G Legname, et al. 2015. "The non-octarepeat copper binding site of the prion protein is a key regulator of prion conversion". *Scientific Reports.* 5.

Table of content

LIST OF FIGURES

LIST OF TABLES

LIST OF ABBREVIATIONS

ASA: amyloid seeding assay

BCS: Bathocuprionedisulfate

BSE: Bovine Spongiform Encephalopathy

CC_1: charged aminoacid cluster 1

CC_2: charged aminoacid cluster 2

CJD: Creutzfeldt-Jakob disease

CPZ: Cuprizone

CWD: Chronic Wasting Disease

DNA: Deoxyribonucleic acid

DRMs: detergent insoluble membrane domains

EM: electron microscopy

ER: endoplasmic reticulum

fCJD: familial Creutzfeldt-Jakob disease

FFI: Fatal familial insomnia

FSE: Feline spongiform encephalopathy

FTIR: Fourier Transform Infrared Spectroscopy

GAGs: glycosaminoglycans

Grb2: Growth factor receptor-bound protein 2

GPI: glycosylphosphatidylinositol

GS: GPI-anchor signal

GSS: Gerstmann-Sträussler–Scheinker

GndHCl: Guanidine hydrochloride

HD: hydrophobic domain

Hu: human

HX-MS: Hydrogen-deuterium exchange mass spectroscopy

IBs: inclusion bodies

IMAC: Immobilized metal ion affinity chromatography

IPTG: isopropyl b-D-galactopyranoside

LRP: Laminin receptor precursor

Mo: mouse

N2a: mouse neuroblastoma cells line

NCAM: neuronal cell adhesion molecule

NMR: nuclear magnetic resonance

NMDAR: *N*-methyl-D-aspartate receptors

NO: nitric oxide

OR: octapeptide-repeat region

ORF: open reading frame

PAGE: Polyacrylamide gel electrophoresis

PCR: Polymerase Chain Reaction

PMCA: Protein Misfolding Cyclic Amplification

Prion: Proteinaceous infectious particle

PrP: prion protein

PrP^{C}: physiological cellular form of PrP

PrP^{Sc}: misfolded, pathogenic form of PrP^{C}, also denoted as prion.

^{Ctm}PrP: C-terminal transmembrane PrP form

^{Ntm}PrP: N-terminal transmembrane PrP form

^{Sec}PrP: secretory PrP

PrP^{*}: partially destabilized folding intermediate of PrP^{C}

PK: proteinase K

PRNP: human prion protein gene

Prnp: prion protein gene in non human species

PTA: phosphotungstate anion (Phosphotungstic acid)

rec: recombinant

RT: room temperature

ScN2a: chronically PrP^{Sc} infected mouse neuroblastoma cells line

SDS: sodium dodecyl sulfate

SEC: Size exclusion chromatoghaphy

SHa: Syrian hamster

SOD: superoxide dismutase

SP: signal peptide

STI-1: stress-inducible protein 1

Tg: transgenic

ThT: thioflavin T

TME: Transmissible Mink Encephalopathy

TSEs: Transmissible spongiphorm encephalopathies

vCJD: variant Creutzfeldt–Jakob disease

WT: wild-type

XAFS: X-ray absorption fine structure

CHAPTER I

INTRODUCTION

1.1 Prion disease

Prion diseases, in human and animals, are a group of fatal neurodegenerative diseases that are also referred to as transmissible spongiform encephalopathies (TSEs). They have a common feature in aberrant metabolism of the aprion protein (PrP) [1]. During the pathogenesis of these diseases, a cellular isoform of the prion protein (PrP^{C}) adopts a pathogenic misfolded conformation denoted as prion (PrP^{Sc}), which accumulates in cells and causes the disease. These diseases are thought to mostly affect the cortex, thalamus, brain stem, cerebellum of the brain and other neuronal tissue [2], and can lead to progressive dementia and may also exhibit some cerebral ataxia [1]. Table 1 includes an overview of some TSEs in human and animals. The disorders can occur spontaneously, genetically or caused by infection [3].

Table 1. Human and animal prion diseases [3,4]

Host	Disease	Mechanism of pathogenesis
Humans	Kuru	Infection through ritualistic cannibalism
	Creutzfeldt-Jakob disease (CJD)	Sporadic, familial or iatrogenic
	Variant Creutzfeldt–Jakob disease (vCJD)	Infection from bovine prions
	Gerstmann-Sträussler–Scheinker syndrome (GSS)	Familial
	Fatal Familial Insomnia (FFI)	Familial
Sheep	Scrapie	Infection
Cattle	Bovine Spongiform Encephalopathy (BSE)	Infection or sporadic
Cervids	Chronic Wasting Disease (CWD)	Infection
Mink	Transmissible Mink Encephalopathy (TME)	Infection

Cats	Feline Spongiform Encephalopathy (FSE)	Infection

In humans, sporadic Creutzfeldt-Jakob disease (sCJD) is the most common form of prion disease. It accounts for about 85% of cases recorded since 1996, with an annual incidence of ~1.5 cases per million worldwide [4]. About 10-15% of prion diseases in humans are caused by mutations in the PrP gene, *PRNP* [5]. Up to date, over 40 different mutations of the PrP gene have been shown to segregate with the heritable human prion diseases (Figure 1). The resulting diseases have been classified as three distinct clinico-pathological phenotypes: familial (f) Creutzfeldt-Jakob disease (fCJD), Gerstmann-Sträussler–Scheinker (GSS) syndrome and Fatal Familial Insomnia (FFI). The acquired forms of the disease are transmitted among humans (iatrogenic CJD and Kuru) or from animals to humans (variant CJD or vCJD). Iatrogenic CJD is caused by using the infected surgical instruments in brain surgery or using human-derived prion-infected growth hormones [6]. Kuru was found in Papua New Guinea due to customary ritualistic cannibalism, which involved the consumption of brain material of dead relatives [7-9]. Another human infectious prion disease is vCJD, which is due to the consumption of prion-infected beef.

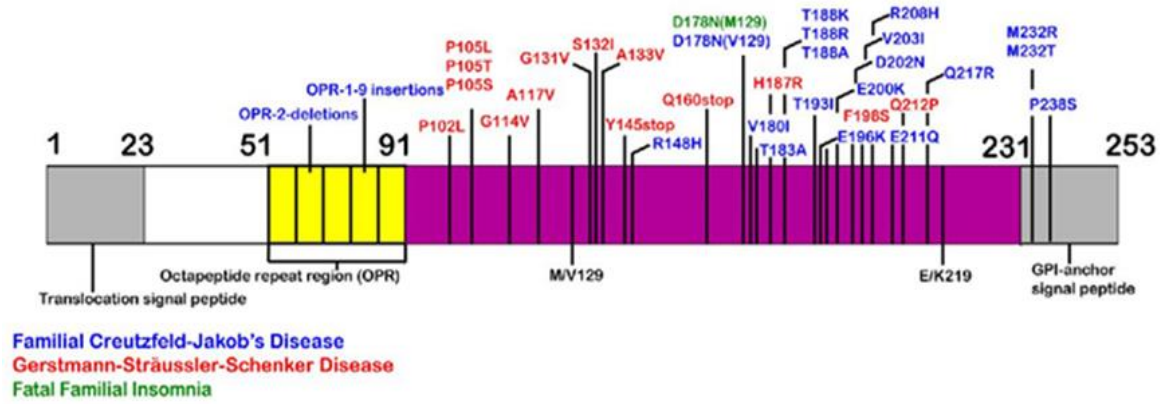

Figure 1. Disease-linked mutations of the prion protein [3].

1.2 The cellular prion protein (PrP^C)

1.2.1 Biogenesis and structure of PrP^C

The prion protein gene (*PRNP* in humans and *Prnp* in other species) is highly conserved across species. In mammals, the DNA sequence of the open reading frame (ORF) encoding PrP generally exhibits around 90% similarity[10]. The human *PRNP* comprises two exons separated by a single intron with the entire ORF located in the second exon [11]. The *Prnp* of mice, sheep and cattle contains three exons with the protein coding sequence located in the third exon [12-14]. The other exons contain untranslated sequences including the promoter and termination sites. The PrP promoter contains multiple copies of GC rich repeats and is devoid of TATA box [15]. In humans, *PRNP* is a single copy gene mapped in the short arm of chromosome 20, which corresponds to the homologous region of mouse chromosome 2 where *Prnp* is located [16]. PrP^C is highly expressed within the central and peripheral nervous systems, although its expression varies among distinct cell types, neurons and brain regions [17]. Transcription and translation of both mRNA and protein usually correlates well and is highly regulated during development. PrP^C is found primarily in neuronal cells but is also normally expressed in a variety of other tissues [18, 19].

The human pre-pro-protein contains 253 amino acids. In the N-terminus of there is located a signal peptide, which regulates trafficking of the protein through the endoplasmic reticulum and the Golgi apparatus to the cell surface. The protein is N-glycosylated at two asparagin residues (181 and 197) located in the C-terminal [20]. In addition, a single disulfide bridge is formed between the cysteine residues at position 179 and 214 [21]. Attachment of a glycosylphosphatidylinositol (GPI) anchor occurs at position 231 after cleavage of GPI-signal peptide [22]. The mature human PrP comprises amino acid 23 to 231 and it is extracellularly attached to the cell membrane via its GPI anchor.

During co-translational translocation in the ER, three topological forms of PrP can be synthesized. Most PrP nascent chains pass completely through the translocon to generate secretory PrP (SecPrP) and follow the traditional exocytic pathway towards the cell surface. Two transmembrane forms were generated by transmembrane insertion of the PrP hydrophobic domain (residues from 110 to 134) in the ER compartment. One form (NtmPrP) integrates into the lipid bilayer with the N-terminus in the ER lumen and the C-terminus retained in the cytosol, whereas the other form (CtmPrP) integrates in the opposite orientation [23]. The role of the atypical forms, CtmPrP and NtmPrP, is still not fully clarified but may be associated with neurotoxicity and cellular death especially in case of inherited prion diseases [24].

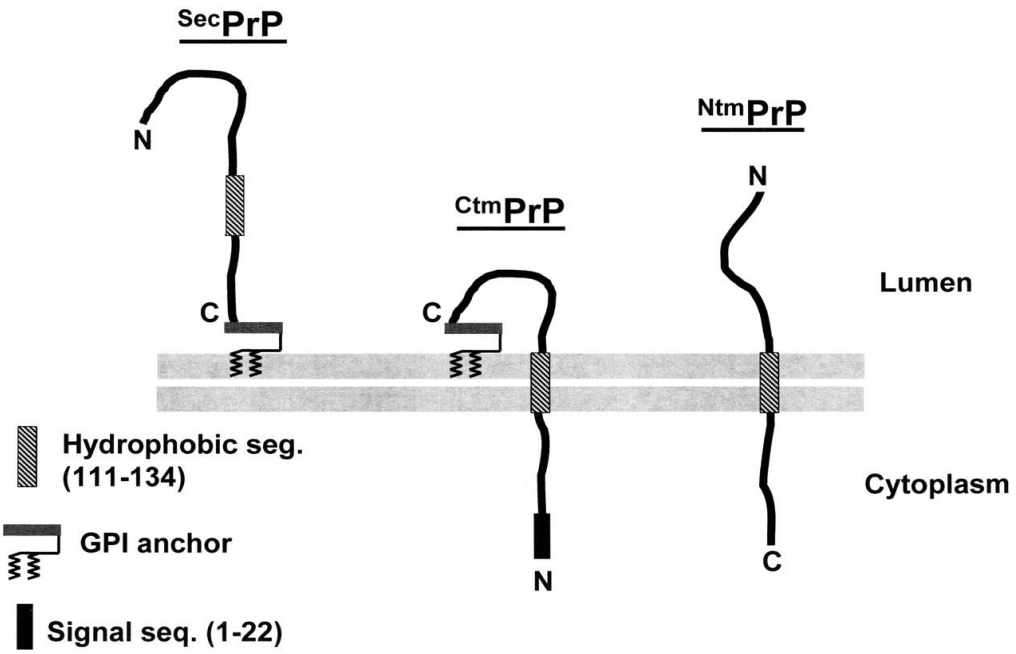

Figure 2. Three topological forms of PrP [25].

The mature PrP^C can be divided in two regions, a flexible unstructured N-terminal region and a C-terminal globular region.

The N-terminal domain contains two positively charged clusters (CC1 and CC2), one at the N-terminus and one close to the hydrophobic domain (HD, residue

111-134). CC1 and CC2 (residue 23-27 and 95-110, respectively) seem be involved in glycosaminoglycans (GAGs) [26, 27] and nucleic acids [28, 29] binding. The highly conserved hydrophobic domain has been shown not to serve as a transmembrane domain at the cell surface [30]. Nonetheless, studies using synthetic systems have shown that peptides from this region can span membranes and suggest that this could occur as part of PrP^C function during cellular trafficking [31, 32]. Small peptides corresponding to the palindromic sequence AGAAAGA of this region can refold into fibrils with β-sheet structure that are toxic to cultured mouse hippocampal cells suggesting that the hydrophobic domain may be an important part of an infectious prion [33, 34]. The octapeptide-repeat region (OR) is also a highly conserved PrP region. The number of the repeated units can vary among species. In HuPrP the OR consists of one nonapeptide, PQGGGGWGQ (residues 51-59) and four repeats of the sequence PHGGGWGQ (residues 60–91). The octapeptide repeats have been shown that it can be the binding sites of copper or other divalent cations such as zinc, nickel, iron and manganese, suggesting a possible role in ion regulation/signaling [35].

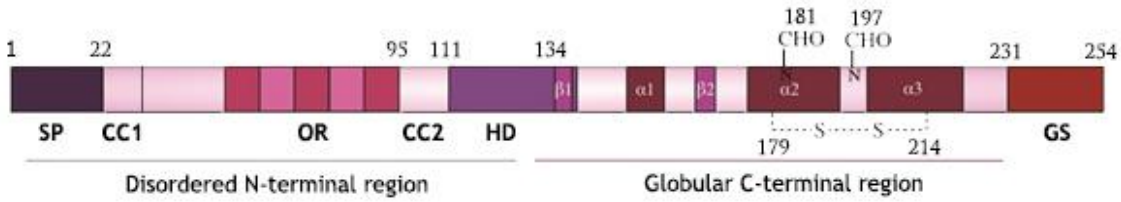

Figure 3. Schematic illustration of primary PrP^C structure. SP: signal peptide, CC1: charged cluster 1, CC2: charged cluster 2, OR: octapeptide repeat region, HD: hydrophobic domain, GS: GPI-anchor signal.

The structure of the C-terminal ordered domain was first determined from mouse PrP using NMR in 1995 [36] and structures from many other species have since been added. The HuPrP structure is composed of three α-helices (α1, α2 and α3) and two very short β-strands which form an antiparallel β-sheet (β1 and β2).

Helices α2 and α3 form the bulk of the structure and are covalently bridged by a disulfide bond between Cys179 and Cys214.[37]

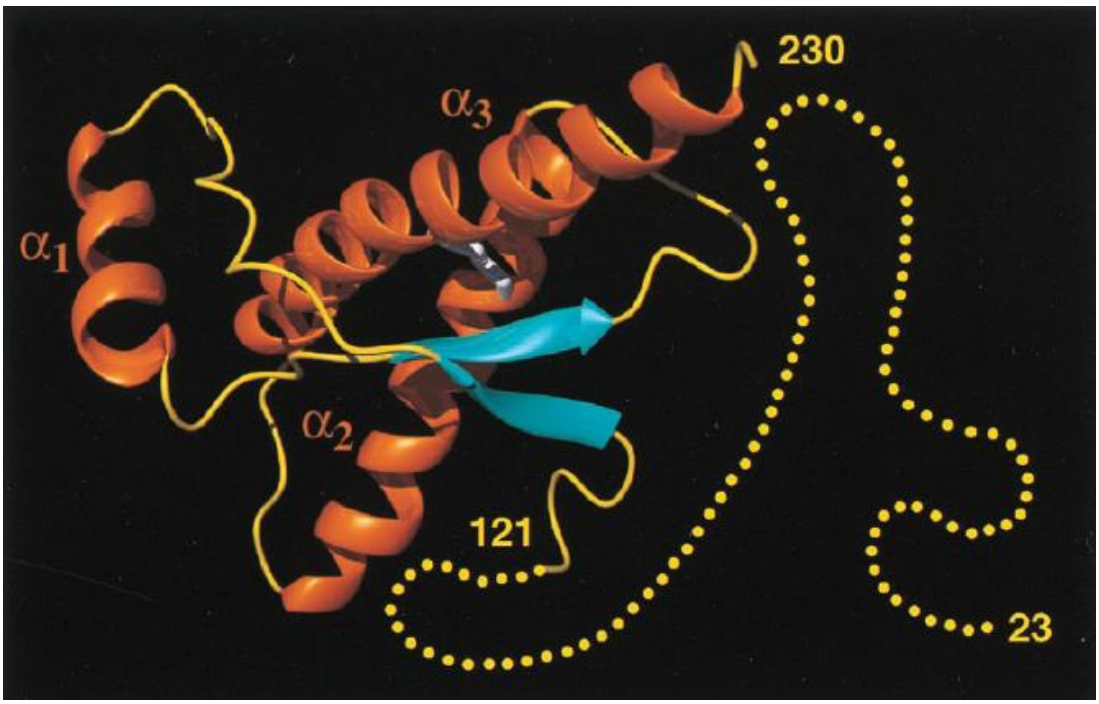

Figure 4. The three-dimensional structure of the human prion protein.
(Modified from [37])

1.2.2 Prion protein trafficking

After its synthesis in the ER, PrP^C is trafficked *via* the Golgi to the cell surface, where it constitutively cycles between the plasma membrane and an endocytic compartment [38]. This process seems to be a complex cellular event and various mechanisms have been proposed to explain it (Figure 5).

In primary cultures of sensory neurons, as well as in neuroblastoma N2a cell, PrP^C has been shown to recycle from the cell surface to endosomes via clathrin-coated pits [39-41]. In addition, the N-terminal positively charged motif, KKRPKP, of PrP^C has been shown to be responsible for localisation of PrP^C in clathrin-coated pits and subsequent internalisation [38, 40]. These findings suggested that PrP^C might be binding, *via* its N-terminal region, to a transmembrane protein containing a localisation signal for coated pits.

Another mechanism of PrP^C internalisation has been proposed following PrP^C localisation studies in various cell models that showed that PrP^C clusters in caveolae or caveolae-like domains [42, 43]. However, caveolae have not been shown to occur on adult mammalian neurons [44], thus the role of caveolae in prion trafficking on neurons is unclear.

Similar to other GPI-anchored proteins, PrP^C is found mainly attached to low-density, detergent insoluble membrane domains (DRMs), rich in cholesterol and sphingolipids [45, 46], also denoted as lipid rafts. Then PrP^C can internalize through a possible pathway that is independent of clathrin and dependent on rafts.

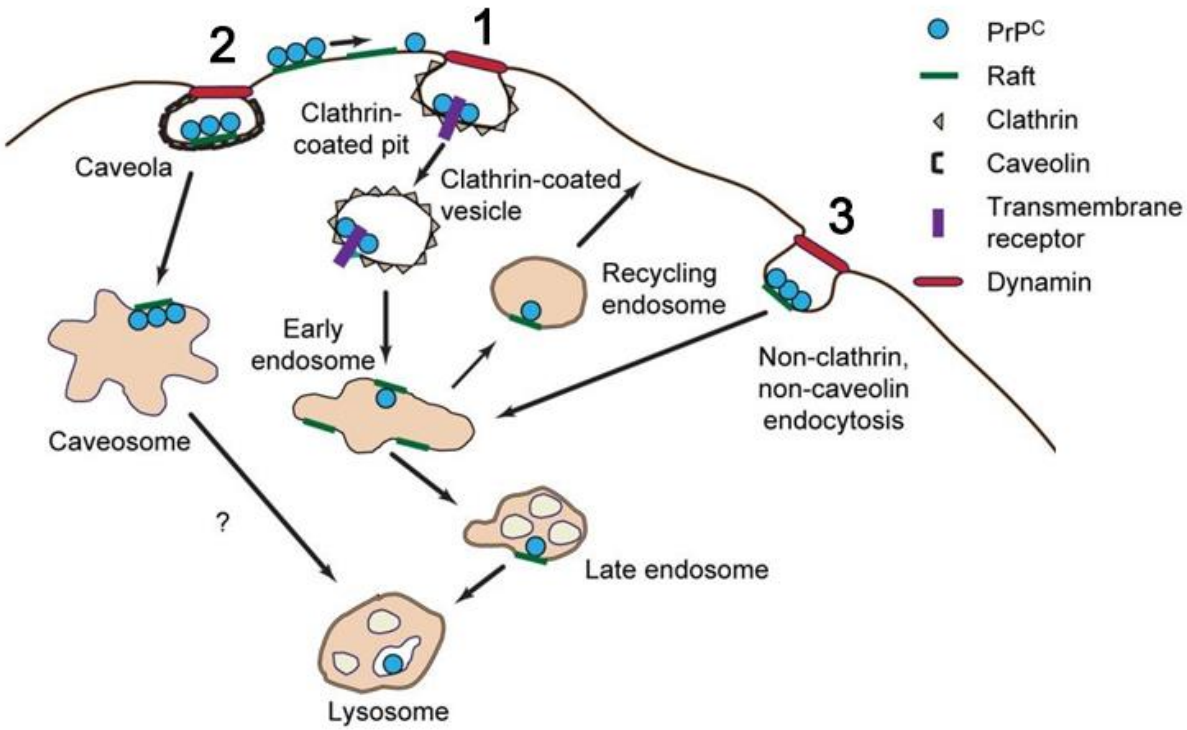

Figure 5. Pathways of PrP^C internalisation[47]. At the plasma membrane, PrP^C can be constitutively internalized. A chief pathway of PrP^C internalization in neuronal cells seems to depend on clathrin-mediated endocytosis (1). Caveolin-related endocytosis and trafficking have been implicated in PrP^C transport in Chinese hamster ovary and glial cells (2). Finally, non-clathrin and non-caveolin but raft-dependent endocytosis has been proposed to participate in the internalization of prion protein (3).

1.2.3 Function of PrP^C

Although PrP^C was discovered over thirty years ago and has been largely studied, its putative physiological function is still unclear. In efforts to determine the function of PrP^C, several lines of PrP^C knockout mice have been produced and investigated.

The first PrP^C-null transgenic mice, called Zurich I (ZrchI), were created by replacing codon 4-187 with a neomycin phosphotransferase expression cassette. These mice showed no behavioural or learning defects [48]. A second study using transgenic mice, called Edinburgh made by an interruption at codon 93 of *Prpn* ORF, gave results similar to those seen for the Zurich I transgenic mice [49]. Based on these studies, they suggested PrP^C is not necessary for normal development. However, contradictory results were obtained by PrP-null transgenic mice, known as Nagasaki, where *Pnrp* has been completely removed. These mice had normal development but at advanced ages developed ataxia and prukinje cell degeneration [50]. The observed phenotype was abolished by reintroduction of PrP^C [50, 51], suggesting that PrP^C have a role in the nervous system.

Other studies involving Zurich I mice showed that these mice had lower anxiety levels suggesting that PrP^C may help the adaptation to stress [52]. Zurich I mice have also shown abnormalities in their circadian rhythms and sleeping patterns, when PrP^C was overexpressed the transgenic mice developed wild type phenotypes [53, 54]. In addition, aged ZrchI mice also showed impairments in short and long term memory [55]. These evidences for significant roles of PrP^C in different behavioral processes suggest that PrP^C could play a regulatory role in synapse formation and function.

Another way to gain insight into the function of PrP^C is to identify proteins that interact and bind to PrP^C. Over the years, a number of candidates have been

identified as potential PrP-binding partners using many different methods, such as yeast two-hybrid screening, co-immunoprecipitation and cross-linking (Table 2). Based on this, some cellular function of PrP^C have been identified, for example: cell adhesion [56-58], synaptogenesis [59], signalling [60], copper homeostasis [61], and neuroprotection [62-64]. However, the physiological relevance of most of the proposed interaction partners is still uncertain and need to be confirmed.

Table 2. Putative PrP interactors [65]

Candidate Interactor	**Candidate Function**	**Identification Method**
Growth factor receptor-bound protein 2 (Grb2)	Signal transduction (adaptor protein)	Yeast two-hybrid; co-immunoprecipitation
Synapsin 1b	Synaptic vesicle trafficking	Yeast two-hybrid; co-immunoprecipitation
TREK-1	Two-pore K^+ channel	Yeast two-hybrid; co-immunoprecipitation
Tubulin	Microtubule subunit	Cross-linking
NRAGE (Neurotrophin receptor-interacting MAGE homologue)	Activator of apoptosis	Yeast two-hybrid; co-immunoprecipitation
Laminin receptor precursor (LRP)	Extracellular matrix interactions	Yeast two-hybrid
Stress-inducible protein 1 (STI-1)	Heat shock protein	Co-immunoprecipitation
Hsp60	Chaperone	Yeast two-hybrid
N-CAM	Cell adhesion	Cross-linking
Bcl-2	Multi-domain anti-apoptotic regulator	Yeast two-hybrid
Caveolin-1	Caveolar coat	Co-immunoprecipitation

1.3 The pathological form of prion protein (PrP^{Sc})

1.3.1 Structure of PrP^{Sc}

The key event in prion disease pathogenesis is the conversion of normal, native conformation PrP^{C} to an abnormal conformation PrP^{Sc}. Although sharing the same sequences, the two isoforms of the prion protein bear several biophysical differences.

Table 3. Biochemical and biophysical characteristics of PrP^{C} and PrP^{Sc}

Properties	PrP^{C}	PrP^{Sc}
Isoform	Monomers	Multimeric aggregates
Protease resistance	No	Stable core (residues ~90-231)
Location	Plasma membrane	Intra- or extracellular
Solubility	Soluble	Insoluble
PK-sensitivity	Sensitive	Partially resistant
α-helices	45%	30%
β-sheets	3%	45%
Infectivity	No	Yes
Turnover	Hours	Days

PrP^{Sc} is insoluble in detergents and can be detected by limited protease digestion that results in a protease resistant molecule of around 142 amino acids referred to as PrP27-30. The protease-resistant core of PrP^{Sc} has been shown to form aggregates and amyloid, which stain with Congo red and show green-gold birefringence, typical of amyloids [66]. But it has been shown that the amyloid properties of PrP^{Sc} are not an obligatory feature of prion diseases [67] and not all PrP^{Sc} molecules are resistant to protease digestion [68]. The other characteristic used to distinguish between the two isoforms is the difference in their secondary structures. Fourier Transform Infrared Spectroscopy (FTIR) and circular dichroism studies have shown that unlike PrP^{C}, which is predominantly α-helix (47% α-helix and only 3% β-sheet), PrP^{Sc} is β-sheet enriched (43% β-sheet and 30% α-helix)[33].

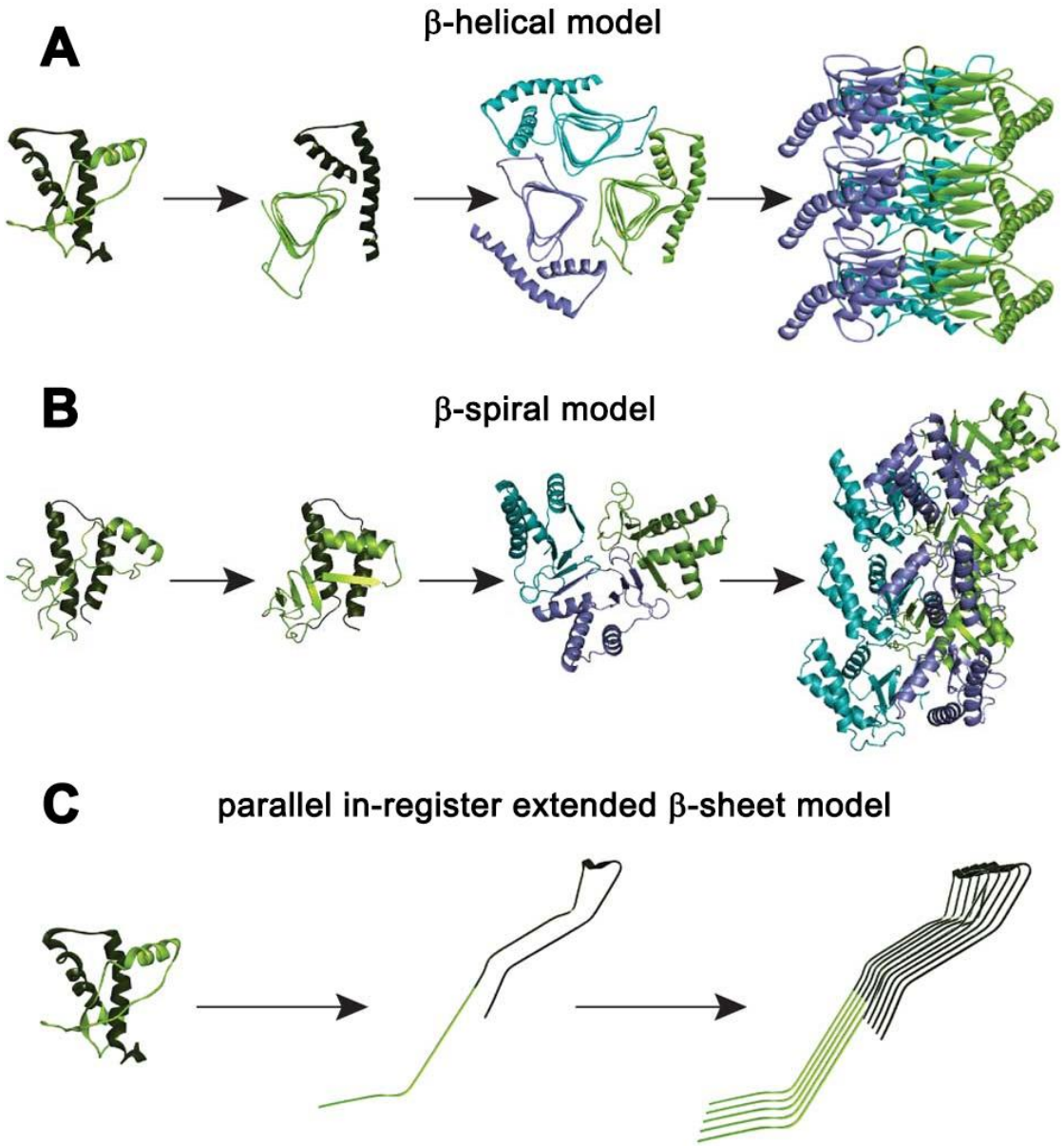

Figure 6. Alternative models proposed for the structure of PrP^{Sc} [69]. (A) The β-helical model, (B) the β-spiral model and (C) the parallel in-register extended β-sheet model.

Because PrP^{Sc} is insoluble and forms aggregates, the atomic structure of PrP^{Sc} is still unclear. However, several structural models have been proposed based on computational modeling or low-resolution biophysical techniques such as X-ray fiber diffraction, electron microscopy (EM) and Hydrogen-deuterium exchange mass spectroscopy (HX-MS). These structural models are β-helical model, β -spiral model and parallel in-register extended β-sheet model.

The first originates from cryo-electron microscopy data and structural modeling, and proposes that PrP^{Sc} forms left-handed β –helix motif in the region from residue 90 to 177, while the C-terminal region (residues 178–230) still maintains the α-helical folding as in PrP^{C} (Figure 6A) [70]. In the spiral model, the proposed PrP^{Sc} structure derives from an all-atom explicit solvent molecular dynamic simulation [71, 72]. According to this model, during prion conversion the two native β-sheets elongate in a longer single β-strand, which forms intermolecular β -sheets with other PrP molecules leading to polymerization. The basic subunit of the oligomers was also modeled according to a trimer. In this model, the three α-helices in PrP^{C} maintain this conformational motif (Figure 6B). Recently, Surewicz *et al* examined by hydrogen-deuterium exchange the structural organization of PrP^{Sc} extracted from transgenic mice expressing unglycosilated PrP^{C} lacking GPI anchor (ΔGPI) and proposed the parallel in-register extended β-sheet model. This model proposes a thorough refolding of PrP^{C} into a structure composed mainly of β-sheets, included a continuum of short β-strands from residue ~90 to the entire C-terminal region (Figure 6C) [73, 74]. Follow up this work, more recently, Groveman and colleagues also proposed the parallel in-regester model for prion-seeded PrP amyloids by using solid-state NMR and molecular dynamics simulations [75].

1.3.2 The “protein-only” hypothesis

The conversion of the cellular form of the prion protein to its pathogenic isoform is the central event of prion diseases. To explain this reaction and prion replication several hypotheses have been proposed. The largely accepted one is the “protein-only” hypothesis proposed by S. B. Prusiner [76]. The protein-only hypothesis, which postulates that prion propagation, results from a change in PrP conformation whereby PrP^{Sc} recruits endogenous PrP^{C} in order to replicate.

Some of the supporting evidence comes from findings that inherited prion diseases are linked to mutations in the *PRNP* gene [77], indicating that a genetic disease may be able to propagate in an infectious way. Another important evidence comes from PrP^{C} knockout (KO) mice, which are resistant to prions thus indicating that PrPC is an absolut requirement in order to develop prion diseases [78].

The other strongest supporting evidence is the synthetic prion. In 2004 the production of synthetic prions *via* the *in vitro* conversion of recPrP was reported and they have been shown to be infectious *in vivo* [79]. As follow-up this experiment, a series of recPrP amyloid fibers were produced and intracerebrally injected in Tg mice overexpressing PrP^{C}. Interestingly, different inocula were able to propagate *in vivo* and induce the formation of different prion strains [80]. Another method for generating synthetic prions is protein misfolding cyclic amplification (PMCA). This methods has improved such *in vitro* amplification systems both with regards to amplification and infectivity, and has helped demonstrate that infectious material can be produced in a cell-free system, which when inoculated into mice leads to a prion disease [81-84]. Recently, Wang *et al.* applied PMCA to produce prion starting from full-length Mo recPrP (recPMCA) using synthetic lipid (POPG) and RNA (isolated from mouse liver) or synthetic polyriboadenylic acid [85-88]. The newly generated PrP^{Sc} was found to be infectious, and the infectivity was maintained after several transmission studies in wild-type mice. The findings that several synthetic prions produced *in vitro* by different methods are able to cause prion diseases have provided the ultimate evidence in support of the protein-only hypothesis [89].

1.3.3 Models for prion replication

Two models to explain the conversion of PrP^{C} to PrP^{Sc} have been proposed.

In the first model, denoted as *template directed-refolding model*, there is an interaction between exogenously introduced PrP^{Sc} and endogenous PrP^{C}, which is induced to transform itself into further PrP^{Sc}. PrP^{Sc} exists as a monomer that is thermodynamically more stable than PrP^{C} but a high energy barrier may prevent spontaneous conversion of PrP^{C} to PrP^{Sc} [90]. There are many studies which support this theory; one particular study uses transgenic (Tg) mice expressing mouse PrP, $MoPrP^{C}$, and Syrian hamster PrP, $SHaPrP^{C}$ [91]. When these mice were injected with $MoPrP^{Sc}$, the infectious particles facilitated the conversion of $MoPrP^{C}$ to $MoPrP^{Sc}$, the same was observed when the Tg mice were inoculated with $SHaPrP^{Sc}$. Thus, indicating only the PrP^{C} with the corresponding sequence to the PrP^{Sc} present, undergo conformational changes. In this model, the critical step in the conversion is the formation of a dimer between PrP^{Sc} and PrP^{C}, and PrP^{C} is assumed to become a partially unfolding intermediate of PrP^{C} (PrP*) before it is induced to misfold into PrP^{Sc} [92]. Some *in vitro* studies have tried to simulate this intermediate by using 2 M guanidinium chloride or sonication [93, 94].

Another proposed pathway of propagation is the *seeded nucleation model*. In this model the conversion between PrP^{C} and PrP^{Sc} is reversible, but the PrP^{Sc} monomer is much less stable than PrP^{C} then the equilibrium is strongly shifted towards PrP^{C}. The seed formation begins very slowly. However, once the seed has formed, monomeric PrP^{C} adopt the conformation of PrP^{Sc} and can efficiently add to the seed. The rate-limiting step in this mechanism is not the conformational conversion step but the seed formation step. This step, responsible for the lag phase in the spontaneous conversion, can be bypassed and accelerated by addition of preformed PrP^{Sc} seeds [95].

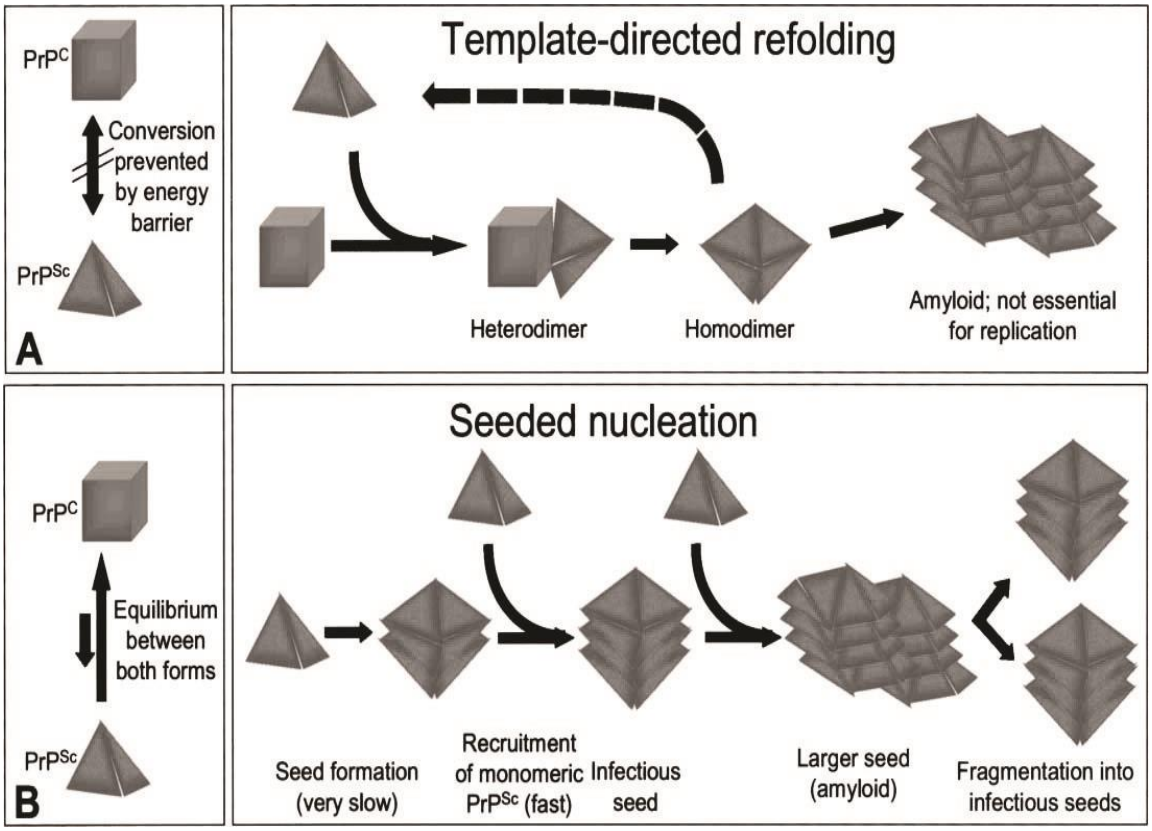

Figure 7. Model for the conversion of PrP^C to PrP^{Sc} [90]. (A) Template directed-refolding model, (B) seeded nucleation model.

1.4 Putative sites for PrP^C-PrP^{Sc} conversion

Most of the prion protein is found in lipid rafts located on the outer side of the plasma membrane [23, 24]. PrP^C serves a short period of time at the surface of the membrane, it has a half-life of 3 to 6 hours [96-98], after which the majority of the cell surface PrP^C undergoes endocytosis. Several studies showed that the prion conversion occurs after PrP^C reaches the cell surface [97, 99, 100]. In addition, PrP^{Sc} formation is also reduced by preventing the transport of PrP^C to the plasma membrane [101]. Then the prion conversion is thought to take place at the cell surface, where the first contact between endogenous PrP^C and exogenous PrP^{Sc} or immediately after its internalization in the endolysosomal compartment.

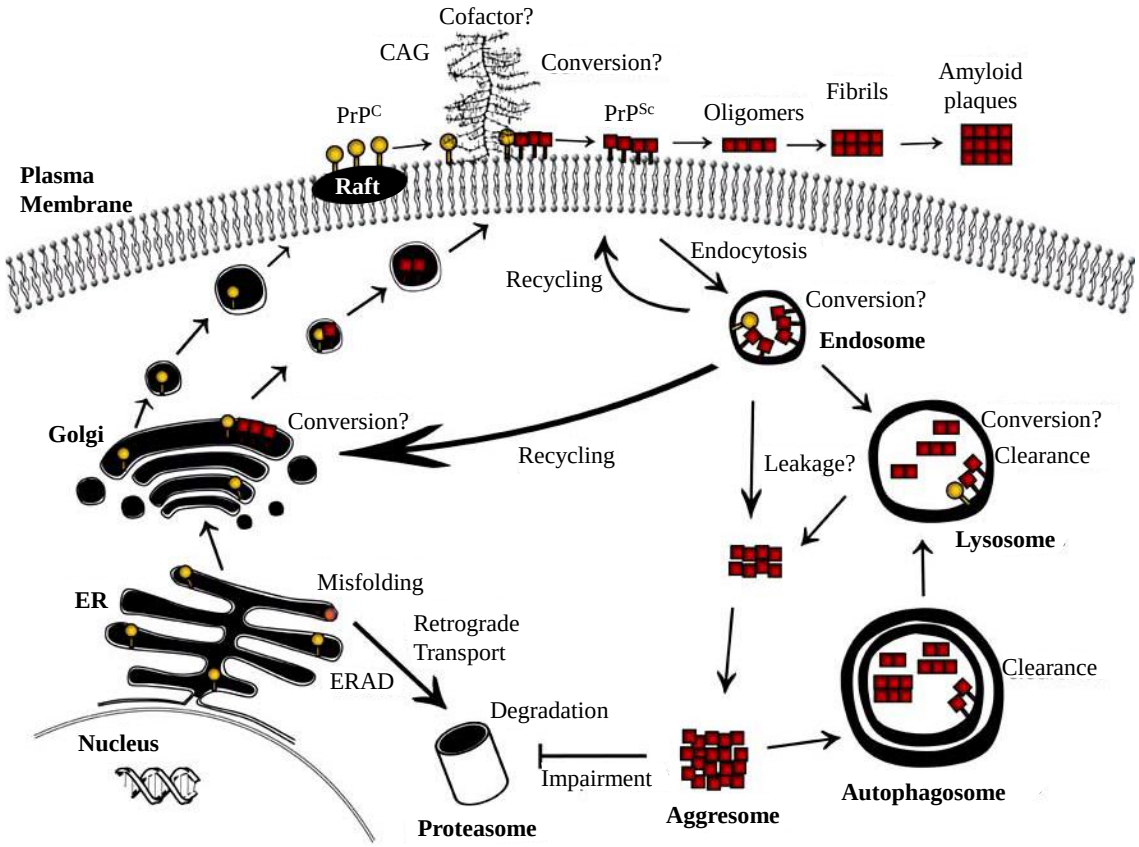

Figure 8. Cell biology of PrP^C and PrP^{Sc} with potential sites of conversion[102].

Some PrP^{Sc} was also found in the Golgi apparatus in N2a cells persistently infected with RML/Chandler scrapie [103]. And also in this cell line infected with RML or 22L scrapie strain, increased PrP^{Sc} levels are along with increased retrograde transport to Golgi and ER [104]. Then another possibility for prion conversion is that PrP^{Sc} undergoes retrograde transport to the Golgi and ER, thereby disturbing the biosynthesis of PrP^C and triggering the formation of the PrP^{Sc} from the PrP^C precursor.

There is still no thorough explanation for the necessity of PrP^C to reach the cell membrane before being converted to PrP^{Sc}. One possibility is the posttranslational modifications that are necessary for prion conversion, therefore PrP^C need to reach the plasma membrane in mature form. Another possibility is that PrP^C will act as a receptor that mediates PrP^{Sc} internalization during infection. Alternatively, the plasma membrane environment might be favorable or contain

some factors needing for the PrP^{C}–PrP^{Sc} interaction and conversion. For example, some studies showed GAGs in cell surface might bind to both PrP^{C} and PrP^{Sc} to generate prion conversion [102, 105].

1.5 Copper and prion diseases

1.5.1 Copper binding to PrP^{C}

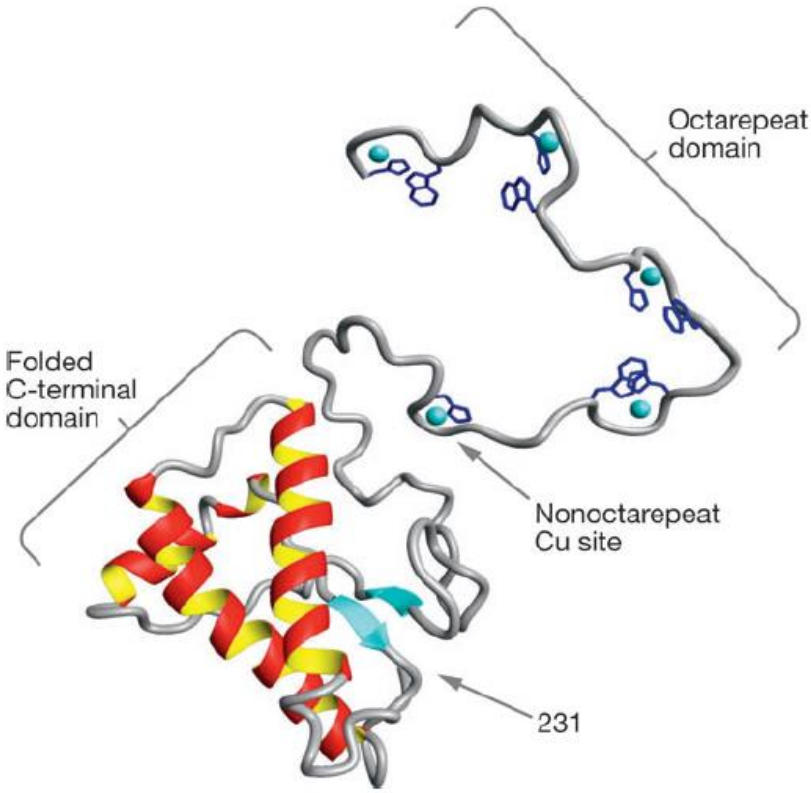

Figure 9. A structural model of the prion protein with its full complement of copper [106]. Each copper in the octarepeat domain interacts with the HGGGW. Electron paramagnetic resonance studies on full-length recombinant protein identified an additional non-octapeptide repeat binding site involving His-96 and His-110.

PrP^{C} has been found that can binds copper and PrP^{C} can be isolated with copper affinity columns [107, 108]. Many studies have used recombinant prion protein to measure the binding affinity of different amino acid sequences of prion protein to copper, and most researchers would agree that copper binds specifically to the N-terminal domain of prion protein [109, 110]. This domain (residues 23 to

126) is highly disordered [111, 112] and there are about five copper binding sites in this domain: four in octapeptide region (residues 60-91) and one in non-octapeptide region (residues 91-111) [113].

The binding of copper at octapeptide repeats binding sites.

The octarepeat region in human prion protein is composed of a sequence of eight amino acids (PHGGGWGQ) repeated four times, each containing a histidine which is generally accepted to be the primary residue responsible for the copper coordination [109, 114]. This region is highly conserved and can bind four copper ions with identical coordination geometry [115, 116]. A crystal structure of the Cu(II) bound octarepeat motif (residues HGGGW) indicates a square-pyramidal geometry [106, 114], involving coordinating nitrogen and oxygen ligands from the main-chain as well as the imidazole side chain. The molecular features of the crystal structure are fully consistent with the structural details elucidated by Electron Paramagnetic Resonance (EPR) (Figure 10) [106].

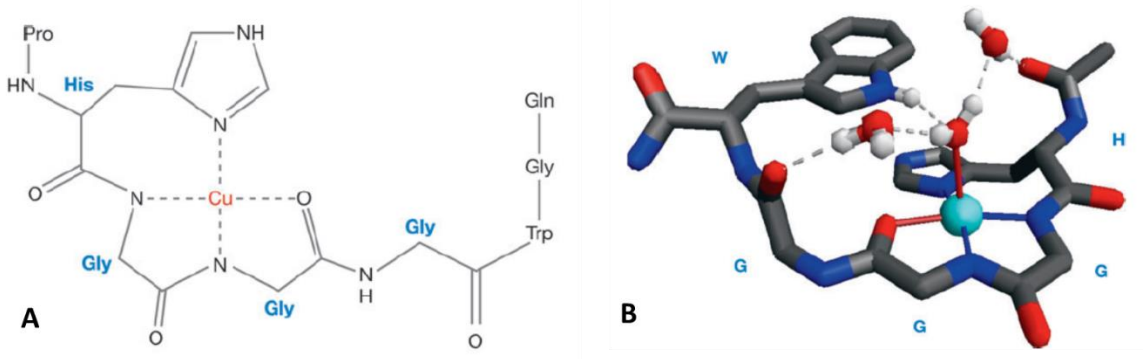

Figure 10. Copper coordination to the octapeptide repeat. A. Chemical details of the copper-octapeptide repeat interaction, determined by electron paramagnetic resonance (EPR) method, B. X-ray crystal structure of the Cu2+-HGGGW complex. (Adapted from [106])

However, the copper coordination to the octapeptide repeat region was also dependent on the degree of copper occupancy on the protein. It has also been shown that at low copper-peptides ratio levels, copper ions will bind with a higher affinity to the octarepeats via multiple His residues [117-119]. Using the Electron

Paramagnetic Resonance (EPR) method, three distinct binding component have identified depending the copper occupancy level [106]. Component 1 dominates at high copper occupancy and reflects the interaction with a single His. Component 2 is an intermediate state in which each copper is coordinated by two His residues, thus forming large intervening loops. Component 2 is coordination is present only as a transition between low copper occupancy of one atom or less and full copper occupancy. Component 3 presents at low copper occupancy only and it is likely to provide the highest affinity copper binding within the octarepeat due to its multi-His coordination.

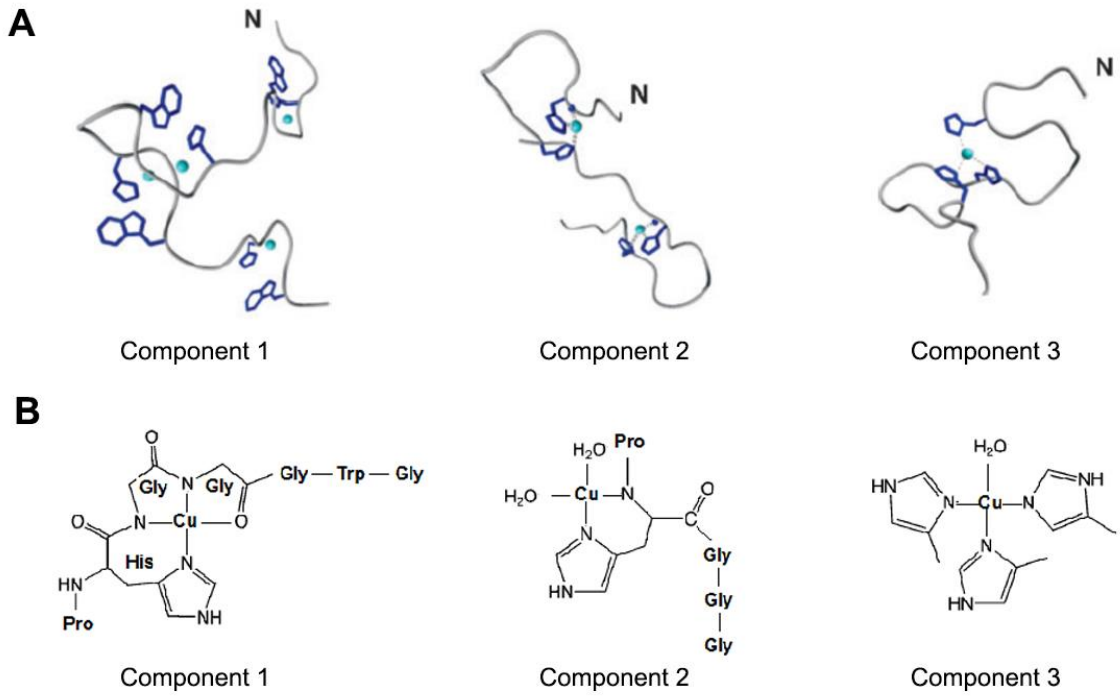

Figure 11. Three components of copper binding to the octapeptide repeat region. A. Octarepeat Cu(II) binding modes with three, two, or one coordinated His residues, B. The 3 models indicating the equatorial coordination modes of copper binding to the octarepeat region are shown (Modified from [106, 120])

The binding of copper at non-octapeptide repeat binding site

Several studies have shown that copper is able to bind outside of the octarepeat region of PrP [121-123]. Work by Jones highlighted these copper binding regions as His96 and His111 in the human protein, in the amyloidogenic

region between residues 90 to 126 [124]. Interestingly, the coordination of copper to this region changed dramatically dependent on pH. There are 3 coordination modes, all of them display a square planar geometry. At pH 7.5 and above, a 4N complex dominates, while at pH6, a ligand rearrangement shifts the coordination to a 3N1O configuration. At low pH, a multi His 2N2O coordination dominates.[120]

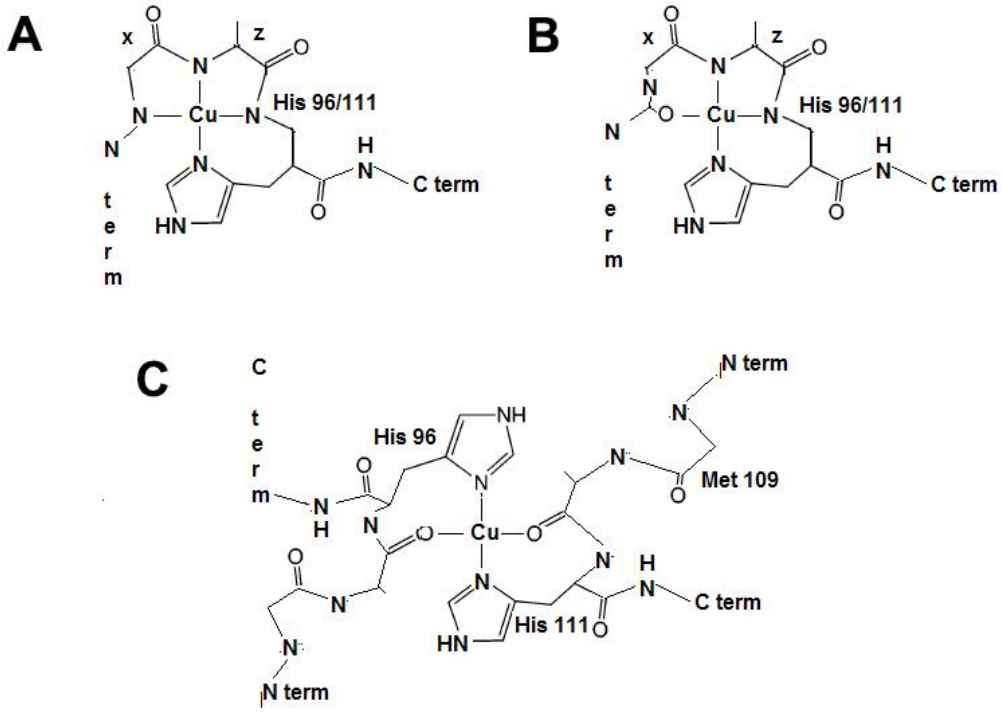

Figure 12. Models of the Cu2+ coordination modes for the non-octapeptide repeat site[120]**. (A)** Component 1 is a 4N complex that dominate at pH 7.5 and above, **(B)** Component 2 is a 3N1O complex that exists at pH 6, **(C)** Component 3 is a 2N2O complex that may exist at pH 5.5.

Copper affinity of prion protein

Early studies suggested that the binding affinities of copper ions to PrP are in the micromolar (μM) range [125, 126]. The first real attempt to assess the affinity of copper for PrP was in the mid 1990s by Hornshaw group. Using X-ray fluorescence, they suggest a Kd at 6.7 μM on synthetic peptides [110] and 14 μM on full length protein [127]. Following this, another group used various spectroscopic techniques and found the affinity for copper within the octarepeat to

be Kd~6 μM when two octarepeat segments were present [115]. However, more recently, some studies showed a much stronger binding affinity, in the femtomolar (fM) range [35, 128]. In 2007, Treiber *et al* used RT-SPR (real time surface plasmon resonance) to assess the affinity of the octapeptide repeat for copper and found the Kd to be in the nanomolar range[129].

Regarding the non-octapeptide repeat binding site, a study of Jones *et al.* shown this site bind copper with nanomolar affinity and was higher than affinity of the octapeptide repeat for copper [124]. In 2007, Treiber and collaborators suggested the affinity of the non-octapeptide repeat site was in the mid-micromolar range[129]. Recently, Nadal *et al.* have reported that the Kd, at pH 7.4, for the amyloidogenic region and octarpeptide repeats (multiple His residue binding mode) at ~20 nM, tighter than copper binding to individual octarepeats (100 nM) [130]. Generally, the binding affinity of copper to PrP is around in the nanomolar range, and the non-octapeptide repeat sites have higher binding affinity than the octapeptide region sites.

1.5.2 Copper and the function of PrP^C

Copper and PrP^C expression

Copper can modulate PrP^C expression by reducing PrP^C mRNA, as well as total PrP^C protein [131]. Along with these changes in PrP^C expression, the amount of PrP^C shed into the extracellular media was also significantly increased. This effect of copper on PrP^C was eliminated by co-treatment with a copper chelator termed cuprizone, indicating that these effects required extracellular copper. Another study has shown that the copper additions significantly increased PrP^C levels in neuronal cells [132]. Furthermore, PrP^C expression levels returned to normal when co-treatment with bathocuprionedisulfate (BCS), another copper

chelator. The ability of copper to modulate the PrP^C expression levels suggest a role of copper in the physiological function of PrP^C.

Copper uptake

PrP^C concentrate at presynaptic membranes, where copper ions are also highly localised [133]. The fact that mice devoid of PrP^C harbour 50% lower copper concentrations in synaptosomal fractions than their WT mice suggests that PrP^C plays a role in the regulation of the copper concentration at the synaptic region of the neuron and also in the re-uptake of metal into the presynaptic cleft [134]. Recent studies show that prion protein has a high degree of structural homology with the ZIP family of zinc ion transporters [135] and altered PrP expression perturbs copper metabolism [136]. Furthermore, copper added to cultured neuroblastoma cells promotes the endocytosis of the PrP^C [137, 138]. Hence, it can be hypothesized that the transport of copper from the extracellular to the intracellular compartment is operated through PrP^C internalisation. Alternatively, PrP^C may act as a copper buffer at the synaptic cleft, capturing copper and handling it over to another membrane transporter.

Copper and neuroprotective role of PrP^C

Based on PrP^C localization in synaptic region and its high affinity for copper ions, several research lines suggest that PrP^C is a neuronal metalloenzyme with SOD-like activity, enabling its effective functioning as an antioxidant in the central nervous system [139]. Recombinant PrP as well as immunoprecipitated murine PrP^C have been shown to harbour the activity of a copper/zinc-dependent superoxide dismutase (SOD), endowing PrP^C with antioxidant capacities [140]. Copper has to be present during PrP^C folding for the protein to show SOD activity. In line with these results, the activity of cytosolic SOD has been reported that decreased in the brains of $PrP^{o/o}$ mice [139] but increased in mice that

overexpressing PrP^C [141]. Moreover, SOD activity in brain lysates from WT mice was reduced after PrP^C depletion using anti-PrP^C antibodies [142]. However, other group showed that the direct assays of SOD activity were inconsistent with some measurements identifying weak dismutase function [141] and others found no activity [143, 144]. These authors proposed that PrP^C may have an antioxidant function, but opposed to enzymatic function, in which PrP binds extracellular Cu(II), thus quenching copper's intrinsic redox activity. Although the role of PrP^C as a SOD or as an oxidative stress-reducer is not yet definitive, PrP^C clearly has a neuroprotective role.

In addition, several studies have also shown that PrP^C may protect against excitotoxic stress in neurons. Removing a 20 residues (105 – 125) from the N-terminal domain of PrP (ΔCR PrP) causes mice to develop the degeneration of cerebellar granule neurons, a typical symptom of excitotoxic stress. This effects of ΔCR PrP can be rescued by co-expression of WT PrP [145, 146]. Other studies using $PrP^{o/o}$ mice have revealed that PrP^C expression at synapses exerts neuroprotection by modulating neuronal excitability [64, 147, 148]. Excitotoxicity occurs in $PrP^{o/o}$ mice as aberrant activity of the N-methyl-d-aspartate receptors (NMDAR) that allows entry of Ca(II) ions into the cell causing nerve cell damage and death. Coexpression of WT PrP^C reverses this effect, allowing PrP^C to interact and inhibit the NDMAR, leading to suppress excitotoxicity and PrP^C requires copper for this process [64, 149]. Recently, Gasperini *et al.* showed that PrP^C exerts copper-dependent neuroprotection by inhibiting NMDAR through S-nitrosylation, a post-translational modification resulting from the reaction of nitric oxide (NO) with cysteines [150]. Comparing WT and $PrP^{o/o}$ mice, they found that NMDAR S-nitrosylation decreased in $PrP^{o/o}$ mice and the treatment with copper chelator decreased NMDAR S-nitrosylation in WT but not in $PrP^{o/o}$ mice. Based on these results, they proposed a neuroprotective mechanism of PrP^C, in which PrP^C-bound

copper ions act as electron acceptors in the reaction between NO and NMDAR cysteine thiols. The consequent S-nitrosylation inhibits the NMDAR and reduces the neurotoxic effect caused by its overactivation.

1.5.3 Relationship of prion diseases and copper

Ever since before the theorem of prion, the relationship of prion diseases and copper metabolism has been already proposed and studied. In early 1970s, Pattison and Jebbett have shown that cuprizone, a copper chelator, as the cause of spongiform lesions in the rodent brain that share a similar histopathology of mouse scrapie [151]. Kimberlin and Millson also found that cuprizone could delay or prevent (with very low inoculation titers) the terminal illness in mice affected by scrapie [152], although their results were not completely reproducible. After falling into ignorance for about two decades, since 2000s, the topic on copper-prion diseases came back into hot debate since copper was found to bind PrP^C [125].

On the basis of previous studies that PrP expression level is strongly correlated with the incubation time [53, 78] and is affected by copper [132, 153, 154] a number of authors have proposed the hypotheses about the impacts of copper on prion disease incubation time. Various *in vivo* experiments have been designed to test this hypothesis and resulted in controversial conclusions about the positive or negative role of copper in prion diseases. Some studies showed that copper plays a positive role in prion diseases since supplementing copper prolong the survival time in infected animals [155, 156]. On the contrary, Canello and collaborators, using a chimeric mouse/human model of E200K on Creutzfeldt-Jakob disease, revealed that copper supplementation resulted in disease acceleration [157]. Additionally, Sigurdsson and colleagues found that copper chelation help delays the onset of the disease [158].

On the other hand, copper has been shown to have the capacity to convert PrP into protease-resistant and detergent-insoluble forms but in a different conformation than PrP^{Sc} [159]. A study of Treiber and colleagues on yeast PrP also showed that yeast grown in copper supplemented media contained PK-resistant PrP [160]. This suggests that copper treatment could induce formation of PK-resistant PrP. Similarly, Nishina and collaborators found the capacity of copper to modulate the protease resistance of PrP^{Sc}, showing that the absence of copper renders PrP^{Sc} 20 times more sensitive to PK digestion [161]. Copper also can helps PrP^{Sc} to recover its infectivity and biochemical properties after reversible denaturation by GdnHCl. However, copper inhibits PrP^{C}-PrP^{Sc} conversion in PMCA [162] and formation of fibrils made from recombinant PrP in an amyloid seeding assay (ASA) [163].

In transgenic mice studies, mice expressing PrP without the octapeptide repeats have extended incubation times despite high PrP expression levels [164]. Owen *et al.* showed that the insertion of additional two to nine octapeptide repeats cause familial prion disease in humans [165]. However, the same study proved that the deletion of an octapeptide repeat did not lead to disease [165]. Interestingly, another report showed that an elderly woman with two-octapeptide repeat deletion showed a rapidly progressive dementia consistent with Creutzfeldt-Jakob disease [166].

In conclusion, several studies have been performed with the aim to find a link between copper and PrP^{Sc} formation, with partially contradictory results. These studies clearly support the role of copper with PrP^{C} in prion disease, but it still remains unclear whether the interaction between PrP^{C} and copper facilitates or inhibits prion formation. Therefore, the topic on copper-prion disease relationship remains huge potential for further investigation.

1.6 Aim of study

The conversion of normal form (PrP^{C}) into the infectious form (PrP^{Sc}) is the key event in prion diseases. Althought there have been numerous studies, the mechanism of prion conversion still remains elusive. Pathological point mutations may help to disclose these molecular mechanisms. Most point mutations linked to inherited prion diseases are clustered in C-terminal globular domain, these mutations may affect secondary structure elements and structure flexibility of the globular domain [167-169] and also accelerate the misfolding process *in vitro* [170-172]. Several structural studies on this globular domain proposed a role of the β2-α2 loop as dynamic "switch" that able to modulate the PrP^{C}-PrP^{Sc} conversion [173, 174]. Interestingly, some point mutations located in the unstructured N-terminal domain. These mutations cause the disease without affecting the kinetics of fibril formation *in vitro* [175, 176]. Moreover, there is little evidence for a direct molecular effect of the mutations in the N-terminus on the globular structure of PrP^{C} [169]. This suggests that N-terminal mutations might affects to the PrP^{Sc} fomation in different way, indicating the potential critical impact of N-terminal domain on prion conversion.

The N-terminal domain of PrP has been shown to have high affinity with copper [109, 110] and the copper binding seems to be involved in physiological functions of PrP^{C} [134, 140, 149, 150] as well as in PrP^{Sc} formation and replication [155, 156, 162, 163]. The treatment of the infectious prion with proteinase K cuts PrP^{Sc} at approximately residue 90 but without loss of infectivity, moreover the Tg mice studies also showed the OR copper-binding sites were not essential for prion infectivity [53], suggesting that this region might not play a role in the prion diseases. Meanwhile, the non-OR region may be relevant because of its location. The non-OR region locates in the protease-resistant core of PrP^{Sc} and is adjacent to the hydrophobic region that contained the palindromic motif sequence

AGAAAAGA involving in structural changes during the early stage of prion conversion [177]. In addition, the Tg mice expressing the PrP mutant in which non-OR and hydrophobic region were deleted developed the diseases with cerebral disorders [178, 179]. The interaction of copper with a peptide including the non-OR and palindromic motif also induced β-sheet formation and aggregation of this segment [180, 181]. These observations raised the question whether the non-OR copper-binding site may have an important role in prion conversion. Therefore, my PhD work aims to evaluate the relationship between the non-OR copper binding site and the prion conversion. The major parts of this work are:

- Evaluating the role of copper binding site in OR and non-OR regions on PrP^{C} to PrP^{Sc} conversion using ScN2a cell conversion assay. In addition, we used synchrotron-based X-ray absorption fine structure (XAFS) technique to study the coordination geometries of Cu(II) in H95Y mutant and the pathogenic mutants (P101L and Q211P, in mouse numbering) and we compared these findings with the WT to find the correlation between the copper coordination and the prion conversion.

- Investigating the spontaneously conversion of non-OR mutants that were expressed in $N2aPrP^{-/-}$ cells. The amyloidogenic potential of recombinant non-OR mutants was also analysed by fibrillization assay.

- Investigating the spontaneous generation of prion disease in Tg mice. The Tg mice expressing H95Y mutant were established and analysed the lifespan, behavior, clinical signs and then examined the brain tissue to determine whether they can develope prion diseases.

CHAPTER II

MATERIALS AND METHODS

2.1 Plasmid construction

2.1.1 Primer design

Primers were designed using the Primer Blast (NCBI) and QuikChange Primer Design (Agilent Technologies).

2.1.2 Cloning of MoPrP variants plasmid for cell transfection and protein production

The mutations were inserted into pcDNA::MoPrP(1-254)WT, pcDNA::MoPrP(1-254)WT3F4 or pET::MoPrP(23-230) by using the QuikChange mutagenenis kit (Agilent Technologies) according to manufacturer's instructions.

PCR parameters were as follows: melting temperature: 95 °C for 30 sec; annealing temperature: 55 °C for 45 sec ; extension temperature: 68 °C for 5 min. These three steps were cycled 16 times. Strand extension was completed at 72 °C for 5 min and reactions cooled to 4 °C. 10 ng of template DNA and 2.5 U *PhuUltra* DNA polymerase was used in each reaction. PCR products were digested by DpnI (1 μL per 20 μL PCR reaction for 1 hour at 37 ºC) prior to transformation into XL-1 Blue supercompetent cells.

Table 4. Primers used for producing His to Tyr mutants

Primer	Sequences
H60Y-F	CAGCCCTACGGTGGTGGCTGGGGACAA
H60Y-R	TTGTCCCCAGCCACCACCGTAGGGCTG
H68Y-F	GGGGACAACCCTATGGGGGCAGCTGG
H68Y-R	CCAGCTGCCCCCATAGGGTTGTCCCC
H76Y-F	AGCTGGGGACAACCTTATGGTGGTAGTTGGG
H76Y-R	CCCAACTACCACCATAAGGTTGTCCCCAGCT
H84Y-F	TGGGGTCAGCCCTATGGCGGTGGATGG
H84Y-R	CCATCCACCGCCATAGGGCTGACCCCA
H95Y-F	CAAGGAGGGGGTACCTATAATCAGTGGAACAAGC
H95Y-R	GCTTGTTCCACTGATTATAGGTACCCCCTCCTTG
H110Y-F	AAAAACCAACCTCAAGTATGTGGCAGGGGCTGC
H110Y-R	GCAGCCCCTGCCACATACTTGAGGTTGGTTTTT

Plasmid DNA was purified using the QIAprep Miniprep Kit (Qiagen). All the constructs were verified by sequencing.

The pET11a expressing the full length MoPrP(23-230) were kindly provided by the group of Prof. Jesús Requena (Universidade de Santiago de Compostela, Spain).

Table 5. Primers used for producing H95X mutants

Primer	**Sequences**
H95R-F	CAAGGAGGGGGTACCAGGAATCAGTGGAACAAGC
H95R-R	GCTTGTTCCACTGATTCCTGGTACCCCCTCCTTG
H95KF	CAAGGAGGGGGTACCAAGAATCAGTGGAACAAGC
H95K-R	GCTTGTTCCACTGATTCTTGGTACCCCCTCCTTG
H95D-F	CAAGGAGGGGGTACCGACAATCAGTGGAACAAGC
H95D-R	GCTTGTTCCACTGATTGTCGGTACCCCCTCCTTG
H95E-F	CAAGGAGGGGGTACCGAGAATCAGTGGAACAAGC
H95E-R	GCTTGTTCCACTGATTCTCGGTACCCCCTCCTTG
H95S-F	CAAGGAGGGGGTACCAGCAATCAGTGGAACAAGC
H95S-R	GCTTGTTCCACTGATTGCTGGTACCCCCTCCTTG
H95T-F	CAAGGAGGGGGTACCACCAATCAGTGGAACAAGC
H95T-R	GCTTGTTCCACTGATTGGTGGTACCCCCTCCTTG
H95N-F	CAAGGAGGGGGTACCAACAATCAGTGGAACAAGC
H95N-R	GCTTGTTCCACTGATTGTTGGTACCCCCTCCTTG
H95Q-F	CAAGGAGGGGGTACCCAGAATCAGTGGAACAAGC
H95Q-R	GCTTGTTCCACTGATTCTGGGTACCCCCTCCTTG
H95C-F	CAAGGAGGGGGTACCTGCAATCAGTGGAACAAGC
H95C-R	GCTTGTTCCACTGATTGCAGGTACCCCCTCCTTG
H95G-F	CAAAAACCAACATGAAGGCTATGGCAGGGGCTGCGG
H95G-R	CCGCAGCCCCTGCCATAGCCTTCATGTTGGTTTTTG
H95P-F	CAAGGAGGGGGTACCCCTAATCAGTGGAACAAGC
H95P-R	GCTTGTTCCACTGATTAGGGGTACCCCCTCCTTG
H95A-F	CAAGGAGGGGGTACCGCCAATCAGTGGAACAAGC
H95A-R	GCTTGTTCCACTGATTGGCGGTACCCCCTCCTTG
H95V-F	CAAGGAGGGGGTACCGTGAATCAGTGGAACAAGC
H95V-R	GCTTGTTCCACTGATTCACGGTACCCCCTCCTTG
H95I-F	CAAGGAGGGGGTACCATCAATCAGTGGAACAAGC
H95I-R	GCTTGTTCCACTGATTGATGGTACCCCCTCCTTG

H95L-F	CAAGGAGGGGGTACCCTGAATCAGTGGAACAAGC
H95L-R	GCTTGTTCCACTGATTCAGGGTACCCCCTCCTTG
H95M-F	CAAGGAGGGGGTACCATGAATCAGTGGAACAAGC
H95M-R	GCTTGTTCCACTGATTCATGGTACCCCCTCCTTG
H95F-F	CAAGGAGGGGGTACCTTCAATCAGTGGAACAAGC
H95F-R	GCTTGTTCCACTGATTGAAGGTACCCCCTCCTTG
H95W-F	CAAGGAGGGGGTACCTGGAATCAGTGGAACAAGC
H95W-R	GCTTGTTCCACTGATTCCAGGTACCCCCTCCTTG

2.1.3 Cloning of HuPrP variants plasmid for EXAFS study

P101L and Q211P mutations were inserted into pET::HuPrP(90-231) by using the QuikChange mutagenenis kit (Agilent Technologies) according to manufacturer's instructions. We used the following primers for the mutagenesis:

- P101L-F: 5'-TGG TTT TTG GCT TAC TCA GCT TGT TCC ACT GA-3'

- P101L-R: 5'-TCA GTG GAA CAA GCT GAG TAA GCC AAA AAC CA-3'

- Q211P-F: 5'-CGC GTG GTT GAG CCG ATG TGT ATC ACC C-3'

- Q211P-R: 5'- GGG TGA TAC ACA TCG GCT CAA CCA CGC G-3'

Plasmid DNA was purified using the QIAprep Miniprep Kit (Qiagen). All the constructs were verified by sequencing.

2.1.4 Cloning of full-length MoPrP H95Y plasmid for Tg mice construction

The MoPrP(1-254, H95Y) was amplified from plasmid pcDNA::MoPrP(1-254, H95Y) by PCR using these primer:

- 5'*Bsi*-MoPrP: 5'-CCT AGT GGT ACC TCG TAC GCA GTC ATC ATG GCG AAC CTT GGC TAC TGG-3'

- 3'*Fse*-MoPrP: 5'-CGC TCA CAA TCG CGG CCG GCC TCA TCC CAC GAT CAG GAA GAT GAG G-3'

The PCR products were then inserted into pJB1 (a modified vector from MoPrP.Xho vector[182], in which *Bsi*WI and *Fse*I sites replaced the *Xho*I site) using *Bsi*WI and *Fse*I restriction sites.

The PCR were performed using the Phusion DNA polymerase (New England Biolab) according to manufacturer's instructions. Plasmid DNA was purified using the QIAprep Miniprep Kit (Qiagen). All the constructs were verified by sequencing.

The pJB1 were kindly provided by the group of Prof. Glenn Telling (Colorado State University, USA).

2.2 Cell culture and transfection

Experiments with mouse cell lines were carried out in a tissue culture facility with strict aseptic technique. All solutions and media were pre-warmed to 37 ^{o}C before using.

2.2.1 Cell lines

N2a mouse neuroblastoma cells were purchased from the American Type Tissue Collection (ATCC CCL131).

N2aPrP$^{-/-}$ cells [183] were kindly provided by the group of Dr. Gerold Schmitt-Ulms (University of Toronto, Canada).

ScN2a cells are N2a cells that cronically infected by Rocky Mountain Laboratory (RML) prion strain.

2.2.2 Cell growth

N2a, N2aPrP$^{-/-}$ and ScN2a cells grew in EMEM media (Invitrogen) supplemented with 10 % fetal bovine serum (FBS, Gibco), 1 % non-essential amino acids, 1 % L-glutamax, 1 % penicillin-streptomycin. Cells were incubated at 37 ^{o}C, 5 % CO_2 in a humidified CO_2 incubator. Growth medium was regularly changed 2-

3 times weekly. When cells reached confluence they were harvested or sub-cultured.

Cells were harvested in cold lysis buffer (10 mM TrisHCl pH 8.0, 150 mM NaCl, 0.5 % Nonidet P-40 substitute, 0.5 % sodium deoxycholate). Cell debris was removed by centrifugation at 1000 g for 5 min in a bench microfuge (Eppendorf). An aliquot was taken off for quantification by BCA protein assay kit (Pierce) and the remaining supernatant was stored at -20 ^{o}C until use.

2.2.3 Cell transfections

Cell transfections were performed using X-tremeGENE 9 DNA Transfection Reagent (Roche) according to the manufacturer guidelines.

Plating of the cells has been performed in a volume of 10 mL Opti-MEM complete medium in a 10 cm plate (Falcon) 24 hours before transfection (corresponding to 30 – 40 % confluency). Cells were incubated overnight. The DNA transfection reagent was prepared by mixing 500 µl Opti-MEM (serum-free medium) and 15 µl X-tremeGENE 9 DNA Transfection Reagent. Following a 5 min incubation at RT, 5 µg plasmid DNA were added to the mixture and incubated for a further 30 min at RT. DNA transfection mixture was added to the cells in a dropwise manner. Cells were incubated with DNA transfection mixture for 18 hours at 37 °C, following which fresh medium was added in replacement.

For transient transfections, 72 hours post-transfection, cell lysates were collected for further analysis.

For stable transfections, 48 hours after transfection cells were splitted into fresh medium containing 1mg/mL Geneticin (Invitrogen). The selective medium was changed every 3–4 days until Geneticin-resistant foci could be identified. After that, the stable cell lines were maintained in medium contains 400 µg/mL Geneticin.

2.3 Methods for the detection of proteins

2.3.1 SDS –polyacrylamide gel electrophoresis (SDS-PAGE)

Samples were boiled at 100 °C for 5 min. Then samples were spun at 16,000 x g for 1 min before loading onto 12 % Tris-Glycine gels. Gels were electrophoresed for 100 min at 120 V (or until the dye front ran off at the end of the gel). PageRuler Plus Prestained Protein Ladder (Thermo Scientific) was used as a molecular weight marker.

2.3.2 Coomassie staining of gels

After electrophoresis, gels were stained in 0.02 % Coomassie R-250 (in 50 % methanol, 10 % acetic acid) in 1 hour with gentle agitation. Gels were de-stained using destaining solution (40 % methanol, 10 % acetic acid) for 2-3 hours or until the protein bands were visible without background staining.

2.3.3 Western blot

After electrophoresis, protein was transferred onto Immobilion PVDF membranes (Millipore) at 250 mA for 150 min or 40 V overnight by Criterion Blotter (Biorad). Membranes were blocked with 5 % non-fat milk powder in TBS-T (0.05 % Tween), incubated with 1:1000 anti-PrP 3F4 antibody (Covance), anti-PrP W226 antibody (epitope W144-N152), anti-PrP 6D11 antibody (epitope T94-P104) or anti-PrP 12B2 antibody (epitope W88-G92) and developed by enhanced chemiluminescence (GE Healthcare). Band intensity was acquired using the UVI Soft software (UVITEC, Cambridge).

2.4 Biochemical assays on PrP^{Sc} and PrP^{C}

2.4.1 Protease-K (PK) digestion

For protease-K (PK) digestion assay, quantified protein lysates were treated with PK (Roche) at 37^{o}C. ScN2a cell lysates were digested with 20 µg/mL of PK for 1 hour, while cell lysates from N2a$PrP^{-/-}$ cells were digested with 1, 2, 3 and 4

μg/mL of PK for 10 minutes. The reactions were stopped by adding 2 mM phenylmethyl-sulphonyl fluoride and the samples were centrifuged at 100,000 g for 1 hour at 4 °C (Optima TL, Beckman Coulter, Inc.). The pellets were resuspended in sample buffer and used in immunoblot as described in *section 2.3*. For the non PK digested sample, 25 μg cell lysates of ScN2a were used. Total PrP^{C} expression levels in $N2aPrP^{-/-}$ and ScN2a cell lysates were normalized on β-actin value using 1:10,000 anti-β-actin Peroxidase (Sigma-Aldrich).

To evaluate the role of copper in prion conversion, ScN2a cells were transiently transfected with pcDNA::MoPrP(1-254)WT3F4 and pcDNA::MoPrP(1-254, H95Y)3F4 plasmids, treated for 48 hours with cuprizone (CPZ, Sigma Aldrich) and immediately collected for lyses, PK digestion and immunoblot as described above.

2.4.2 Deglycosylation of proteins using Endo-H or PNGase-F

For glycosidase assay, protein lysates were treated with Endo-H or PNGase-F enzymes (New England Biolabs) according to the manufacturer instructions.

9 μL cell lysate (1-20 μg protein) was denatured with 1 x glycoprotein denaturing buffer (0.5 % sodium dodecylsulfate (SDS), 1 % β-mercaptoethanol) at 95 °C for 5 minutes. After that samples were chilled on ice and centrifuged 10 seconds before incubation with 1500 U of Endo-H or PNGase-F in 1 x G5 or G7 reaction buffer, 1% NP-40 at 37 ^{o}C overnight with vigorous shaking. The reaction was stopped by freezing at -20 ^{o}C.

2.4.3 Solubility assay

Cell lysates containing 50 μg of total protein was adjusted to a final volume of 0.5 mL in lysis buffer containing Complete Protease Inhibitors (Roche). Samples were incubated on ice for 20 min before being centrifuged at 100,000 g, 1 hour, 4 °C. The supernatant was recovered and the pellet resuspended in an equal volume

of 5 % (wt/vol) Sarkosyl buffered with 10 mM Tris, pH 8.0. Samples were then methanol precipitated for further analysis by Western blot.

2.5 Immunofluorescence

2.5.1 Immunofluorescence for the detection of PrP and organelles

Cells were cultured for 1 day in each well of a 24-well plate containing a poly-L-lysine coated coverslip and appropriate culture medium. Medium was removed and cells were washed with 1X PBS. Cells were fixed for 20 min in 4% paraformaldehyde (PFA) in PBS at RT then washed twice for 15 min with 1X PBS. Fixed cells were blocked in 10% FBS, 0.3% Triton X-100 diluted in PBS for 1 hour at RT. After blocking, cells were incubated at 4°C O/N with primary antibody in dilution buffer (1% FBS in PBS with 0.3% Triton X-100). Cells were washed twice with 1X PBS for 15 min. After that, cells were incubated for 1 hour at RT with secondary antibody conjugated with AlexaFluor (1:500; Invitrogen) in dilution buffer. Finally, cells were washed twice for 15min with 1X PBS. The coverslips were taken out and dried naturally. Coverslips were mounted in DAPI and subsequently placed on glass slides and stored at 4ºC. Images were acquired with a DMIR2 confocal microscope equipped with Leica Confocal Software (Leica). Primary antibodies used to detect PrP are D18 mAb for endogenous MoPrPs, and 3F4 mAb for transfected MoPrPs. All organelle markers were purchased from Abcam, as were the ER marker (antiCalnexin), the early endosome marker (anti-EEA1), the recycling endosome (antiTransferrin receptor Tfn), the late endosome marker (anti-Mannose-6 phosphate receptor M6PR) and the lysosome marker (anti-LAMP2).

2.5.2 Surface staining

Cells were placed on ice for 15 min then stained with Opti-MEM containing anti-PrP 3F4 mAb (1:1000) for 20 min. After the fixation, cells were washed with PBS for 3 times to remove residual fixative. Finally, cells were

incubated with fluorescence-conjugated secondary antibody without permeabilization.

2.5.3 Endocytosis imaging

Cells were surface-labeled on ice with anti-PrP 3F4 mAb in Opti-MEM, and returned to 37°C for 1 hour to induce PrP internalization. Later, cells were washed twice with PBS, treated with 0.5% trypsin on ice for 90 sec to remove surface proteins, and fixed for 20 min at RT in 4% PFA. Cells were permeabilized with 0.2% Triton X-100 for 5 min at RT, blocked for 1 hour in 2% FBS in PBS, and stained with AlexaFluor-488 anti-mouse antibody for 1 hour. Finally, coverslips were washed with PBS for 3-4 times and mounted on glass [184].

2.6 X-ray Absorption measurements

Note: All X-ray absorption measurements were performed by the group of Prof. Paola D'Angelo (Department of Chemistry, University of Rome "La Sapienza", Rome, Italy).

2.6.1 Sample preparation

Refolded proteins were concentrated to 1.5-2 mM using Amicon centrifugal cells (Millipore). Samples with 1:1 Cu(II):WT and mutants HuPrP(90-231) ratio were prepared in 25 mM NaOAc pH 5.5 and 25 mM MOPS buffer pH 7.0. The Cu(I):WT and mutants HuPrP(90-231) complexes were generated reducing Cu(II) with 40 mM ascorbate.

2.6.2 X-ray absorption experiments

X-ray absorption spectra were recorded at the European Synchrotron Radiation Facility (ESRF) on beam line BM30B FAME35, under ring conditions of 6.0 GeV and 180 mA. All the spectra were collected at 15 K. The spectra were collected at the Cu K-edges in fluorescence mode using a solid state 30-element Ge detector, with sample orientation at 45° to incident beam. The X-ray photon beam

was vertically focused by a Ni−Pt mirror, and dynamically sagittally focused in the horizontal size. The monochromator was equipped with a Si(111) double crystal, in which the second crystal was elastically bent to a cylindrical cross section. The energy resolution at the Cu K-edge is 0.5 eV. The spectra were calibrated by assigning the first inflection point of the Cu foil spectrum to 8981. All the spectra were collected at 10 K. For the Cu(II) samples photo reduction was observed and thus the beam was moved to different spots of the sample at each scan. During collection, data were continuously monitored in order to insure sample homogenity across the multiple spots and cells. Complete data sets were collected for samples 1 to 14. For each sample, 12 spectra were recorded with a 7 s/point collection statistic and averaged. The collection time was 25 min for each spectrum.

2.6.3 EXAFS data analysis

EXAFS data analysis was performed using the GNXAS code, which is based on the decomposition of the EXAFS signal (defined as the oscillation with respect to the atomic background cross-section normalized to the corresponding K-edge channel cross-section) into a summation over n-body distribution functions $\gamma(n)$, calculated by means of the multiple-scattering (MS) theory36. The analysis of the EXAFS spectra was carried out starting from the coordination model previously determined30. In particular, Cu(II) was found to be coordinated to H95, H110, and two additional low Z ligands (oxygen or nitrogen donors) in the inner shell and to a sulphur-donating ligand, which was assigned to M108. The final fit included also one close oxygen-donating ligand that was assumed to derive from solvent, although it could also be derived from a protein ligand such as a Q97. Based on this model, theoretical EXAFS spectra were calculated to include contributions from first shell two-body signals, and three-atom configurations associated with the His rings. The model $\chi(k)$ signal has been then refined against the experimental data by using a least-squares minimization procedure in which structural and nonstructural

parameters are allowed to float. The structural parameters are bond distance (R) and bond variance (σ2R) for a two-body signal, the two shorter bond distances, the intervening angle (θ), and the six covariance matrix elements for a three-body signal. During the minimization procedures, the magnitudes of the Debye−Waller terms for the imidazole rings were assumed to increase with distance, and imidazole ring atoms at similar distances from the copper ion were assigned the same value. The EXAFS spectra of Cu(II)-HuPrP(90-231, H95Y or P101L or Q211P) and Cu(I)-HuPrP(90-231, H95Y or P101L or Q211P) were analyzed trying out different possible models including either one or two histidine ligands and a sulfur coordinating atom. In all cases two additional nonstructural parameters were minimized, namely E_0 (core ionization threshold) and S_0^2 (many body amplitude reduction factor). The quality of the fits was determined by the goodness-of-fit parameters, R_i [185], and by careful inspection of the EXAFS residuals and their Fourier Transforms.

2.7 Preparation of PrP^{Sc} or PrP^{res} seed by sodium phosphotungstic acid (PTA)

1 mg of ScN2a or N2a$PrP^{-/-}$ cell lysate was used for PTA precipitation by adding 500 μL of PBS containing 4 % sarkosyl, complete protease inhibitor (Roche) and 0.5 % PTA, with constant shaking 350 rpm, at 37 °C for 1 hour and centrifuged 14,000 g for 30 min at RT. The pellet was washed with 500 μL of PBS/2% Sarkosyl/protease inhibitor and then centrifuged the pellet again at 14,000 × g for 30 min at RT. After that, the pellet was resuspended in 150 μL of sterile distilled water and stored at −80 °C until use.

2.8 Protein misfolding cyclic amplification (PMCA)

Brains from wild type mice were harvested after perfusion, and 10 % homogenate was prepared in conversion buffer (1 % Triton-X100, 5 mM EDTA,

and 150 mM NaCl in PBS pH 7.2) with the addition of Complete Protease Inhibitors (Roche), divided in single-experiment aliquots and keep at –80 ºC.

Sample were mixed with substrate and subjected to 96 cycles of PMCA with the use of a microsonicator (model Q700, Qsonica). Each cycle consisted of 29 minutes 30 seconds of incubation at 37 °C, followed by a 30-second pulse of sonication set at a potency of 250 W. After one round, an aliquot of the amplified material was diluted 1:10 into fresh brain homogenate, mixed well and performed an additional round of PMCA cycles.

Amplified samples were treated with 100 μg/mL proteinase K at 37 °C for 1 hour with shaking. The reaction was stopped by SDS-PAGE sample buffer, and samples were loaded into SDS-PAGE followed by immunobloting as previously described in *section 2.3*.

2.9 Preparation of recombinant proteins

2.9.1 Protein expression

All recombinant MoPrP and HuPrP variants in this study were expressed and produced in LB medium (10 g trypton, 5 g yeast extract, 10 g NaCl) according to the following protocol: freshly transformed 100 mL overnight culture of *E. coli* BL21 (DE3) cells was added to 2 L of LB medium plus ampicillin (100 μg/mL) in a Biostat B plus 2 L bioreactor (Sartorius) which allows for an automated control of pH, temperature and pO2. The expression was induced at 0.8 OD_{600} with 1 mM IPTG. The cells were harvested 12 hours after induction by centrifugation at 4000 g, 4 °C for 30 min.

2.9.2 Isolation of inclusion bodies

Bacteria pellet was resuspended in 25 mM Tris-HCl, 5 mM EDTA, 0.8 % TritonX-100, 0.4 % Deoxycholic acid, 1 mM PMSF, pH 8 and lysed by Panda plus homogenizer at 4 ºC. Bacteria cells were disrupted by three cycles of mechanical

lysis at 1500 bar. Inclusion bodies (IBs) were collect by centrifugation at 10,000 g, 30 min, 4 °C, washed one time with washing buffer (25 mM Tris-HCl, 5 mM EDTA, 0.8 % Triton-X100, pH 8), and then with cold water two times. Washed IBs were solubilized in 5 volumes of 8 M GndHCl, and then removed bacterial debris by centrifugation at 10,000 g, 30 min, 4 °C.

2.9.3 Protein purification

The dissolved IBs in 8 M GndHCl were diluted to 6 M GndHCl using 50 mM Tris, 1 M NaCl, pH 8.0 then loaded onto a 5 mL HisTrap crude column (GE Healthcare) in binding buffer (2 M GndHCl, 500 mM NaCl, 20 mM Tris, 20 mM imidazole, pH 8.0). After that, the column was washed with 3 column volume (CV) of binding buffer and eluted with a gradient from 0-100 % of elution buffer (5 M GndHCl, 500 mM NaCl, 20 mM Tris, 500 mM imidazole, pH 8.0) at 5 mL/min in 20 min. Finally, the PrP-contained fractions were loaded onto gel filtration column (Superdex 200 26/60, GE) and eluted with 6 M GndHCl, 25 mM Tris-HCl, 5 mM EDTA, pH 8 at a flow rate of 2 mL/min. Purified protein was analyzed by SDS-PAGE. Protein concentration was determined by UV at 280 nm and stored at −80 °C before use.

2.9.4 Protein refolding

Purified prion proteins were rapidly diluted to a final concentration of 0.1 mg/mL using 25 mM Tris, 5 mM EDTA, pH 8.0. Then the samples were dialyzed against refolding buffer (20 mM NaOAc, 0.005% NaN3, pH 5.5) using a 3 kDa molecular weight cut-off (MWCO) membrane (Spectra/Por), until a final GndHCl concentration of about 10 µM.

2.10 Monitoring the kinetics of *in vitro* amyloid formation

To monitor the formation of amyloid fibrils in our samples, we use a protocol adapted from Colby et al. [186]. The refolded prion protein was prepared to 2X

stock solution by dilution buffer (4 M GndHCl in PBS pH 7.0) to concentration of 200 μg/mL protein and 2 M GndHCl. Then stock solution was dilution two times in PBS pH 7.0, 2 M GndHCl, 20 μM ThT. For seeding experiments, 4 μL resuspended PTA pellet was diluted into 400 μL of water and 20 μL of the diluted sample was added to each well.

The fibrillization reaction was performed in a final volume of 200 μL in 96-well plate (BD Falcon) and each well was added one 3-mm glass bead (Sigma-Aldrich) for increasing agitation. The plate was continuous shaking at 37 ^{o}C on a plate reader (Spectramax M5, Molecular Device). The kinetics of fibril formation was monitored by reading fluorescence intensity every 10 min at 444 nm excitation and 485 nm emission. The lag phase was estimated based on 10 % of the ThT fluorescence increasing.

2.11 Generation and detection of transgenic mice

MoPrP mutant transgenes (H95Y or H95.110Y) containing mouse regulatory sequences were excised from the plasmid pJB::MoPrP(1-254, H95Y) by using the restriction endonuclease *Not*I. These fragments were then microinjected into the pronucleus of 200 fertilized FVB mice eggs, which were implanted into pseudopregnant FVB females. This work was done at the transgenic mouse facility of Cyagen Biosciences Inc (USA).

DNA was prepared from tail of F0 offspring mice was used to screen for transgene integration by a PCR assay using specific primers. The primers used were 5′-GAA CTG AAC CAT TTC AAC CGA G-3′ and 5′-AGA GCT ACA GGT GGA TAA CC-3′. The presence of PCR-amplified products of 800 bp indicated the presence of MoPrP mutant transgenes. Transgenic F0 mice were crossed with WT mice to obtain an F1 generation that was also screened using PCR amplification as above. Homozygous transgenic lines were established in two steps. Founders were

backcrossed to homozygous null animals MoPrP$^{-/-}$ (*Prnp*$^{-/-}$) to obtain homozygosity for the null mutation. Interbreeding within the same transgenic line yielded homozygosity for the MoPrP mutant constructs. These work with transgenic mice were performed in collaboration with the group of Prof. Juan-María Torres at Centro de Investigación en Sanidad Animal (CISA-INIA), Madrid, Spain.

2.12 PK immunoblot analysis of mouse brain homogenates

10 % (wt/vol) brain homogenates from frozen tissues were prepared in lysis buffer (100 mM sodium chloride, 10 mM EDTA, 0.5 % Nonidet P40, 0.5 % sodium deoxycholate in 10 mM Tris-HCl, pH 7.4). Aliquots of cleared lysate equivalent to 100 µg were digested with 50 µg/mL of PK for 1 hour at 37 °C. Reactions were terminated by the addition of phenylmethanesulfonyl fluoride (PMSF, 5 mM). Treated homogenates were analysed by immunoblot using anti-PrP 12B2 antibody.

2.13 Cell viability

Cells were seeded in a 96-well tissue culture plate one day before transfection and then transiently transfected with MoPrP constructs. Seventy-two hours after the transfection, the medium was removed and the cells were incubated with 200 µL of MTT (Sigma) working solution (5 mg/mL of MTT in sterile PBS) for 4 hours at 37 °C. Cell viability was assessed by the conversion of MTT (yellow) to a formazan product (purple). The solution was removed and formazan products were dissolved by adding 200 µL of DMSO to each well. The optical density was read at 570 nm and the background subtracted at 690 nm using a VersaMax plate reader (Molecular Device). Each assay was performed in duplication of 4 wells.

2.14 Statistical analysis

Data were expressed as mean plus standard error of mean (SEM; sd√n). Data were compared by 2-tailed t-tests and considered significantly different when

$P<0.05$. Degree of significance was expressed as follows: $P<0.05$*; $P<0.01$**; $P<0.001$***, unless otherwise specified.

CHAPTER III

RESULTS

3.1 Role of fifth copper binding site in prion conversion

3.1.1 The non-OR H95Y mutation promotes prion conversion

Expression of exogenous PrP in a prion-infected mouse neuroblastoma (ScN2a) cell results in its conversion to PrP^{Sc}, so it is a useful tool to study prion conversion. In this study, we engineered the MoPrP constructs to include the human-specific 3F4 epitope (Met substitutions at residues 108 and 111), known not to interfere with the conversion process (Figure S1) and allow distinguishing exogenous MoPrP from endogenous MoPrP [103, 187, 188]. To investigate the role of copper binding sites of prion protein, we created MoPrP mutants in which single His residues along the entire N-terminal domain were replaced by Tyr (denoted as H60Y, H68Y, H76Y, H84Y and H95Y mutations). The His residue 110 was not considered in this experiment because it is located inside the 3F4 epitope, so replacing His110 would destroy the epitope and the anti-PrP 3F4 mAb cannot recognize mutants (Figure S3).

The substitution of histidine by tyrosine in MoPrP constructs were not toxic for cells (Figure S2) and also did not affect PrP expression as all constructs shared a similar PrP expression level (Figure 13). Meanwhile the PK-resistant profiles displayed interesting results. When a histidine in the OR was replaced by tyrosine, it had no significant effect on prion conversion, and all OR mutants (H60Y, H68Y, H76Y, H84Y) displayed the same PK-resistant PrP^{Sc} levels as WT. Conversely, the non-OR mutant (H95Y) yielded in significantly higher PrP^{Sc}, around 3 times more than the others (Figure 13), providing the first evidence for the role of this mutation in prion replication.

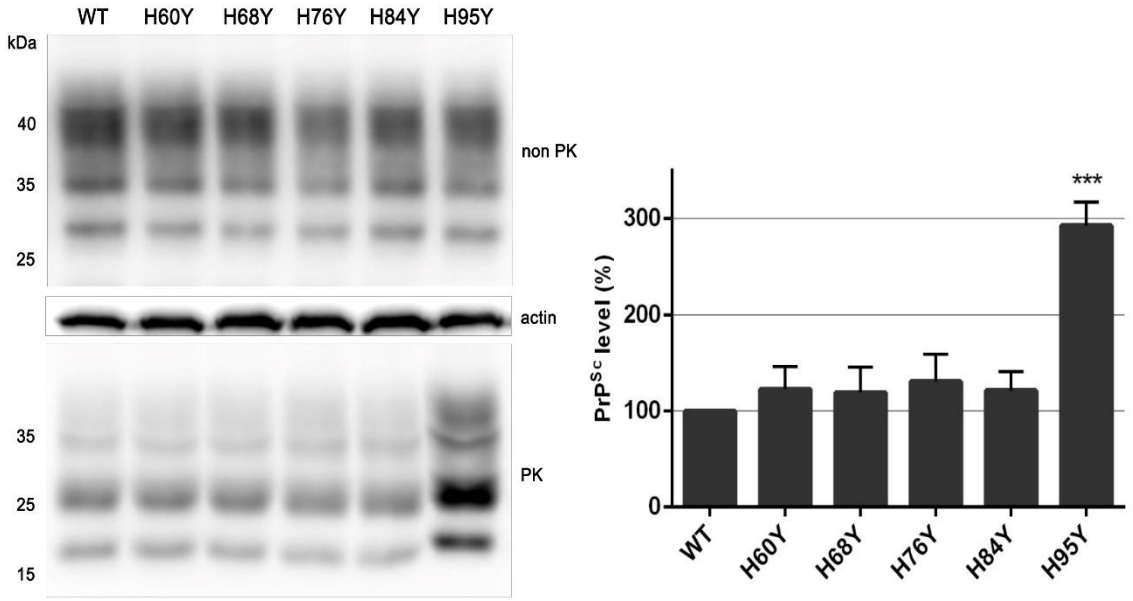

Figure 13. The non-OR H95Y mutation promotes prion conversion. (A) For non-PK experiment, 50 μg of undigested lysates was applied to each lane; β-actin was used as internal control. For PK experiment, 500 μg of cell lysate was digested with PK (20 μg/mL) at 37°C for 1 hour. PrPs were detected by anti-PrP 3F4 mAb. (C) Quantitative analysis of PK-resistance levels (PrP^{Sc}) in transfected constructs. (n = 4, ***p< 0.001).

3.1.2 Cuprizone removal of copper increased level of PrP^{Sc} in MoPrP WT but not in H95Y

Because H95 binds copper, it is likely that the removal of this copper ligand might accelerate prion replication in ScN2a cells. Therefore, the absence of copper from the non-OR region could promote this pathological process. To verify this hypothesis, we treated ScN2a cells transfected either with WT or H95Y with cuprizone (CPZ), a well-known selective Cu(II) chelator that does not affect cell viability and cannot cross plasma membranes [189]. After 48 hours of CPZ treatment, PK-resistance levels were evaluated.

CPZ treatments on WT ScN2a cells promoted a significant increase in PrP^{Sc}-PK resistance levels upon 10μM CPZ additions, suggesting that PrP^{C} in the apo form is more susceptible to PrP^{Sc} conversion (Figure 14). The PrP^{Sc} levels remained

a plateau among control and CPZ-treated H95Y ScN2a cells but always higher than PrP^{Sc} level in the WT cells as presented previously. These data were consistent with the hypothesized mechanism whereby H95Y mutant was per se sufficient to generate high amount of PrP^{Sc} molecules. Copper appeared as a pivotal modulator of this process since its absence from PrP^{C} seemed to promote prion conversion.

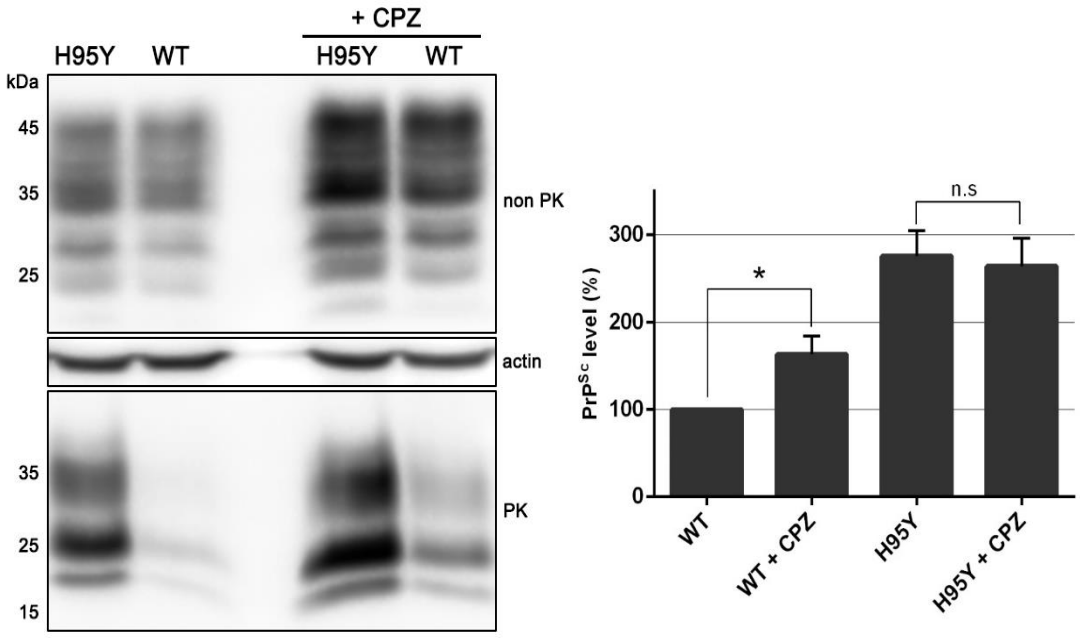

Figure 14. Cuprizone removal of copper increased level of PrP^{Sc} in MoPrP WT but not in H95Y. (A) After transfection, ScN2a cells were treated for 48 hours with cuprizone (CPZ) and collected for PK digestion assay. For non-PK experiment, 50 µg of undigested lysates was applied to each lane. For PK experiment, 500 µg of cell lysates was digested with PK (20 µg/mL) at 37°C for 1 hour. MoPrPs were detected by anti-PrP 3F4 antibody. (B) Quantitative analysis of PrP^{Sc} PK-resistance levels in WT and H95Y MoPrP transfected ScN2a cells treated with 10 µM CPZ (n = 3, **P*< 0.05, n.s: non-significant)

3.1.3 Localization and trafficking of H95Y mutant in N2a cell

PrP WT and H95Y mutant were expressed in N2a cells and selectively visualized by immunofluoresence with the 3F4 mAb. The 3F4-tagged WT and H95Y PrPs were found predominantly on the cell surface, with some intracellular punctated deposits in perinuclear region. The distribution of WT and mutant PrPs found in this study is similar to previous reports [190, 191] (Figure 15).

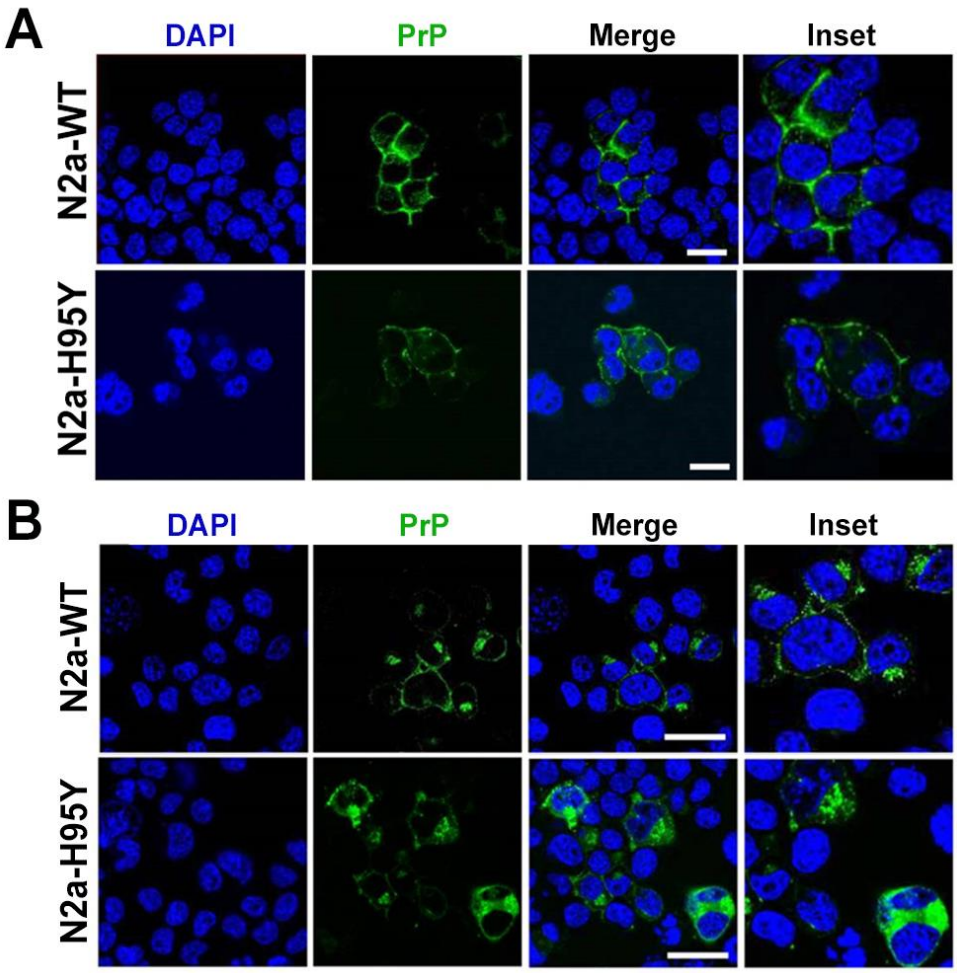

Figure 15. H95Y mutant is predominantly expressed on cell surface as wild-type PrP^C. (A) Cell surface staining. PrPs on cell surface were detected by anti-PrP 3F4 mAb without permeabilization. **(B)** Combined cell surface and intracellular staining. PrPs were detected by anti-PrP 3F4 mAb with permeabilization. Insets represent magnifications of some cells in the merge images. Blue fluorescence for nucleus, green fluorescence for PrP. Scale bars: 24 μm.

PrP^C is trafficked through the secretory pathway to the cell surface, but not all PrP^C remain on the cell surface after their delivery there. PrP^C has been demonstrated that it is rapidly and constitutively endocytosed by the endosomal system [40] and copper has been previously implicated in the endocytic trafficking of PrP^C [137, 192]. Therefore, we investigated whether the alteration of copper binding of PrP by removing H95 may have an effect on the endocytosis. For this purpose, cells were surface-labeled on ice with anti-PrP 3F4 mAb and returned to

37 °C to induce PrP internalization. After that the extracellular PrP^C were removed by trypsin, so only endocytosed PrPs were detected. We observed that both PrP WT and H95Y exhibited intracellular fluorescence signals corresponding to endocytosed PrPs, indicating that H95Y was efficiently efficiently endocytosed as WT (Figure 16). We concluded that replacing of histidine by tyrosine at His95 do not impair PrP^C internalization from cell surface.

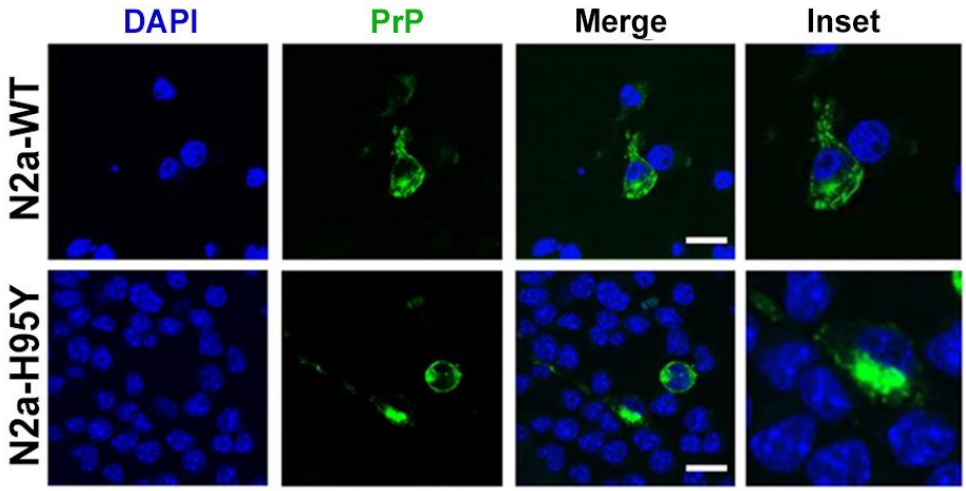

Figure 16. Substitution of histidine by tyrosine at H95 does not impair PrP endocytosis. Cells were surface-labeled on ice with anti-PrP 3F4 mAb and returned to 37 °C to induce PrP internalization. Only endocytosed PrPs were detected after removing surface proteins by trypsin. Insets show magnifications of cells in the merge images. Blue fluorescence for nucleus, green fluorescence for PrP. Scale bars: 24 µm.

To further investigate the sub-cellular localization and trafficking of PrP^C, we analyzed the localization patterns of 3F4-tagged WT and H95Y mutant with some organelle markers. The results showed that most PrP^C WT is found on cell surface, while there is a small portion in the endosomes and lysosomes (Figure 17A). These results are consistent with those obtained from previous studies that analyzed the localization of WT PrP^C in different cell lines [193, 194]. In cells expressing the H95Y mutant, PrP^C is still mainly expressed on cell surface. In addition, a smaller fraction of H95Y mutant was found in the late endosomes and lysosomes as PrP WT. However, a significant population of intracellular H95Y

mutant showed co-localization with EEA1 (an early endosome marker) and Tfn (a recycling endosome marker), suggesting an accumulation of H95Y mutant in early and recycling endosomes (Figure 17B).

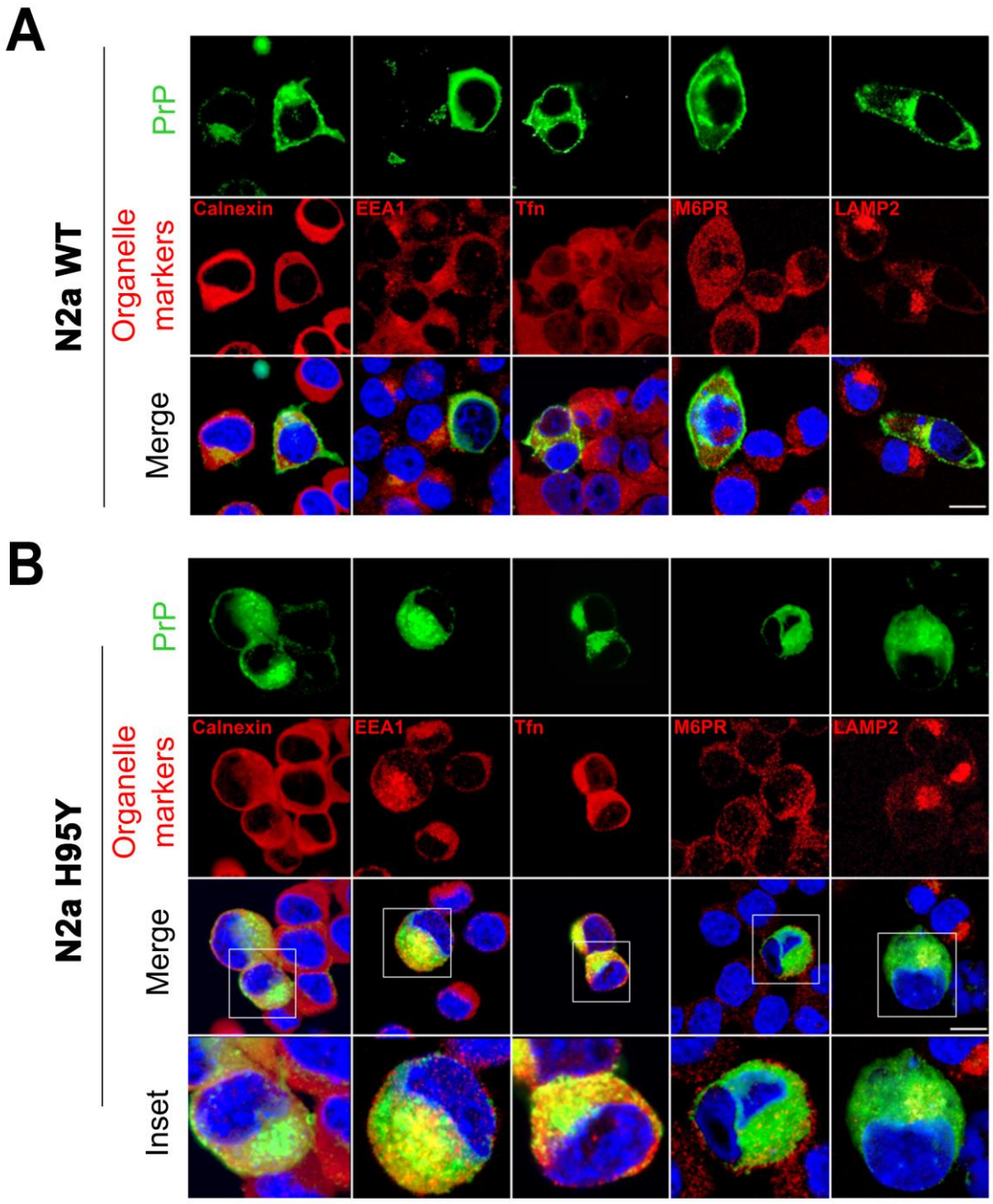

Figure 17. The H95Y mutant displays intracellular accumulation in early and recycling endosomes. PrP localization in N2a cells expressing the MoPrP WT (A) or the MoPrP H95Y (B). Nuclei are labeled with DAPI (blue), PrPs are detected by 3F4 antibody (green), while organelle markers, as Calnexin (ER marker), EEA1

(early endosomes marker), Tfn (recycling endosomes marker), M6PR (late endosomes marker) and LAMP2 (lysosomes marker), are labeled in red. Insets show a magnification of the merged panels (white boxed areas). Scale bars: 12 µm.

Endosomal compartments have been known as acidic compartments [195-197]. This acidic pH has been suggested as a critical condition for changes in PrP conformation [198]. Previous studies have shown that the transition of PrP from its native state to soluble oligomers is a pH-dependent process [199] and the acidic conditions is favor for the existence of soluble PrP oligomers [200]. Additionally, various studies demonstrated that PrP^{Sc} is detected throughout endosomal compartments, being particularly abundant in recycling endosome and the endosomal recycling compartment was identified as the likely site of prion conversion [201, 202]. Therefore, the accumulation of H95Y mutant in early and recycling endosomes, a proposed suitable environment for PrP^{Sc} formation might be an appropriate explanation for promotion effect on prion conversion of H95Y mutant.

3.1.4 Effect of the H95Y mutation on the copper coordination

In order to have more insight into the effect of H95Y mutation, we investigated the copper coordination in non-OR region of this mutant. High resolution techniques, as NMR or X-ray spectroscopy, are not able to detect any structural information in this region due to its intrinsic flexibility. Then we used the synchrotron-based X-ray absorption fine structure (XAFS) technique to study the coordination geometries of copper in H95Y mutant. In addition, we also analysed the copper binding in non-OR region of pathological mutations in the globular domain (Q211P, in mouse numbering) and in the N-terminal unstructured region (P101L, in mouse numbering). To have better comparision with these pathogenic mutation, truncated HuPrP(90-231) variants which are devoid of the OR were used in these experiments.

Copper coordination in the non-OR region of WT HuPrP

At pH 5.5, EXAFS spectra of Cu(II)- and Cu(I)-HuPrP(90-231) are almost identical, indicating that the coordination environment of copper in HuPrP(90-231) is the same despite its oxidation state. Quantitative analysis of the EXAFS spectra indicated that in both oxidation states, copper ion is coordinated by two His residues (H95 and H110, in mouse numbering) with Cu-N distance of 1.98 Å, by two low Z ligands (either oxygen or nitrogen atoms at 1.98 Å) and by one sulphur scatterer at longer distance (*i.e.* 3.25 Å) (Figure 18).

While at pH 5.5 the EXAFS spectra are almost identical for both copper oxidation states, at pH 7.0 EXAFS signals show markedly different features over the full k-range. The quantitative analysis of the EXAFS data indicates that at pH 7.0 only a single His coordinates the metal ion in both oxidation states, thus suggesting that one of the two His residues (H95 or H110) moves away from the metal. EXAFS data concerning Cu(II)-HuPrP(90-231) at pH 7.0 could be modeled as a four coordinate copper center with one His at 1.99 Å, and three N/O scatterers at 1.99 Å with a more distant sulphur scatterers at 3.47 Å. As far as the Cu(I)-HuPrP(90-231) protein is concerned, the EXAFS analysis revealed a three-fold coordination with one His at 1.98 Å, one N/O scatterers at 2.00 Å and one sulphur scatterer at 2.27 Å (Figure 18).

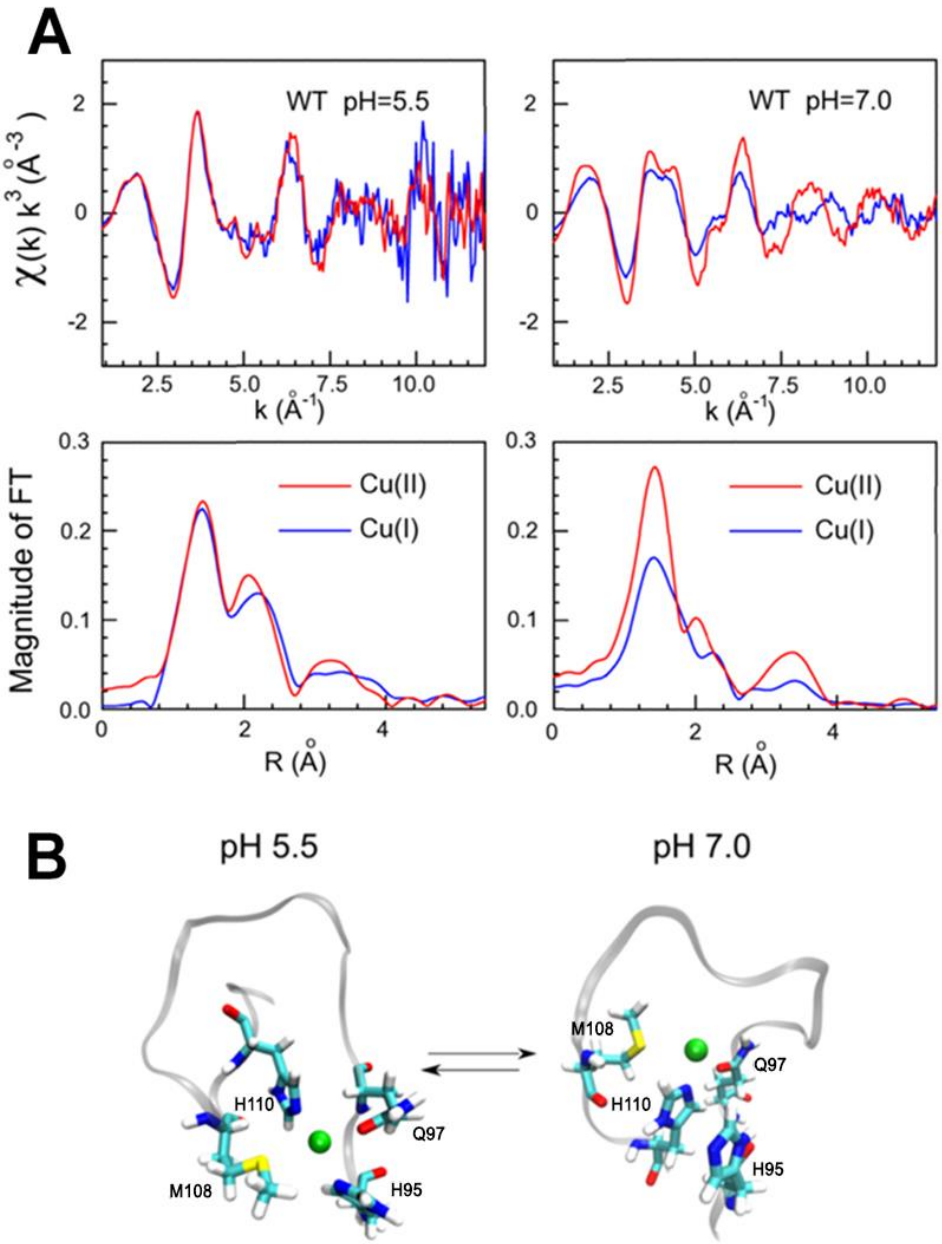

Figure 18. Copper coordination in the non-OR region of HuPrP WT. (A) k3-weighted EXAFS spectra and Fourier transforms of the experimental data of Cu(II) and Cu(I) bound to HuPrP(90-231) WT at pH 5.5 and 7.0. (B) Schematic representations of copper binding sites in HuPrP(90-231) WT

Copper coordination in H95Y mutant

At pH 5.5, the Cu K-edge EXAFS data for H95Y, compared to the WT protein, exhibited a clear modification in the coordination environment. This variation is explained by the existence of a single His in the non-OR region of the

H95Y mutant, hampering the coordination of the Cu(II) ion with two His residues (Figure 19). Conversely, at pH 7.0 the EXAFS spectra of the H95Y mutant and WT proteins are almost identical, thus suggesting that H110 is involved in the copper binding site in both cases. In addition, the EXAFS data showed that the H95Y mutant maintains the same coordination environment around the Cu(II) ion when increasing pH from 5.5 to 7.0. The analysis of the EXAFS data revealed the presence of a four coordinate copper center almost identical to that of the WT protein at pH 7.0, with the H110 residue at 2.00 Å from the ion. In sum, the copper coordination of H95Y mutant is independently of the pH and similar to copper coordination of WT at pH 7.0. Interestingly, the pathogenic mutants, HuPrP Q211P and P101L, shared the same coordination pattern as H95Y mutants at both pH 5.5 and 7.0 (Figure S4).

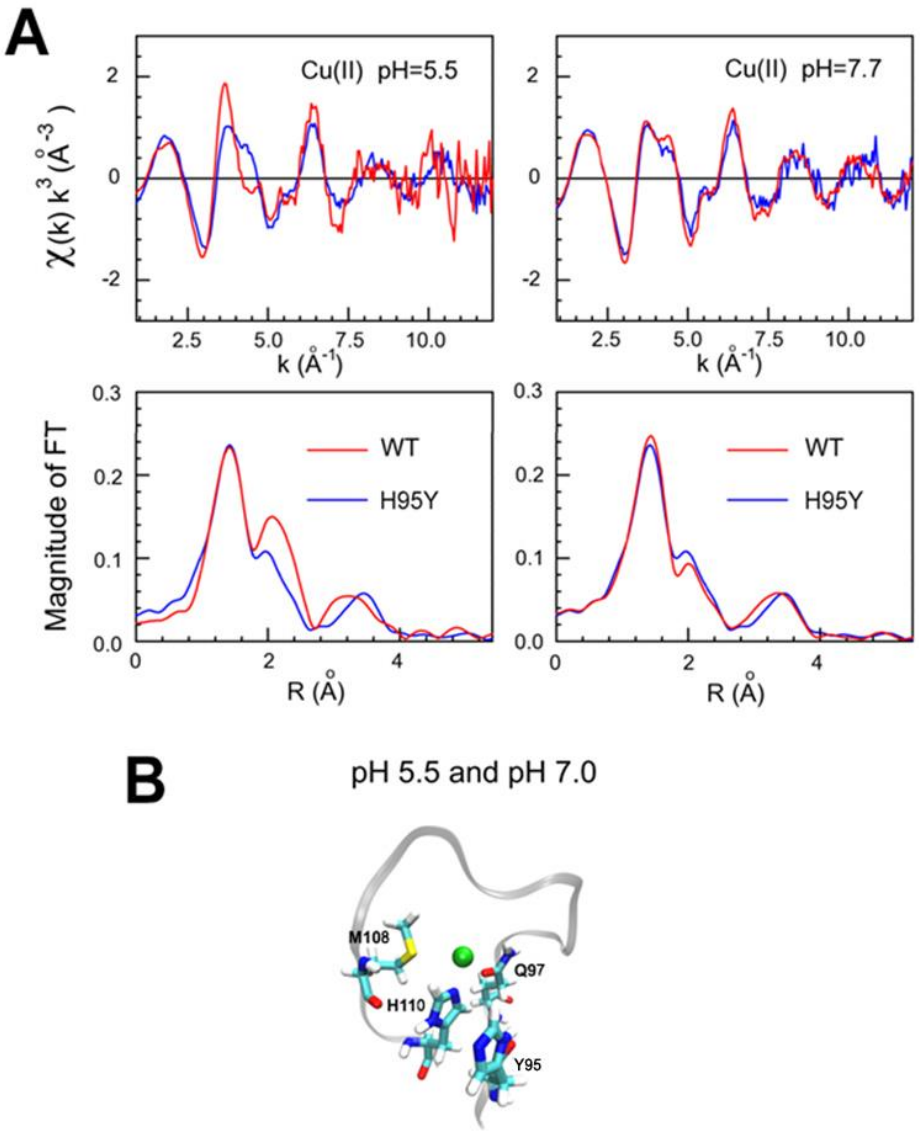

Figure 19. Copper coordination in the non-OR region of HuPrP H95Y. (A) k3-weighted EXAFS spectra and Fourier transforms of the experimental data of Cu(II) bound to HuPrP(90-231) WT and H95Y at pH 5.5 and 7.0. **(B)** Schematic representations of copper binding sites in HuPrP(90-231) H95Y.

3.1.5 Amino acid scanning reveals H95 as a "hot spot" for prion conversion

In order to investigate further the potential role of the fifth copper-binding site in prion conversion, we created the amino acid scanning at H95, in which all possible amino acid substitutions were introduced. Then the influence of this substitution on the conversion efficiency was evaluated based on PK-digestion assay in ScN2a cells.

Western blot analysis of ScN2a cells transfected with H95X (where X means any amino acids) mutants revealed a very interesting result. The expression level of H95X mutants was almost equal to that of WT, but the PK-resistant level showed large variation. When H95 was replaced by neutral or small amino acid (A, G, C, S, T, N, Q, P), the PrP^{Sc} level was almost similar to WT. Remarkably, in the case of hydrophobic amino acid substitutions (F, Y, L, M, V, W, I), the prion conversion was highly promoted featuring high PrP^{Sc} level in ScN2a cells when transfected with these mutants. In some case, such as F, V, I, the PrP^{Sc} level were 2-3 times higher than WT. Meanwhile, only a small amount of PrP^{Sc} was detected in the mutants with charged amino acid residues (D, E, R, K) at H95, suggesting that prion replication was inhibited by the presence of these mutations at codon 95. These data showed that the hydrophobicity of amino acid at H95 might have an impact on PrP^{C}-PrP^{Sc} conversion. Therefore, the fifth copper-binding site represents a "hot spot" for prion conversion, because by changing the amino acid at this position, the prion conversion process could be promoted or inhibited.

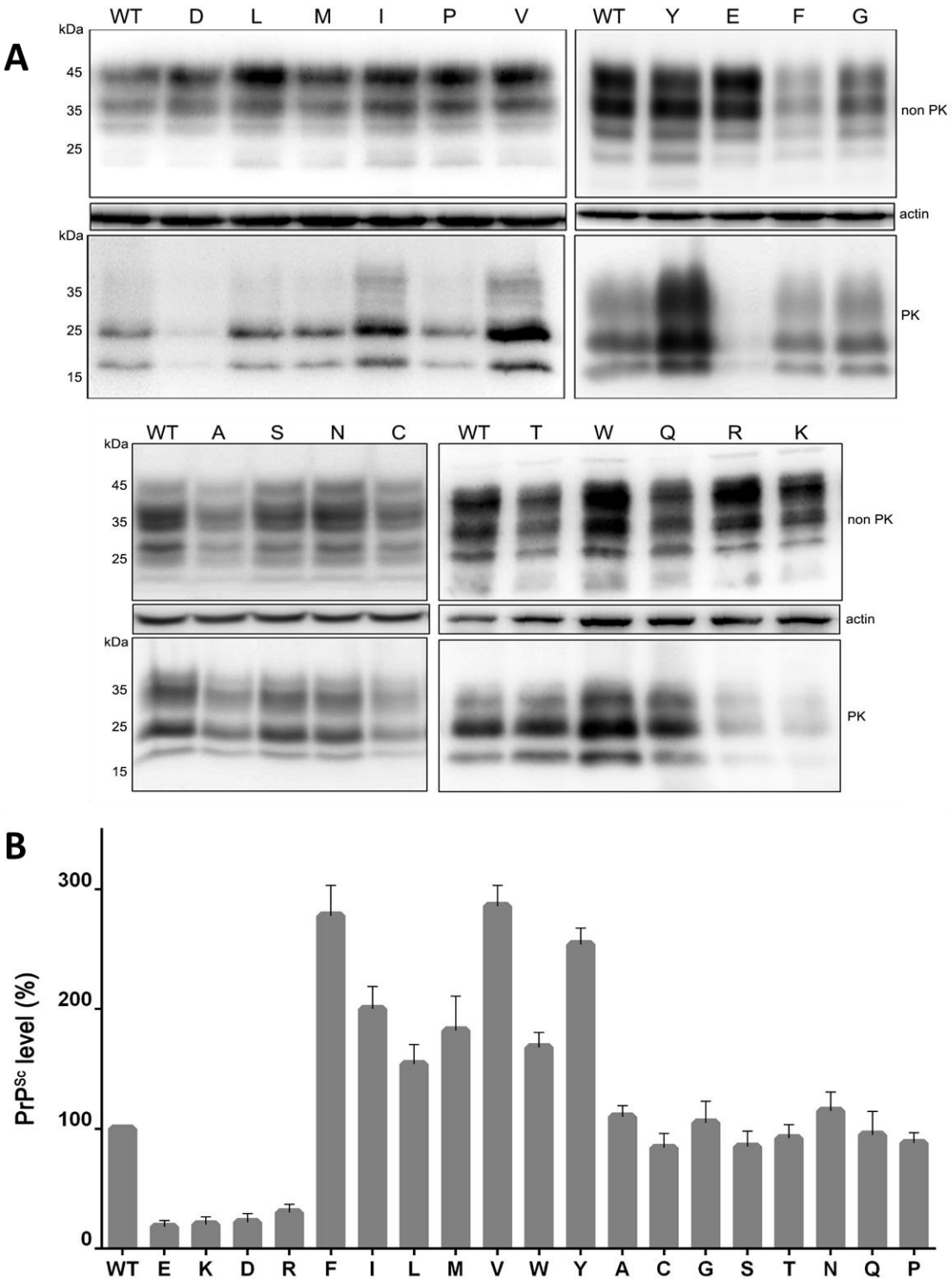

Figure 20. Effects of amino acid substitutions at His95 to prion conversion process. (A) For non-PK experiment, 50 μg of undigested lysate was applied to each lane, β-actin was used as internal control. For PK experiment, 500 μg of cell lysates was digested with PK (20 μg/mL) at 37°C for 1 hour. PrPs were detected by anti-PrP 3F4 mAb. (C) Quantitative analysis of PK-resistance levels (PrP^{Sc}) in transfected constructs.

3.2 Non-OR mutants induce *de novo* generation of prions *in vitro*

3.2.1 Generation of stable N2aPrP$^{-/-}$ cells expressing PrP WT and non-OR mutants

As mentioned before, when replacing histidine by tyrosine at Histidine 110 residues, we altered the 3F4 epitope (Figure S3), therefore we could not use the ScN2a cells system for experiments with mutations at H110. In addition, to avoid any possible influence of endogenous PrP^{C} on the *de novo* generation of prions, we used the N2aPrP$^{-/-}$ cells that did not express PrP (Figure 21), that were subsequently stably transfected with WT or non-OR mutants PrPs. Plasmids pcDNA::MoPrP(1-254), pcDNA::MoPrP(1-254, H95Y), pcDNA::MoPrP(1-254, H110Y) and pcDNA::MoPrP(1-254, H95Y/H110Y) were used for transfection of N2aPrP$^{-/-}$ cells. Following selection, we obtained Geneticin-resistant N2aPrP$^{-/-}$ cells indicating the integration of plasmid DNA into genomic DNA so selected cells had the ability to constitutively express the PrP gene. To determine whether PrP^{C} was stably expressed at the protein level, western blot was performed. The clones which had positive signal were selected and designated N2aPrP$^{-/-}$-WT, N2aPrP$^{-/-}$-H95Y, N2aPrP$^{-/-}$-H110Y and N2aPrP$^{-/-}$-H95Y/H110Y (Figure 21).

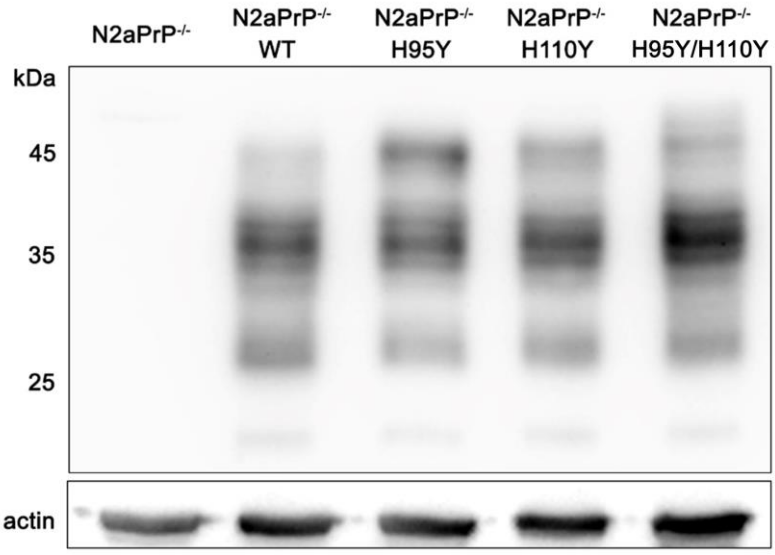

Figure 21. Expression of PrP^{C} in N2aPrP$^{-/-}$ constructs. Fifty μg of cell lysate was applied to each lane. PrPs were detected with anti-PrP W226 mAb.

3.2.2 The non-OR mutants share similar glycosylation patterns and proteolytic features as WT PrP^C

PrP^C is synthesized in the endoplasmic reticulum (ER). During biogenesis, PrP^C is co-translationally directed into the secretory pathway to reach the cell surface. The maturation of PrP^C is achieved by the attachment of two N-linked complex carbohydrate moieties, the disulfide bond formation and the addition of a GPI anchor at its C-terminus. To elucidate whether the mutants could alter cellular maturation processes, we analysed the glycosylation patterns and proteolytic features of PrP mutants.

First, the expression of PrP^C was analysed by immunoblot (Figure 22A), which demonstrated that, like WT, the H95Y, H110Y and H95Y/H110Y mutant PrP^C had similar glycosylation patterns with three bands corresponding to the diglycosylated, monoglycosylated and unglycosylated PrP^C forms. This result indicated that non-OR mutations PrPs did not affect the glycosylation of PrP^C.

After that, we performed the deglycosylation assays using Endo-H and PNGase-F. Endo-H is a highly specific endoglycosidase, which cleaves asparagine-linked mannose rich oligosaccharides, but not highly processed complex oligosaccharides from glycoproteins. Therefore, Endo-H is used to monitor posttranslational modification in the Golgi apparatus. Because glycoproteins acquire Endo-H resistance upon transport to the Golgi compartments, Endo-H sensitivity is considered a sign of protein immaturity [203]. Meanwhile, PNGase-F is able to remove most N-glycans and used to detect glycoproteins.

Immunoblotting of all MoPrP constructs treated with Endo-H showed no difference between WT and mutated PrP glycoforms (Figure 22C). The treatments with the PNGase-F also displayed the same patterns between constructs with a clearly band at molecular weight of about 25 kDa, which was identical to unglycosylated PrP^C (Figure 17B). Meanwhile, bands with higher molecular weight

(35-45 kDa) corresponding to mono and diglycosylated PrP^C were undetected. Taken together, these data suggested that these mutant proteins were successfully processed through ER and Golgi compartments during their maturation.

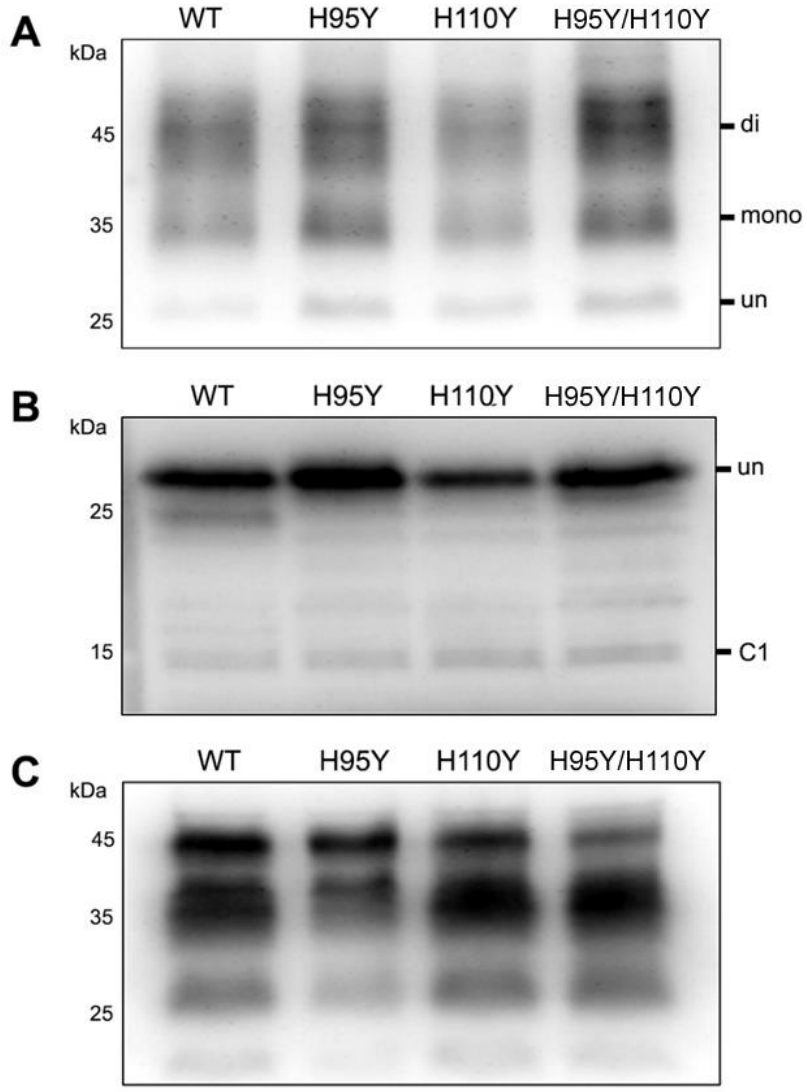

Figure 22. The non-OR mutations share the same glycosylation patterns and proteolytic characteristics as PrP WT. (A) 50 μg of cell lysate was applied to each lane. (B) Lysates were either digested with PNGase F or (C) Endo H. PrPs were detected with anti-PrP W226 mAb. The positions of diglycosylated, monoglycosylated and unglycosylated forms of PrP^C and the C-terminal fragment (C1) are on the right of blot.

In the PNGase assay, the immunoblot also showed an additional band of about 15 kDa (Figure 22B), corresponding to the major C-terminal fragment of PrP^C

(C1 fragment). Similar to many other cell surface proteins, PrP^{C} can be differentially cleaved at specific sites to generate various fragments. In normal tissues and cells, PrP^{C} is mainly cleaved at the 110/111 or 111/112 peptide bonds (termed α-cleavage), yielding the C-terminal fragment (C1) tethered to the plasma membrane and releasing the corresponding N-terminal fragment (N1) [204-206]. Although in H110Y and H95Y/H110Y mutants, H110 at cleavage site was replaced by Tyr, C1 fragment has been still detected. This suggested that the substitution of histidine by tyrosine at H110 did not affect the α-cleavage process.

3.2.3 The non-OR mutants do not alter the solubility and protease resistant profile of PrP^{C}

PrP^{Sc} can be distinguished from PrP^{C} by several biochemical properties, of which detergent insoluble and protease resistance stand out as the most prominent [207, 208]. Here we examined the PrP^{C} mutants to test whether the His-to-Tyr substitution could alter these features of PrP^{C}.

To investigate solubility, cell lysates were extracted in lysis buffer and centrifuged at high speed. Subsequently, the pellets and supernatants were tested for the presence of PrPs. The insolubility of PrP mutants slightly increases compared to WT, but this difference was not statistically significant. In $N2aPrP^{-/-}$ WT, almost all PrP^{C} was found in the supernatant fraction while only 4% was in the pellet. Similarly, less than 7% of PrP was detected in the insoluble fraction of non-OR mutants (Figure 23).

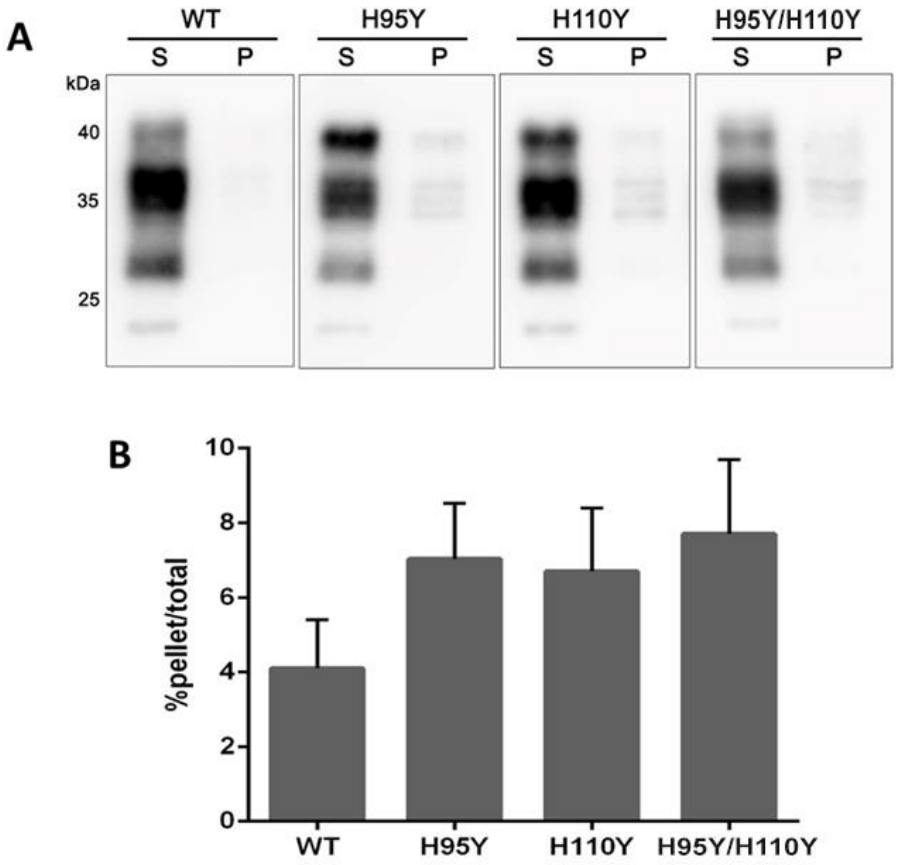

Figure 23. Solubility of PrP is slightly decreased in non-OR mutants. (A) N2aPrP$^{-/-}$ cells stably expressed WT and non-OR mutants. Supernatant (S) and pellet (P) fractions from cell lysates were collected following 100,000 × g centrifugation. PrPs were detected by anti-PrP W226 mAb. (B) Solubility profile of each PrP, determined by the relative densitometry of the pellet signal relative to the total of pellet and supernatant signal.

Similarly, when examining the sensitivity of non-OR mutants to protease digestion, we found that PrP mutants were rapidly digested by PK, just as WT was. In this experiment, PrPs were treated with increased concentrations of PK and the reaction was performed at 37^{o}C in 10 min in order to better monitor PK-resistance levels. The single mutations (H95Y, H110Y) shared almost the same PK-resistance profile with WT; while the double mutations (H95Y/110Y) had slightly higher PK-resistance levels yet statistically not significant (Figure 24).

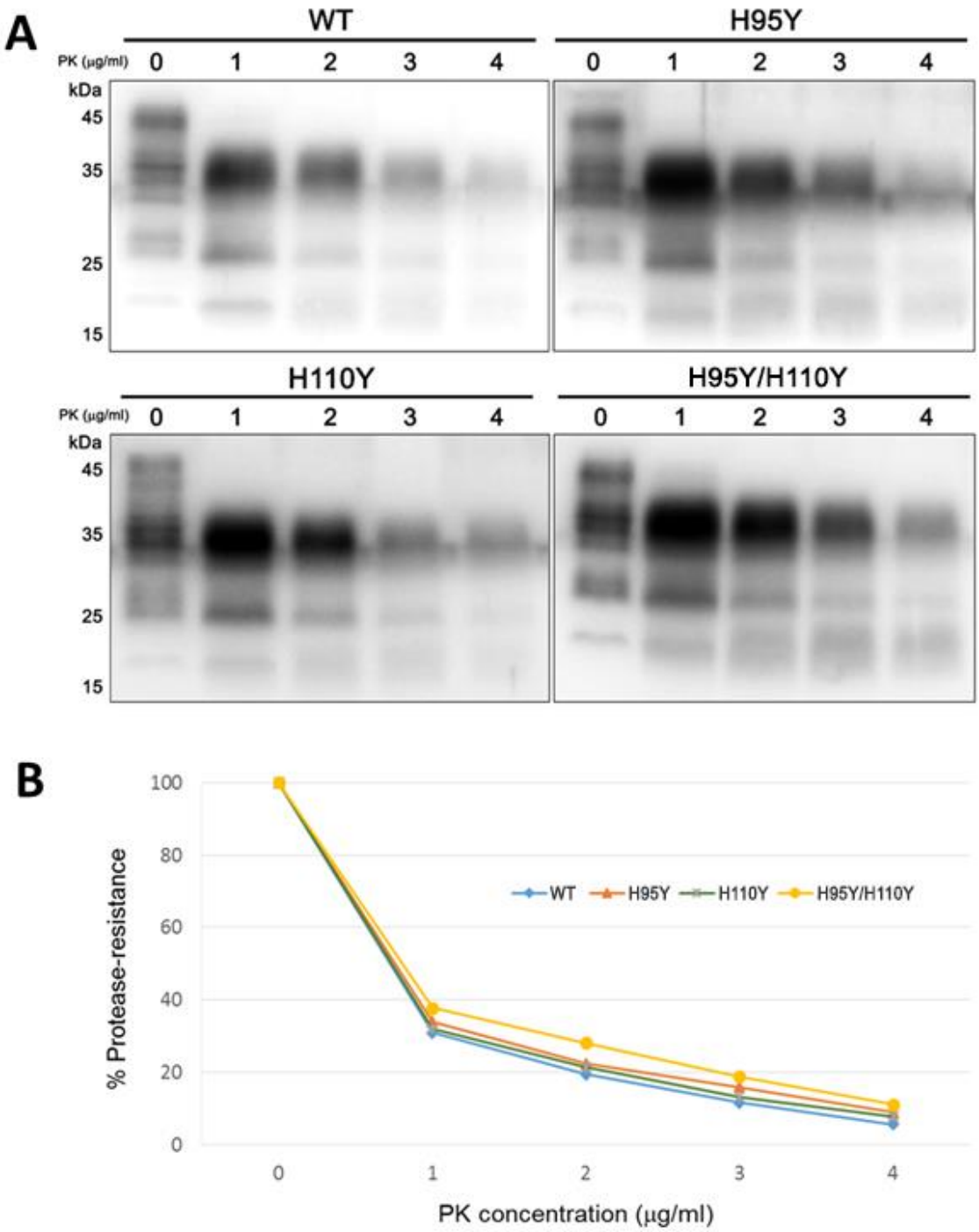

Figure 24. The WT PrP^C and non-OR mutants displayed similar PK-resistance profile when expressed in N2a$PrP^{-/-}$ cells. N2a$PrP^{-/-}$ cells stably expressed WT and non-OR mutants. (A) 100 µg cell lysates were treated with 1 to 4 µg/mL of PK at 37°C for 10 min, 25 µg of undigested cell lysate was loaded in the case of the untreated sample. PrPs were detected by anti-PrP W226 mAb. (B) PK resistant profile of each PrP, determined by the relative densitometry of the treated sample relative to the untreated sample signal.

3.2.4 Substitution of Histidine by Tyrosine at non-OR copper-binding site accelerates fibrillization process

In order to study the impacts of His-to-Tyr replacement in the non-OR region on fibril formation, recMoPrP mutants were produced and applied to fibrillization assays. Experiments were performed at pH 7.0 in the presence of 2M GndHCl. We used this chaotropic agent at this concentration was demonstrated to facilitate aggregation efficiency [209]. The kinetics of filbrillization were monitored by measuring changes in Thioflavin T (ThT) fluorescence intensity. This dye show strong increase of fluorescence upon binding to β-sheet rich structures like amyloid aggregates, hence is used as a marker for newly generated amyloid structural motives [210].

The typical sigmoidal curves of amyloid formation were obtained for both recMoPrP WT and recMoPrP mutants (Figure 25). All mutants formed fibrils faster than the recMoPrP WT as indicated by their shorter lag phases. In unseeded experiments (Figure 25 A, B), the fibrillization reaction of recMoPrP WT showed the longest lag phase (48 ± 7.3 hours). The single mutations, H95Y and H110Y, shared similar kinetic profiles with a shorter lag phase than WT, indicating that both mutations can significantly promotes protein fibrillization. Then, when replacing both His by Tyr, the double mutation H95Y/H110Y displayed the shortest lag phase (23.4 ± 3.7 hours) as a result of the cumulative effect. Similar results were also noted in the seeded experiments. In these experiments, PrP^{Sc} seeds purified using phosphotungstate (PTA) precipitation [186] were added into the reactions and the seeding effect was clearly observed in all cases. In the presence of PrP^{Sc} seed, recMoPrP H95Y/H110Y was rapidly converted to amyloid fibrils with only 10 hours of lag phase. The single mutations needed around 13 hours before ThT fluorescence intensity started to increase. Meanwhile PrP^{Sc} seed reduced the lag phase of recMoPrP WT to 20 hours. In sum, non-OR mutants had higher intrinsic

amyloidogenic potential as compared to MoPrP WT, of which the double mutant H95Y/H110Y had highest fibrillization propensity.

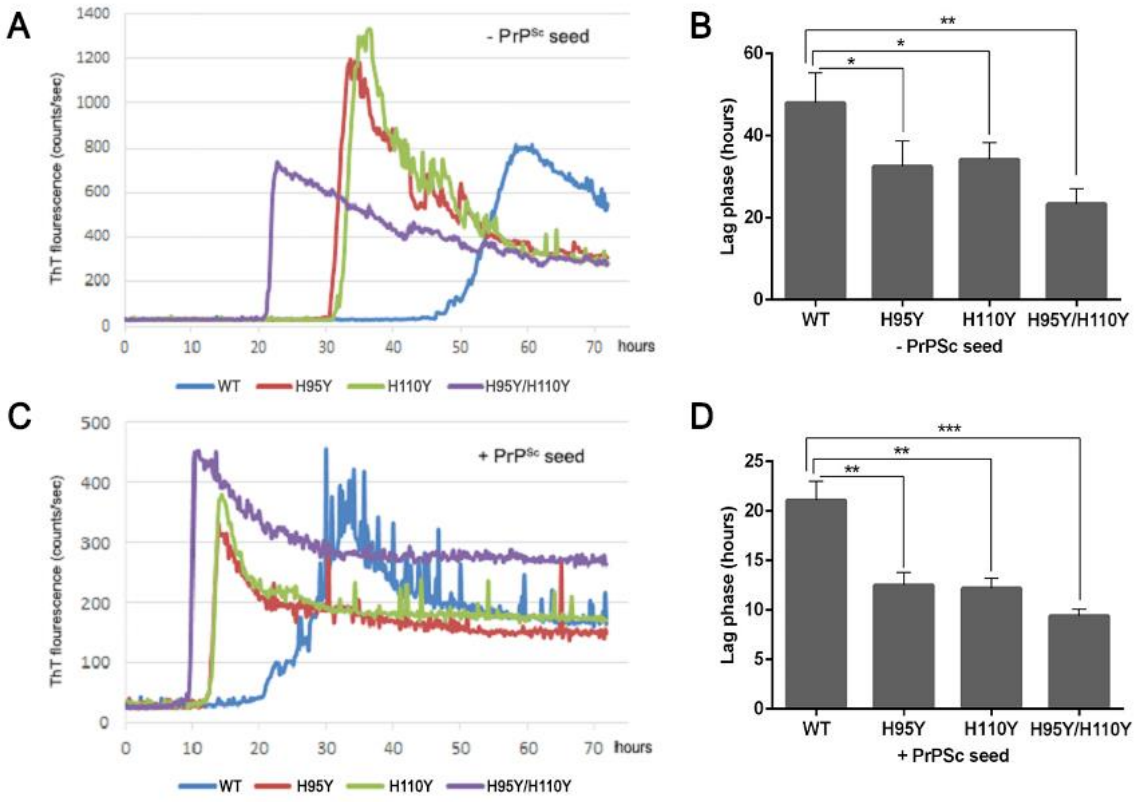

Figure 25. recMoPrP non-OR mutants dramatically promote polymerization processes. recMoPrP WT (WT), recMoPrP H95Y (H95Y), recMoPrP H110Y (H110Y), recMoPrP H95Y/H110Y (H95Y/H110Y) were adding into fibrillization reactions. The kinetics of MoPrP fibrillization with (C) or without (A) PrP^{Sc} seeds at pH 7.0, 2 M GndHCl. Mean value of lag phase in the presence (D) or absence (B) of PrP^{Sc} seeds were determined and compared. (n = 4, *$p<0.05$, **$p<0.01$, ***$p<0.001$).

3.2.5 Non-OR mutants-derived seeds accelerates PrP polymerization in the amyloid seeding assay

Although, non-OR mutants expressed in $N2aPrP^{-/-}$ did not present similar characteristics of PrP^{Sc}, the results from the fibrillization assays showed that they had high fibrillization propensity and form fibrils faster than the WT PrP. Furthermore, H95Y mutant expressed in ScN2a cell also accelerated the prion

conversion. On the basis of these results, we reasoned whether the non-OR mutants expressed in N2aPrP$^{-/-}$ cells might spontaneously convert and behave as an infectious prion. To test this hypothesis, we examined the amyloid seeding assay (ASA), a method that is able to detect PrP^{Sc} (both PK sensitive and resistant) from different human or animal infected brain samples [186, 211].

Non-OR mutant "seeds" were isolated from N2aPrP$^{-/-}$-H95Y, N2aPrP$^{-/-}$-H110Y, N2aPrP$^{-/-}$-H95Y/H110Y cell lysates by PTA precipitation, and seeds from N2aPrP$^{-/-}$-WT cells were also isolated and used as a control. After that, seeds were added into the reactions containing recMoPrP WT as substrate, 2 M GdnHCl, pH 7.0 under continuous shaking for 72 hours at 37 ^{o}C. In case of unseeded reactions used as a negative control, the lag phase of the fibrillization process took around 50 hours. When scrapie seeds were added to the reactions, the amyloid formed much more rapidly, resulting in the reduction of the lag phase to 20 hours. Interestingly, non-OR mutants-derived seeds also showed seeding activity. All three mutants, H95Y, H110Y, H95Y/H110Y had the same effects. Seeds derived from these mutants accelerated the formation of amyloid. The lag phases for these reactions were about 35 hours, corresponding to a 30% reduction compared to unseeded reactions. Surprisingly, the lag phase for H95Y/H110Y-seeded reaction was the same as the lag phase for H95Y or H110Y-seeded reactions although results from the above fibrillization assay showed H95Y/H110Y had higher fibrillization propensity and could form amyloid faster than H95Y or H110Y. On the other hand, seeds prepared from N2aPrP$^{-/-}$-WT cells did not show any significant change in the lag phase: these reactions still had a lag phase of 50 hours, similar to the unseeded reactions.

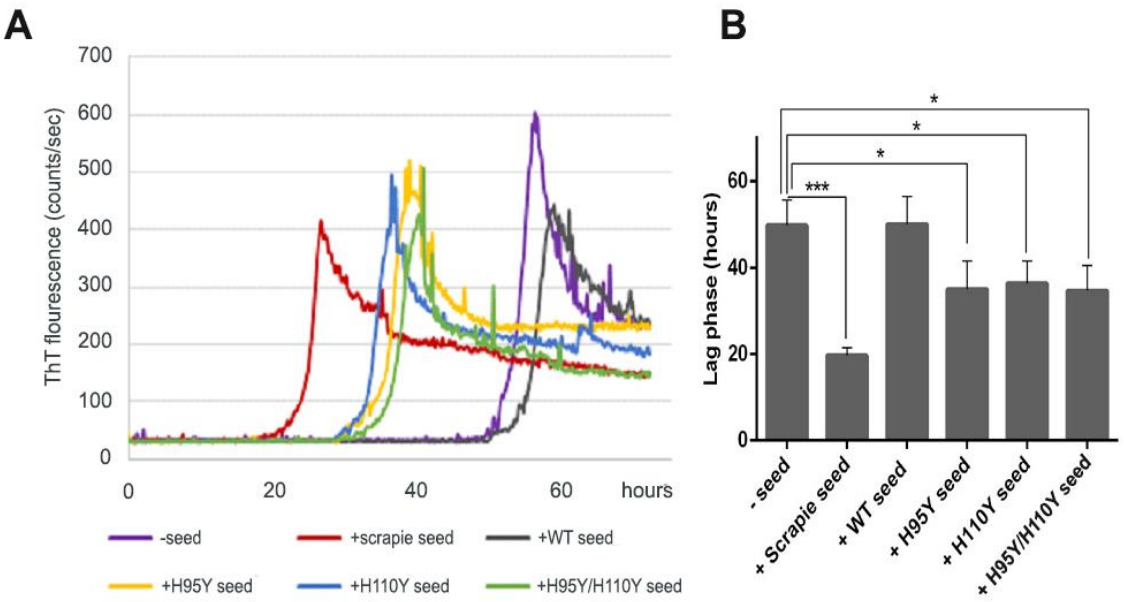

Figure 26. Non-OR mutants-derived seeds accelerates PrP polymerization. (A) The kinetics of MoPrP fibrillization in unseeded and seeded conditions. recMoPrP WT were adding into fibrillization reactions in 2M GndHCl, pH 7.0. Seeds were prepared from cell lysate of ScN2a (scrapie), N2aPrP$^{-/-}$ WT (WT), N2aPrP$^{-/-}$ H95Y (H95Y), N2aPrP$^{-/-}$ H110Y (H110Y), N2aPrP$^{-/-}$ H95Y/H110Y (H95Y/H110Y). (B) Mean values of lag phase were determined and compared. (n = 4, * *p<0.05*, ****p<0.001*).

3.2.6 Spontaneous PrP^{res} generation in N2aPrP$^{-/-}$ cells expressing MoPrP H95Y as detected by PMCA

Protein Misfolding Cyclic amplification (PMCA) is a technique that takes advantage of the nucleation-dependent prion replication process to promote prion conversion in test tube. PMCA consists of cycles of accelerated prion replication, each cycle is composed of two phases. During the first phase the sample containing small amounts of PrP^{Sc} and an excess of PrP^{C} are incubated to induce growing of PrP^{Sc} polymers. In the second phase the sample is subjected to sonication to break down the polymers, multiplying the number of nuclei. After each cycle, the number of seeds increases in an exponential fashion [212]. Thus, PMCA is able to detect the equivalent of a single molecule of infectious PrP^{Sc} [213]. This technique also

propagates prions that maintain high infectivity, strain properties and species specificity [213].

In this experiment, the cell lysates from N2aPrP$^{-/-}$, N2aPrP$^{-/-}$WT and N2aPrP$^{-/-}$H95Y were used as samples for PMCA reactions. The substrates were prepared from FVB WT brain homogenates. After the first and second rounds, we could not detect any PrP^{Sc} in any samples. In the third round, the immunoblot of N2aPrP$^{-/-}$, N2aPrP$^{-/-}$ WT samplez still showed a negative result, indicating no PrP^{res} was present in these samples. Meanwhile, sample from N2aPrP$^{-/-}$ H95Y displayed a positive result. When N2aPrP$^{-/-}$ H95Y cell lysates were directly added to reactions, the PK-resistant PrP^{res} were not detectable. However, when we concentrated N2aPrP$^{-/-}$H95Y cell lysates by phosphotungstate (PTA) precipitation, the PrP^{res} were clearly detected in this sample. This can be explained because there likely was only an extremely small amount of PrPres present in N2aPrP$^{-/-}$ H95Y cell lysates, which we could not detect directly using N2aPrP$^{-/-}$ H95Y cell lysates as sample. Using PTA precipitation, a method widely used to concentrate PrP^{Sc} for diagnostic purposes [186, 214], PrP^{res} in N2aPrP$^{-/-}$ H95Y cell lysates were concentrated to the detectable concentration. These results were consistent with the fibrillization assay result, suggesting that MoPrP H95Y expressed in N2aPrP$^{-/-}$ cells spontaneously converted into PrPres, which could be detected by both ASA and PMCA.

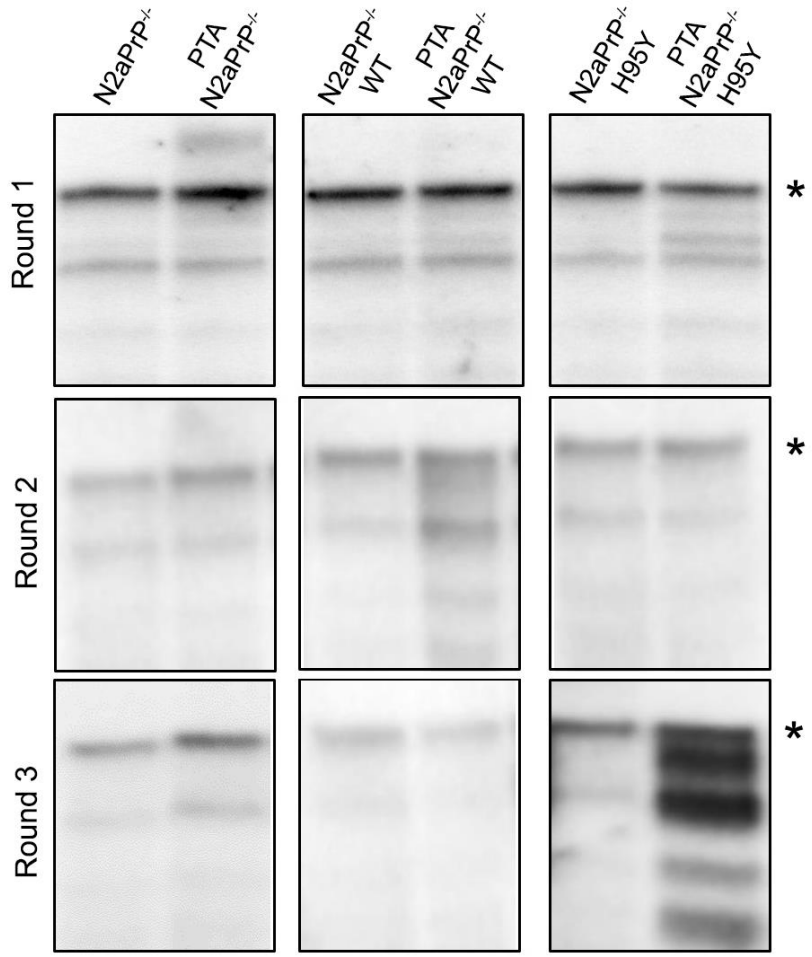

Figure 27. Detection and replication of spontaneous PrP^{res} in $N2aPrP^{-/-}$ expressing MoPrP H95Y using PMCA. 20 µL of reactions were treated with 100 µg/mL of PK at 37 ºC for 1 hour. PrPs were detected by anti-PrP 6D11 mAb. (*) unspecific band.

3.3 Spontaneous generation of prion disease in Tg mice

3.3.1 Establishment of Tg mice overexpressing MoPrP H95Y

To establish Tg mice, we used the plasmid pJB1, a modified vector from MoPrP.Xho vector. This vector was demonstrated to provide relatively high levels of transgene-encoded polypeptides in the brains and hearts of Tg mice [182]. MoPrP H95Y-coding sequence was inserted into pJB1, resulting in plasmid pJB::MoPrP(1-254, H95Y). After that, H95Y mutant transgenes containing mouse regulatory sequences were excised from the plasmid pJB::MoPrP(1-254, H95Y)

and microinjected into the pronucleus of fertilized FVB mice eggs. Mice with transgene integration were screened by PCR using specific primers (Figure S8). Seven lines (founders) of MoPrP H95Y heterozygous Tg mice carrying the endogenous murine *Prnp* gene (*Prnp*$^{+/+}$ H95Y$^{+/-}$) were obtained. Tg lines H95YMoPrP-22, H95YMoPrP-40 and H95YMoPrP-51 were selected on the basis of their expression levels, and bred to homozygosity in a murine *Prnp* null background. To achieve this expression, selected lines were crossed with *Prnp* null mice (*Prnp*$^{-/-}$) to achieve transgene-hemizygous lines (*Prnp*$^{-/-}$ H95Y$^{+/-}$).

Transgene expression levels were determined in brain homogenates and compared with PrP^{C} levels found in FVB WT brain homogenates. Because we did not use 3F4 tag in this experiment, we could not discriminate transgene expression from endogenous expression. Therefore, PrP^{C} expression levels in Tg mouse with PrP$^{C+/+}$ background is included also transgene PrP H95Y and endogenous PrP WT. However, to facillitate the determination of transgene expression level, we use the brain homogenates from Tg mice with PrP$^{C-/-}$ background (Figure 28). Based on that, we found Tg lines H95YMoPrP-22, H95YMoPrP-40 and H95YMoPrP-51 have transgene expression at ~6X, 1X and ~0.5X, respectively. MoPrP H95Y expressed in 22, 40 and 51 Tg lines also showed an electrophoretic profile similar to that of wild-type.

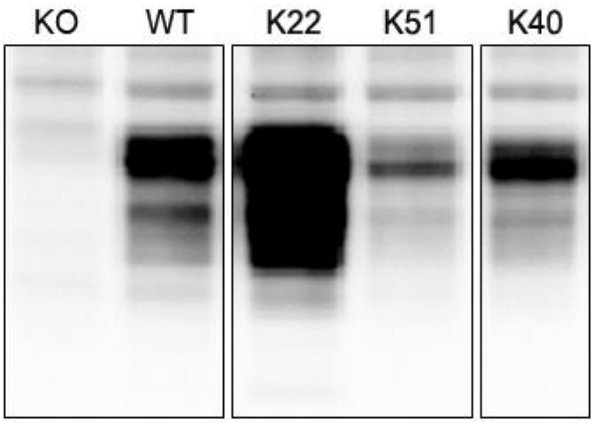

Figure 28. Immunoblots of brain extracts from Tg mice. Equivalent amounts of total protein were loaded into each lane. MoPrPs were detected by anti-PrP 12B2 mAb. K22, K40, K51: represent for Tg lines H95YMoPrP-22, H95YMoPrP-40 and H95YMoPrP-51 in $PrP^{C-/-}$ background.

3.3.2 Spontaneous disease in transgenic mice expressing MoPrP H95Y

According to preliminary results, Tg mice expressing MoPrP H95Y (lines 22, 51) spontaneously develop prion disease. These mice showed neurological clinical signs and reduced survival times compared to FVB wild-type mice (Table 5). In Tg line 22 expressing MoPrP H95Y at high levels, Tg mice in $PrP^{+/+}$ background (X22) were found dead at 108±19 days, while the lifespan of Tg mice in $PrP^{-/-}$ background (K22) was 96±6 days. Interestingly, disease also developed in H95YMoPrP-51 mice expressing low levels of MoPrP H95Y. Two Tg mice in $PrP^{+/+}$ background (X51) were found dead at 443 and 467 days. Although the incubation period of these mice was longer than line 22 and only 33% (2/6) mice developed disease, it indicates that H95Y mutation might cause *de novo* prion diseases when expressed in Tg mice, even in low level expression.

Table 6. Transgene expression level and survival times of Tg mice expressing MoPrP H95Y

Line	Transgene expression level	Total PrPC expression level	Mean incubation period ± SEM (days)
FVB WT ($Prpn^{+/+}$)		1X	>600 (0/6)
X22 ($Prpn^{+/+}$ $H95Y^{+/-}$)	6X	7X	108±19 (20/20)
K22 ($Prpn^{-/-}$ $H95Y^{+/-}$)	6X	6X	96±6 (5/5)
X40 ($Prpn^{+/+}$ $H95Y^{+/-}$)	1X	2X	>350 (0/4, ongoing)
K40 ($Prpn^{-/-}$ $H95Y^{+/-}$)	1X	1X	>350 (0/3, ongoing)
X51 ($Prpn^{+/+}$ $H95Y^{+/-}$)	0.5x	1.5X	443*, 467*, >500 (2/6, ongoing)
K51 ($Prpn^{-/-}$ $H95Y^{+/-}$)	0.5X	0.5X	>220 (0/6, ongoing)

The enhanced resistance to protease digestion is a primary feature to discriminate between PrP^{C} and PrP^{Sc} [207, 208]. Since some Tg mice H95YMoPrP spontaneously developed disease, we examined the presence of PrP^{Sc} in the brains of these Tg mice. Brain homogenates from Tg mice showing clinical signs and developing disease were prepared and applied to PK digestion assay. The results revealed that protease-resistant PrP was observed in the brain homogenate of all Tg mice that developed disease (X22, K22 lines and two X51 mice) (Figure 29). These preliminary results are very promising, neuropathologic and histopathologic studies will be performed to further evaluate these Tg mice.

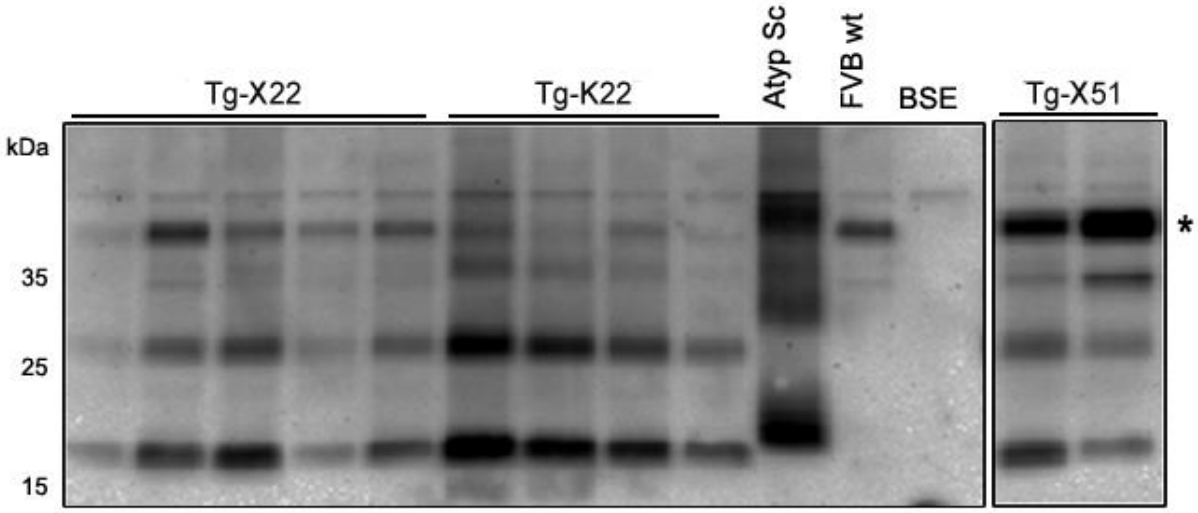

Figure 29. Western blot of brain PrP^{res} in mice expressing MoPrP H95Y. An atypical sheep scrapie brain has been included as positive control, a FVB mouse brain as negative control. In BSE, the 12B2's epitope is cleaved by PK digestion process then it was also included as negative control of the 12B2 mAB. PrPs were detected by anti-PrP 12B2 mAb. (*) incomplete-digested band.

CHAPTER IV

DISCUSSION

Discussion

The central molecular event in prion diseases is the conversion of PrP^{C} into the pathological and infectious prions termed PrP^{Sc}, whose mechanism of formation and transmission remains unclear in spite of numerous investigations. It is well established that PrP^{C} specifically binds to copper, an essential trace metal. Moreover, copper seems to play an important role for PrP^{C} stability and prion conversion [163, 215-219]. Nevertheless, results obtained from these studies showed contradiction, demanding further research to clarify the connection between copper and PrP^{Sc} formation.

In this study, to investigate the copper-PrP^{Sc} relationship, we introduced the substitutions of Histidine by Tyrosine at N-terminal copper binding sites to abolish the binding of copper in these regions. Using the ScN2a cell conversion assay, we found that prion replication was not affected by the lack of each histidine in the OR. This result was in agreement with previous studies, confirming that the deletion of an octapeptide repeat did not lead to prion disease [165]. Moreover, PK treatment of PrP^{Sc} removes residues 23 to approximately 90 without loss of infectivity, suggesting that the OR domain does not play a role in prion conversion. Conversely, when we replaced His by Tyr at the non-OR region, the H95Y mutant strongly promoted the conversion of PrP^{C} to PrP^{Sc}, suggesting that the non-OR copper binding site is much more crucial for prion propagation. Based on the fact that H95 has a higher copper affinity than a single OR copper binding site [106, 123, 220, 221] and localises in the PrP^{Sc} region that typically remains after proteolytic cleavage, we proposed that H95 may have a role in PrP^{Sc} formation. In agreement with this hypothesis, H95Y mutant expressed in $N2aPrP^{-/-}$ spontaneously converted into PrP^{res} that had seeding activity in ASA and it was detected by PMCA.

The question is why H95Y mutant can cause spontaneous conversion. Structural studies revealed that the N-terminal of the prion protein (residue 23-127) is highly disordered [115] without any regular secondary structure [222, 223]. Therefore, instead of causing a significant change in structure like other pathogenic mutations in the globular domain, H95Y might alter the interaction between distinct portions in the protein structure, whose changes are required for oligomerization into fibrillar species. This hypothesis was supposed by a recent publication by Thakur and colleagues [224]. In this study, they found that copper bound to PrP could induce interactions between N- and C-terminal regions, in which the N-terminal region (residues 90–120) became proximal to helix-1 (residues 144–147) and its nearby loop region (residues 139–143). These regions were shown to promote aggregation [225-227] and the helix-1 region also played a prominent role in prion replication [228]. Therefore, they proposed that the interactions between these regions and the N-terminal region (residues 90–120) might regulate prion conversion. In this study, we found that H95Y mutant caused a modification on Cu(II) coordination in the non-OR region. In PrP WT Cu(II) was anchored to two histidine at pH 5.5, and only one histidine at pH 7. Conversely, in H95Y mutants copper was bound only to one histidine independently of the pH. This might lead to the change of aforementioned interactions, promoting prion replication.

In addition, our analysis showed that H95Y mutant induced PrP^{C} accumulation in the acidic endosomal compartments, a putative site for prion conversion. Therefore, the alteration of copper coordination of H95Y mutant seems corresponding to its accumulation in acidic endosomes. Taken together, we proposed a model in which the copper binding had a protective role in prion conversion. In acidic condition, copper bound to non-OR region might stabilize this segment when coordinated by H95 and H110, inducing transient short or long range interactions between C-terminal domain and N-terminal region, such as an

interaction between residues 90–120 and residues 139-147 (including helix-1 and its nearby loop region), preventing the conversion from PrP^{C} to PrP^{Sc}. Copper might act as a key modulator of this process since the removal of copper led to promoted prion conversion, as observed in CPZ-treatment experiments.

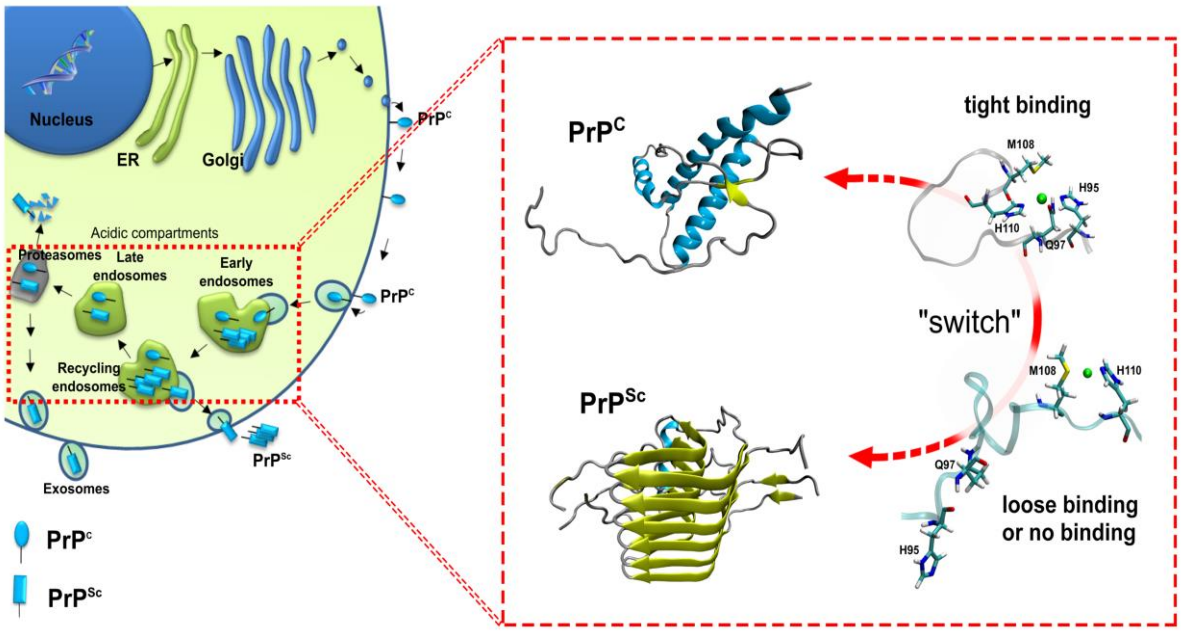

Figure 30. Model for the non-OR region molecular switch at acidic pH. In acidic conditions as endosomal compartments, PrP^{C} binds "tightly" to copper in the non-OR region hinder the conversion from PrP^{C} to PrP^{Sc}. When PrP^{C} binds "loosely" or doesn't bind to copper in non-OR region, PrP^{C} is more prone to the conversion. As PrP^{Sc} model we used the HET-s (218-289) 2KJ3 PDB structure.

In this study, we also investigated the copper coordination in the pathogenic mutations P101L and Q211P. Q211P mutation situates in C-terminal globular domain and is responsible for a rare GSS syndrome characterized by mild amyloid PrP deposition in patients [229]. This mutation induces prominent structural differences, including disruption of the C-terminal part of the α3 helix, solvent exposure of hydrophobic residues and a different orientation of α2 and α3 helices. These changes lead to th reduction of the PrP stability and promote the prion conversion [168]. P101L locates in the flexible N-terminus of PrP and is the most common mutation associated with the GSS disease. Differently from C-terminal

pathogenic mutations, P101L has no or little effect on the thermodynamic stability of PrP [172] but influences the structure and propagation of PrP^{Sc} [229, 230]. Although their impacts on the structure and stability of PrP are different, they interestingly share the same copper coordination on non-OR region, in which copper is bound only to H110 at both pH 5.5 and 7.0, similar to H95Y mutant. These data suggest that in addition to thermodynamic destabilization, the alteration of copper binding in non-OR region might also contribute to promoting spontaneous generation of prions of Q211P mutant. In case of P101L mutation, while other structural studies revealed no significant difference between WT and its structure [231], based on the perturbation of the copper coordination in the non-OR region, our models may appropriately explain why this mutation cause disease. Moreover, the data from these mutations strongly support our hypothesis about the role of non-OR region as molecular switch for prion conversion.

Based on this model, not only H95 but H110 might have a similar role in prion conversion. In our results, the H110Y and H95Y/H110Y mutant expressed in $N2aPrP^{-/-}$ cells also converted spontaneously into PrP^{res}, which can be detected by ASA. On the other hand, substituting H95 by all possible amino acids, we found that the effect of these mutants on prion conversion has a large fluctuation and seems to depend on the substitute's hydrophobicity. The hydrophobic amino acids promoted, while the charged amino acids inhibited conversion. This revealed that H95 could be an important "hot spot" for prion conversion, as this site might acts as a molecular switch that can "turn on" or "turn off" prion conversion. Considering the proposed model, we think that these mutants might differently change copper coordination leading to different effects on PrP^{Sc} formation; therefore further studies on copper coordination of these mutants are needed to explore this issue.

Moreover it will be very interesting if we consider the role of other metals. Other metals have been suggested to bind to PrP^{C}, these include manganese, zinc,

and nickel [35, 124, 138, 232-234]. Recombinant PrP has been shown to bind to manganese *in vitro*, and the binding of manganese to PrP potentially results in the conversion of the protein to an abnormal isoform with properties reminiscent of PrP^{Sc} [234, 235]. In particular, manganese-bound PrP shows greater protease resistance [236], increased β-sheet content, the ability to aggregate [237], and the ability to seed polymerization of prion protein [235]. Interestingly, prion infected mice have dramatic differences in blood, muscle, and brain metal content as compared to the non-infected mice [238]. These infected mice showed increased manganese and decreased copper content. Thus, it has been suggested that substitution of copper with manganese could bring about changes in PrP, initiating prion disease [234]. Brazier *et al.* (2008) [239] indicated that the main manganese binding site is associated with H95. Therefore, manganese may be related to the role of the fifth copper binding site. Because manganese binds to H95 at a lower affinity than copper, the binding of copper precedent here was in a normal condition. The adjustment in copper coordination might lead to the replacement of copper with manganese, promoting the conversion of PrP^{C} to PrP^{Sc}. Considering that the dual impact of these metals might bring about a better answer for the role of H95 in prion conversion.

We also used a new Tg mice expressing the H95Y mutant. The preliminary results showed that these Tg mice spontaneously developed prion diseases as they showed clinical signs with a shortened lifespan and they present PK-resistant PrP^{res} in brain. Interestingly, Tg mice with low expression level of H95Y mutant also developed diseases. Although, these experiments are still ongoing and further analyses will be carried out, these preliminary results clearly point to an important role of H95 in prion conversion. In addition, these Tg mice may be useful for further studying of the relationship between copper and prion disease and also for studying physiological functions of the fifth copper binding site. Moreover, the non-OR

region has recently been found as the principal site for amyloid-β peptide (Aβ) oligomer binding and modulating Aβ neurotoxicity [240]. Therefore, H95YMoPrP Tg mice can be used as an animal model for investigating the interaction between the non-OR region and Aβ oligomers to possibility define a relation among copper, PrP^{C} function and oligomeric Aβ in neurodegenerative disorders.

In conclusion, our findings in this work provide valuable evidences for the critical role of the non-OR copper-binding site in prion conversion. In this work, by using ScN2a cell conversion assay, we found that H95Y mutant promoted PrP^{Sc} formation, and this mutant accumulated in the acidic endosomal compartments. Here we also used EXAFS method to define the copper coordination in non-OR region of WT and H95Y mutant. The difference of these coordination revealed the role of copper binding in this region to PrP^{Sc} formation. Based on these data, we proposed the model, in which the non-OR region acts as a critical molecular "switch" for prion conversion with copper as a modulator. The tight binding of copper in non-OR region induces transient interaction between C-and N-terminal domain, and prevents the conversion from PrP^{C} to PrP^{Sc}. The loose binding or absence of copper lead to the opposite effect that accelerated the PrP^{Sc} formation. The EXAFS data from P101L and Q211P mutations shared similar behavior of non-OR copper coordination and they were highly in line with the proposed model. In addition, this model was proven by the results from N2a$PrP^{-/-}$ cells expressing non-OR mutants. The non-OR mutants on these cells could spontaneously convert into PrP^{res} molecules at detectable level of ASA and PMCA method. We also estabished Tg mice expressing H95Y mutant as *in vivo* model for examing our hyposthesis. Interestingly, in preliminary results, these Tg mice also developed diseases, providing an additional evidence for a pivotal role of non-OR region in prion conversion. These findings are remarkable because this is the first time that a proposed mechanism of prion conversion has been described at biochemical,

structural and functional level. This hypothesis should be considered when studying the pathogenic point mutations, especially the N-terminal mutations.

APPENDIX

SUPPLEMENTARY INFORMATION

A. The 3F4–epitope tag has no effect on prion conversion

The 3F4-epitope tag is a powerful tool to distinguish between exogenous and endogenous MoPrPs. To confirm that this tag has no effect on prion replication, we transiently transfected ScN2a cells with vector pcDNA::MoPrP(1-254)WT or pcDNA::MoPrP(1-254)WT3F4. 72 hours after transfection, cell lysates were collected and treated with PK to evaluate PrPSc PK-resistance levels. Immunoblotting with anti-PrP W226 antibody showed the similarity in PK-resistance PrP^{Sc} levels between cells expressing PrP WT with and without 3F4-tag (Figure S1).

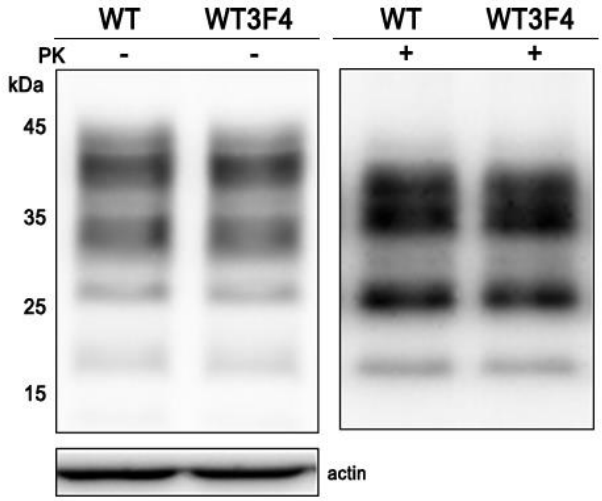

Figure S1. The 3F4–epitope tag has no effect on prion conversion. For non-PK experiment, fifty μg of undigested lysates was applied to each lane, β-actin was used as internal control. For PK experiment, five hundred μg of cell lysates was digested with PK (20 μg/mL) at 37 °C for 1 hour. PrPs were detected by anti-PrP W226 mAb.

B. PrP mutants with the substitution of histidine by tyrosine are not toxic to ScN2a cells

To evaluate the toxicity of mutants, ScN2a were transfected with MoPrP constructs. Seventy-two hours after the transfection, the medium was removed and the MTT assay was performed as described. The result showed that all cells shared a similar viability, around 100 % compared to un-transfected cells

(**Figure S2**). This indicated that the expressions of WT3F4 and mutants had no toxicity effect on ScN2a cells.

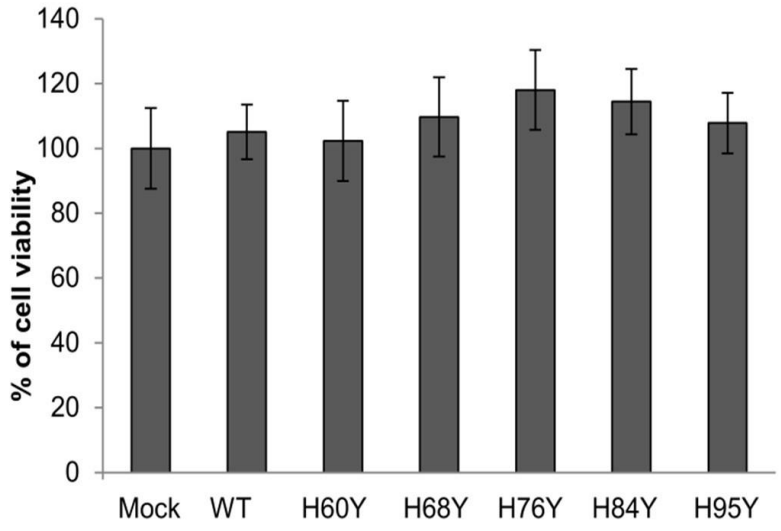

Figure S2. The histidine substitutions in the OR and non-OR regions are not toxic for cell culture.

C. Substitution of histidine by tyrosine at H110 leads to destroy 3F4 epitope

His residue 110 is located inside the 3F4 epitope. So substitution of His110 will change the amino acid sequences of this region, destroying the epitope, thus anti-3F4 antibody cannot recognize it. To examining this, we created two constructs with the replacement of histidine by tyrosine at H110. These constructs were transfected into N2a cell, and their expression was checked by western blot using anti-3F4 antibody.

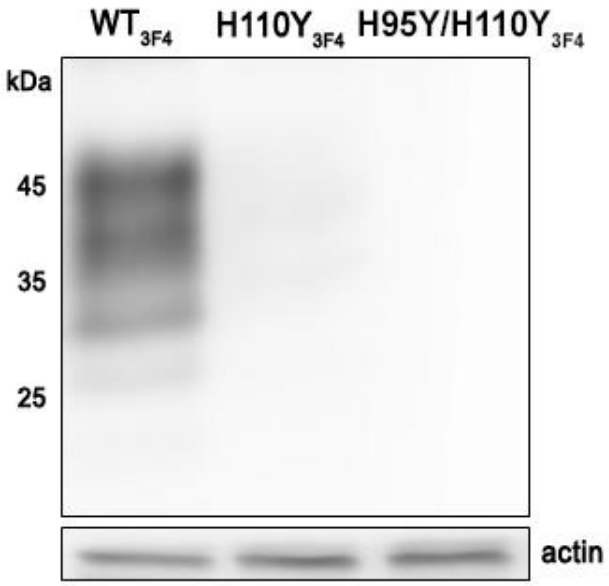

Figure S3. Substitution of histidine by tyrosine at H110 leads to destroy 3F4 epitope. Fifty μg of cell lysates was applied to each lane, β-actin was used as internal control. PrPs were detected by anti-PrP 3F4 mAb.

In positive control sample, MoPrP WT3F4 was recognized, showing clear signal on immunoblot membrane. In contrast, H110Y3F4 and H95Y/H110Y3F4 constructs were not recognized by anti-3F4 antibody in this experiment. Therefore, 3F4 tag cannot be used for studies in which His110 is replaced by other amino acid.

D. Copper coordination in the non-OR region of pathogenic mutants P101L and Q211P

The structures of Cu(II) and Cu(I) binding sites were investigated in Q211P and P101L HuPrP mutants at both pH 5.5 and 7.0 values. The EXAFS data of the mutants share the same coordination pattern observed for the WT at pH 7.0, where the copper ion is coordinated by a single His, namely H110 (Figure S4AB). While in the WT the copper ion -at both oxidative states- changes coordination losing the contact with H95 at pH 7.0, in the pathogenic mutants copper is bound only to H110 independently of the pH.

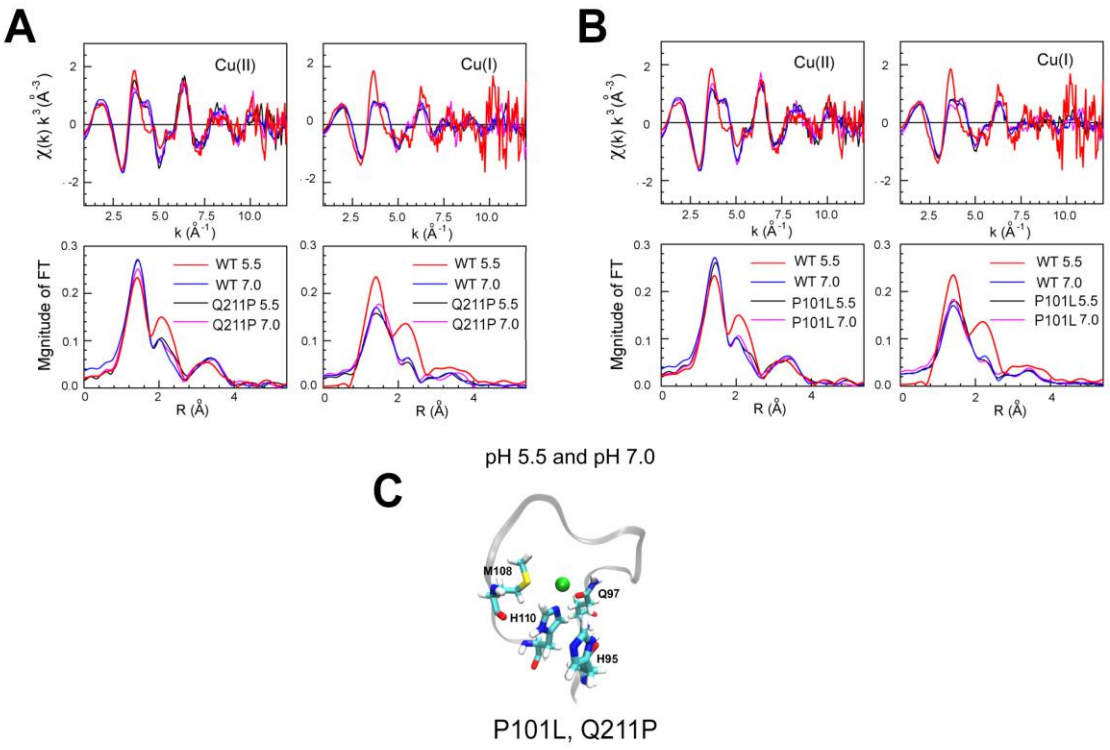

Figure S4. Comparison between copper coordination of pathological P101L, Q211P and HuPrP WT. (A) k3-weighted EXAFS spectra and Fourier transforms of Cu(II) and Cu(I) bound to HuPrP(90-231) WT and Q211P at pH 5.5 and 7.0 and **(B)** of Cu(II) and Cu(I) bound to WT HuPrP(90-231) and P101L at pH 5.5 and 7.0. **(C)** Schematic representations of copper binding sites in the HuPrP(90-231) Q211P and P101L.

E. Expression and purification of recombinant PrP

All MoPrP and HuPrP variants were cloned into plasmid pET11a. The recombinant proteins were produced in *E. coli* BL21(DE3) in LB medium. As a reference, here we showed results of the MoPrP23-231 WT only.

Large-scale protein expression was achieved using a 2 L bioreactor which allowed an automated pH, stirrer, temperature and pO2 control. Fermentation was carried out at 37 ºC, pH 7.0 and pO2 30 %. The fermentation profile was presented in Figure S5. At the end of the fermentation process, bacterial yield was 9-10 g/L of paste with a final OD600 nm of 7-8. By using 1 mM IPTG as inducer, MoPrP was overexpressed in bacterial cells with clear band in SDS-PAGE (Figure S5).

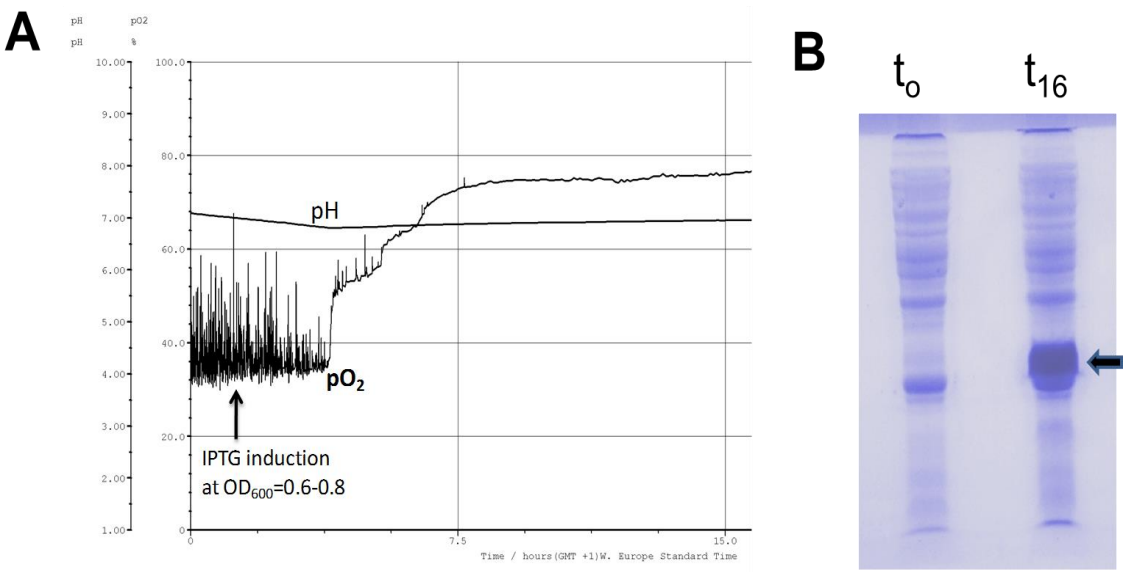

Figure S5. Fermentation and expression of MoPrP23-231 in *E. coli* BL21 (DE3). (A) Profile of fermentation process. **(B)** Expression of MoPrP23-231 in *E. coli* BL21 (DE3), t_0: before induction, t_{16}: 16 hours after induction.

MoPrP23-231 were expressed in BL21(DE3) as insoluble inclusion bodies. Therefore they needed to be solubilized in in 8 M GndHCl and purified under denature condition. MoPrP23-231 contains muti-His region in N-terminal, so it can bind to metals as copper, nikel... Rely on this characteristic, MoPrP23-231 were first purified by Immobilized metal ion affinity chromatography (IMAC) using Histrap column. After the first purification step (Figure S6A), the proteins were considerably pure with only a small number of contaminant bands. Fractions containing PrP from this step were loaded into SEC column to obtain a highly purified protein (Figure S6B).

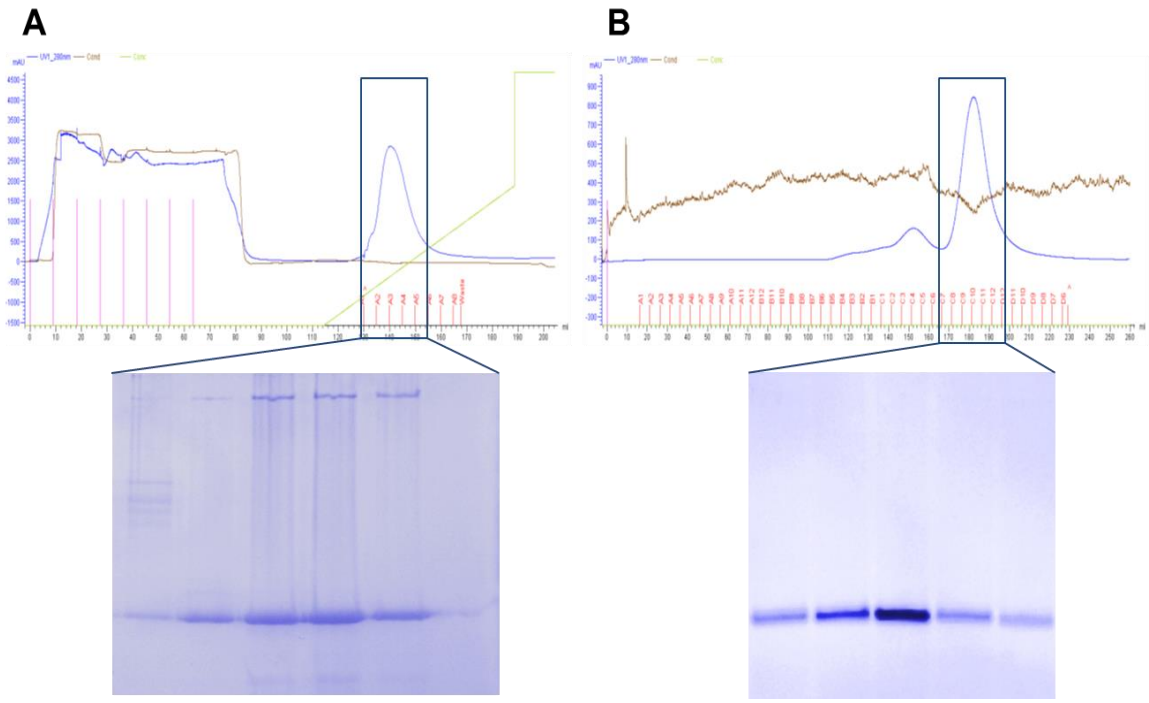

Figure S6. Purification of MoPrP23-231. (A) Purification of MoPrP23-231 by Histrap column, **(B)** Purification of MoPrP23-231 by Size exclusion chromatography.

F. Establishment of Tg mice expressing MoPrP H95Y

MoPrP H95Y-coding sequences were inserted into pJB1, resulting in plasmid pJB::MoPrP(1-254, H95Y). MoPrP mutant transgenes (H95Y) containing mouse regulatory sequences were excised from the plasmid pJB::MoPrP(1-254, H95Y) by using the restriction endonuclease *Not*I. These fragments were then microinjected into the pronucleus of fertilized FVB mice eggs, which were implanted into pseudopregnant FVB females. DNA prepared from tail of F0 offspring mice was used to screen for transgene integration by a PCR assay.

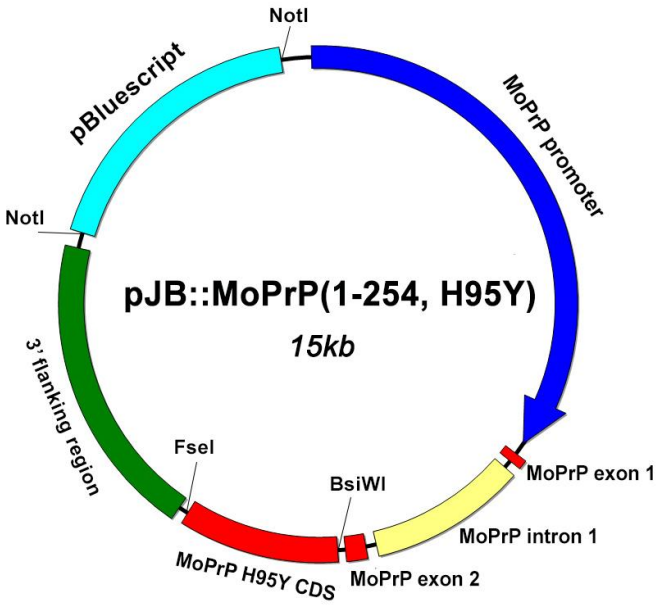

Figure S7. Maps of plamid pJB::MoPrP(1-254, H95Y).

Two PCR assay were used to screen and confirm the integration of transgene into F0 mice genome.

- PCR assay 1:
- Transgene PCR primer F1: GAA CTG AAC CAT TTC AAC CGA G
- Transgene PCR primer R1: AGA GCT ACA GGT GGA TAA CC
- Internal control PCR primer F: ACT CCA AGG CCA CTT ATC ACC
- Internal control PCR primer R: ATT GTT ACC AAC TGG GAC GAC A
- Annealing Temp: 55 ^{o}C
- Transgene PCR product size: 800 bp
- Internal control PCR product size: 413 bp
- PCR assay 2:
- Transgene PCR primer F2: TGG CGA ACC TTG GCT ACT G
- Transgene PCR primer R2: GTG ATA TTG ACG CAG TCG TGC
- Internal control PCR primer F: ACT CCA AGG CCA CTT ATC ACC
- Internal control PCR primer R: ATT GTT ACC AAC TGG GAC GAC A
- Annealing Temp: 62 ^{o}C
- Transgene PCR product size: 550 bp
- Internal control PCR product size: 413 bp

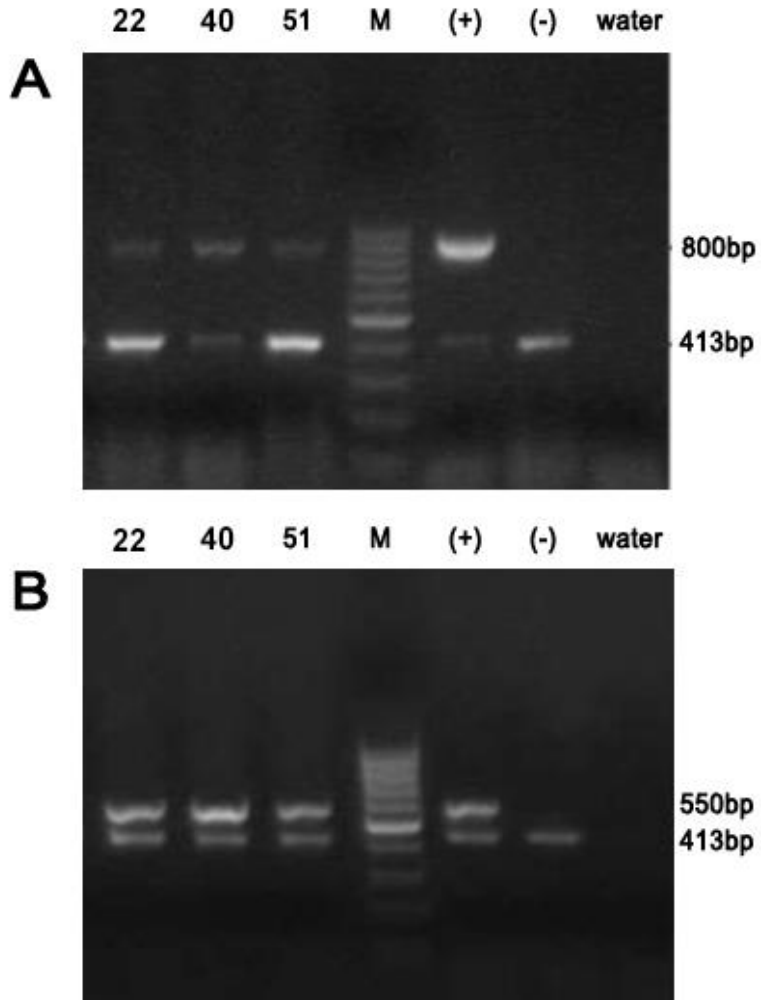

Figure S8. PCR assay for screening Tg mice. (A) PCR assay 1**. (B)** PCR assay 2. The internal control PCR targets the endogenous mouse Actb (beta-actin) locus. Positive control is 400 ng of mouse genomic DNA spiked with an amount of transgene injection DNA that is equivalent to 5 copies of transgene per diploid mouse genome. Wild-type control is 400 ng of mouse genomic DNA.

BIBLIOGRAPHY

1. Prusiner, S.B., *The prion diseases.* Brain Pathol, 1998. **8**(3): p. 499-513.
2. Ross, C.A. and M.A. Poirier, *Protein aggregation and neurodegenerative disease.* Nat Med, 2004. **10 Suppl**: p. S10-7.
3. Colby, D.W. and S.B. Prusiner, *Prions.* Cold Spring Harb Perspect Biol, 2011. **3**(1): p. a006833.
4. Ladogana, A., et al., *Mortality from Creutzfeldt-Jakob disease and related disorders in Europe, Australia, and Canada.* Neurology, 2005. **64**(9): p. 1586-91.
5. Mastrianni, J.A., *The genetics of prion diseases.* Genet Med, 2010. **12**(4): p. 187-95.
6. Koch, T.K., et al., *Creutzfeldt-Jakob disease in a young adult with idiopathic hypopituitarism. Possible relation to the administration of cadaveric human growth hormone.* The New England journal of medicine, 1985. **313**(12): p. 731.
7. Gajdusek, D.C., *Unconventional viruses and the origin and disappearance of kuru.* Science, 1977. **197**: p. 943-960.
8. Alpers, M.P., *Kuru: implications of its transmissibility for the interpretation of its changing epidemiologic pattern*. 1968.
9. Glasse, R., *Cannibalism in the Kuru region of New Guinea.* Transactions of the New York Academy of Sciences, 1967. **29**(6): p. 748.
10. Schatzl, H.M., et al., *Prion protein gene variation among primates.* J Mol Biol, 1995. **245**(4): p. 362-74.
11. Puckett, C., et al., *Genomic structure of the human prion protein gene.* Am J Hum Genet, 1991. **49**(2): p. 320-9.
12. Inoue, S., et al., *Characterization of the bovine prion protein gene: the expression requires interaction between the promoter and intron.* J Vet Med Sci, 1997. **59**(3): p. 175-83.
13. Westaway, D., et al., *Structure and polymorphism of the mouse prion protein gene.* Proc Natl Acad Sci U S A, 1994. **91**(14): p. 6418-22.
14. Basler, K., et al., *Scrapie and cellular PrP isoforms are encoded by the same chromosomal gene.* Cell, 1986. **46**(3): p. 417-28.
15. Premzl, M., et al., *The prion protein gene: identifying regulatory signals using marsupial sequence.* Gene, 2005. **349**: p. 121-34.
16. Lee, I.Y., et al., *Complete genomic sequence and analysis of the prion protein gene region from three mammalian species.* Genome Res, 1998. **8**(10): p. 1022-37.
17. Linden, R., et al., *Physiology of the prion protein.* Physiol Rev, 2008. **88**(2): p. 673-728.
18. Kretzschmar, H.A., et al., *Scrapie prion proteins are synthesized in neurons.* Am J Pathol, 1986. **122**(1): p. 1-5.
19. Brown, H.R., et al., *The mRNA encoding the scrapie agent protein is present in a variety of non-neuronal cells.* Acta Neuropathol, 1990. **80**(1): p. 1-6.

20. Bolton, D.C., R.K. Meyer, and S.B. Prusiner, *Scrapie PrP 27-30 is a sialoglycoprotein.* J Virol, 1985. **53**(2): p. 596-606.

21. Safar, J., et al., *Molecular mass, biochemical composition, and physicochemical behavior of the infectious form of the scrapie precursor protein monomer.* Proc Natl Acad Sci U S A, 1990. **87**(16): p. 6373-7.

22. Stahl, N., et al., *Scrapie prion protein contains a phosphatidylinositol glycolipid.* Cell, 1987. **51**(2): p. 229-40.

23. Hegde, R.S., et al., *A transmembrane form of the prion protein in neurodegenerative disease.* Science, 1998. **279**(5352): p. 827-34.

24. Stewart, R.S., B. Drisaldi, and D.A. Harris, *A transmembrane form of the prion protein contains an uncleaved signal peptide and is retained in the endoplasmic Reticulum.* Mol Biol Cell, 2001. **12**(4): p. 881-9.

25. Harris, D.A., *Trafficking, turnover and membrane topology of PrP.* Br Med Bull, 2003. **66**: p. 71-85.

26. Yin, S., et al., *Human prion proteins with pathogenic mutations share common conformational changes resulting in enhanced binding to glycosaminoglycans.* Proc Natl Acad Sci U S A, 2007. **104**(18): p. 7546-51.

27. Pan, T., et al., *Cell-surface prion protein interacts with glycosaminoglycans.* Biochem J, 2002. **368**(Pt 1): p. 81-90.

28. Takemura, K., et al., *DNA aptamers that bind to PrP(C) and not PrP(Sc) show sequence and structure specificity.* Exp Biol Med (Maywood), 2006. **231**(2): p. 204-14.

29. Mashima, T., et al., *Unique quadruplex structure and interaction of an RNA aptamer against bovine prion protein.* Nucleic Acids Res, 2009. **37**(18): p. 6249-58.

30. Stahl, N., D.R. Borchelt, and S.B. Prusiner, *Differential release of cellular and scrapie prion proteins from cellular membranes by phosphatidylinositol-specific phospholipase C.* Biochemistry, 1990. **29**(22): p. 5405-12.

31. Forloni, G., et al., *Neurotoxicity of a prion protein fragment.* Nature, 1993. **362**(6420): p. 543-6.

32. Glover, K.J., et al., *Conformational dimorphism and transmembrane orientation of prion protein residues 110-136 in bicelles.* Biochemistry, 2001. **40**(44): p. 13137-42.

33. Gasset, M., et al., *Perturbation of the secondary structure of the scrapie prion protein under conditions that alter infectivity.* Proc Natl Acad Sci U S A, 1993. **90**(1): p. 1-5.

34. Goldfarb, L.G., et al., *Synthetic peptides corresponding to different mutated regions of the amyloid gene in familial Creutzfeldt-Jakob disease show enhanced in vitro formation of morphologically different amyloid fibrils.* Proc Natl Acad Sci U S A, 1993. **90**(10): p. 4451-4.

35. Jackson, G.S., et al., *Location and properties of metal-binding sites on the human prion protein.* Proc Natl Acad Sci U S A, 2001. **98**(15): p. 8531-5.

36. Riek, R., et al., *NMR structure of the mouse prion protein domain PrP(121-231).* Nature, 1996. **382**(6587): p. 180-2.

37. Zahn, R., et al., *NMR solution structure of the human prion protein.* Proc Natl Acad Sci U S A, 2000. **97**(1): p. 145-50.

38. Shyng, S.L., M.T. Huber, and D.A. Harris, *A prion protein cycles between the cell surface and an endocytic compartment in cultured neuroblastoma cells.* J Biol Chem, 1993. **268**(21): p. 15922-8.

39. Shyng, S.L., J.E. Heuser, and D.A. Harris, *A glycolipid-anchored prion protein is endocytosed via clathrin-coated pits.* J Cell Biol, 1994. **125**(6): p. 1239-50.

40. Sunyach, C., et al., *The mechanism of internalization of glycosylphosphatidylinositol-anchored prion protein.* EMBO J, 2003. **22**(14): p. 3591-601.

41. Taylor, D.R., et al., *Assigning functions to distinct regions of the N-terminus of the prion protein that are involved in its copper-stimulated, clathrin-dependent endocytosis.* J Cell Sci, 2005. **118**(Pt 21): p. 5141-53.

42. Vey, M., et al., *Subcellular colocalization of the cellular and scrapie prion proteins in caveolae-like membranous domains.* Proc Natl Acad Sci U S A, 1996. **93**(25): p. 14945-9.

43. Kaneko, K., et al., *COOH-terminal sequence of the cellular prion protein directs subcellular trafficking and controls conversion into the scrapie isoform.* Proc Natl Acad Sci U S A, 1997. **94**(6): p. 2333-8.

44. Morris, R.J., C.J. Parkyn, and A. Jen, *Traffic of prion protein between different compartments on the neuronal surface, and the propagation of prion disease.* FEBS Lett, 2006. **580**(23): p. 5565-71.

45. Naslavsky, N., et al., *Characterization of detergent-insoluble complexes containing the cellular prion protein and its scrapie isoform.* J Biol Chem, 1997. **272**(10): p. 6324-31.

46. Taylor, D.R. and N.M. Hooper, *The prion protein and lipid rafts.* Mol Membr Biol, 2006. **23**(1): p. 89-99.

47. Campana, V., D. Sarnataro, and C. Zurzolo, *The highways and byways of prion protein trafficking.* Trends Cell Biol, 2005. **15**(2): p. 102-11.

48. Bueler, H., et al., *Normal development and behaviour of mice lacking the neuronal cell-surface PrP protein.* Nature, 1992. **356**(6370): p. 577-82.

49. Manson, J.C., et al., *129/Ola mice carrying a null mutation in PrP that abolishes mRNA production are developmentally normal.* Mol Neurobiol, 1994. **8**(2-3): p. 121-7.

50. Sakaguchi, S., et al., *Loss of cerebellar Purkinje cells in aged mice homozygous for a disrupted PrP gene.* Nature, 1996. **380**(6574): p. 528-31.

51. Nishida, N., et al., *A mouse prion protein transgene rescues mice deficient for the prion protein gene from purkinje cell degeneration and demyelination.* Lab Invest, 1999. **79**(6): p. 689-97.

52. Nico, P.B., et al., *Altered behavioural response to acute stress in mice lacking cellular prion protein.* Behav Brain Res, 2005. **162**(2): p. 173-81.

53. Fischer, M., et al., *Prion protein (PrP) with amino-proximal deletions restoring susceptibility of PrP knockout mice to scrapie.* EMBO J, 1996. **15**(6): p. 1255-64.

54. Tobler, I., et al., *Altered circadian activity rhythms and sleep in mice devoid of prion protein.* Nature, 1996. **380**(6575): p. 639-42.

55. Criado, J.R., et al., *Mice devoid of prion protein have cognitive deficits that are rescued by reconstitution of PrP in neurons.* Neurobiol Dis, 2005. **19**(1-2): p. 255-65.

56. Graner, E., et al., *Cellular prion protein binds laminin and mediates neuritogenesis.* Brain Res Mol Brain Res, 2000. **76**(1): p. 85-92.

57. Schmitt-Ulms, G., et al., *Binding of neural cell adhesion molecules (N-CAMs) to the cellular prion protein.* J Mol Biol, 2001. **314**(5): p. 1209-25.

58. Santuccione, A., et al., *Prion protein recruits its neuronal receptor NCAM to lipid rafts to activate p59fyn and to enhance neurite outgrowth.* J Cell Biol, 2005. **169**(2): p. 341-54.

59. Kanaani, J., et al., *Recombinant prion protein induces rapid polarization and development of synapses in embryonic rat hippocampal neurons in vitro.* J Neurochem, 2005. **95**(5): p. 1373-86.

60. Mouillet-Richard, S., et al., *Signal transduction through prion protein.* Science, 2000. **289**(5486): p. 1925-8.

61. Vassallo, N. and J. Herms, *Cellular prion protein function in copper homeostasis and redox signalling at the synapse.* J Neurochem, 2003. **86**(3): p. 538-44.

62. Kuwahara, C., et al., *Prions prevent neuronal cell-line death.* Nature, 1999. **400**(6741): p. 225-6.

63. Bounhar, Y., et al., *Prion protein protects human neurons against Bax-mediated apoptosis.* J Biol Chem, 2001. **276**(42): p. 39145-9.

64. Khosravani, H., et al., *Prion protein attenuates excitotoxicity by inhibiting NMDA receptors.* J Cell Biol, 2008. **181**(3): p. 551-65.

65. Westergard, L., H.M. Christensen, and D.A. Harris, *The cellular prion protein (PrP(C)): its physiological function and role in disease.* Biochim Biophys Acta, 2007. **1772**(6): p. 629-44.

66. Prusiner, S.B., et al., *Scrapie prions aggregate to form amyloid-like birefringent rods.* Cell, 1983. **35**(2 Pt 1): p. 349-58.

67. Wille, H., S.B. Prusiner, and F.E. Cohen, *Scrapie infectivity is independent of amyloid staining properties of the N-terminally truncated prion protein.* J Struct Biol, 2000. **130**(2-3): p. 323-38.

68. Gambetti, P., et al., *A novel human disease with abnormal prion protein sensitive to protease.* Ann Neurol, 2008. **63**(6): p. 697-708.

69. Diaz-Espinoza, R. and C. Soto, *High-resolution structure of infectious prion protein: the final frontier.* Nat Struct Mol Biol, 2012. **19**(4): p. 370-7.

70. Govaerts, C., et al., *Evidence for assembly of prions with left-handed beta-helices into trimers.* Proc Natl Acad Sci U S A, 2004. **101**(22): p. 8342-7.

71. DeMarco, M.L. and V. Daggett, *From conversion to aggregation: protofibril formation of the prion protein.* Proc Natl Acad Sci U S A, 2004. **101**(8): p. 2293-8.

72. DeMarco, M.L., et al., *Structural properties of prion protein protofibrils and fibrils: an experimental assessment of atomic models.* Biochemistry, 2006. **45**(51): p. 15573-82.

73. Cobb, N.J., et al., *Molecular architecture of human prion protein amyloid: a parallel, in-register beta-structure.* Proc Natl Acad Sci U S A, 2007. **104**(48): p. 18946-51.

74. Smirnovas, V., et al., *Structural organization of brain-derived mammalian prions examined by hydrogen-deuterium exchange.* Nat Struct Mol Biol, 2011. **18**(4): p. 504-6.

75. Groveman, B.R., et al., *Parallel in-register intermolecular beta-sheet architectures for prion-seeded prion protein (PrP) amyloids.* J Biol Chem, 2014. **289**(35): p. 24129-42.

76. Prusiner, S.B., *Molecular biology of prion diseases.* Science, 1991. **252**(5012): p. 1515-22.

77. Collinge, J., *Prion diseases of humans and animals: their causes and molecular basis.* Annu Rev Neurosci, 2001. **24**: p. 519-50.

78. Bueler, H., et al., *Mice devoid of PrP are resistant to scrapie.* Cell, 1993. **73**(7): p. 1339-47.

79. Legname, G., et al., *Synthetic mammalian prions.* Science, 2004. **305**(5684): p. 673-6.

80. Colby, D.W., et al., *Design and construction of diverse mammalian prion strains.* Proc Natl Acad Sci U S A, 2009. **106**(48): p. 20417-22.

81. Supattapone, S., *Prion protein conversion in vitro.* J Mol Med (Berl), 2004. **82**(6): p. 348-56.

82. Castilla, J., et al., *In vitro generation of infectious scrapie prions.* Cell, 2005. **121**(2): p. 195-206.

83. Barria, M.A., et al., *De novo generation of infectious prions in vitro produces a new disease phenotype.* PLoS Pathog, 2009. **5**(5): p. e1000421.

84. Deleault, N.R., et al., *Cofactor molecules maintain infectious conformation and restrict strain properties in purified prions.* Proc Natl Acad Sci U S A, 2012. **109**(28): p. E1938-46.

85. Wang, F., X. Wang, and J. Ma, *Conversion of bacterially expressed recombinant prion protein.* Methods, 2011. **53**(3): p. 208-13.

86. Wang, F., et al., *Generating a prion with bacterially expressed recombinant prion protein.* Science, 2010. **327**(5969): p. 1132-5.

87. Wang, F., et al., *Genetic informational RNA is not required for recombinant prion infectivity.* J Virol, 2012. **86**(3): p. 1874-6.

88. Zhang, Z., et al., *De novo generation of infectious prions with bacterially expressed recombinant prion protein.* FASEB J, 2013. **27**(12): p. 4768-75.

89. Le, N.T., et al., *Synthetic prions and other human neurodegenerative proteinopathies.* Virus Res, 2015. **207**: p. 25-37.

90. Aguzzi, A. and M. Polymenidou, *Mammalian prion biology: one century of evolving concepts.* Cell, 2004. **116**(2): p. 313-27.

91. Prusiner, S.B., et al., *Transgenetic studies implicate interactions between homologous PrP isoforms in scrapie prion replication.* Cell, 1990. **63**(4): p. 673-86.

92. Cohen, F.E., et al., *Structural clues to prion replication.* Science, 1994. **264**(5158): p. 530-1.

93. Kaneko, K., et al., *Molecular properties of complexes formed between the prion protein and synthetic peptides.* J Mol Biol, 1997. **270**(4): p. 574-86.

94. Kocisko, D.A., et al., *Cell-free formation of protease-resistant prion protein.* Nature, 1994. **370**(6489): p. 471-4.

95. Jarrett, J.T. and P.T. Lansbury, Jr., *Seeding "one-dimensional crystallization" of amyloid: a pathogenic mechanism in Alzheimer's disease and scrapie?* Cell, 1993. **73**(6): p. 1055-8.

96. Caughey, B., et al., *Prion protein biosynthesis in scrapie-infected and uninfected neuroblastoma cells.* J Virol, 1989. **63**(1): p. 175-81.

97. Caughey, B. and G.J. Raymond, *The scrapie-associated form of PrP is made from a cell surface precursor that is both protease- and phospholipase-sensitive.* J Biol Chem, 1991. **266**(27): p. 18217-23.

98. Borchelt, D.R., et al., *Scrapie and cellular prion proteins differ in their kinetics of synthesis and topology in cultured cells.* J Cell Biol, 1990. **110**(3): p. 743-52.

99. Borchelt, D.R., A. Taraboulos, and S.B. Prusiner, *Evidence for synthesis of scrapie prion proteins in the endocytic pathway.* J Biol Chem, 1992. **267**(23): p. 16188-99.

100. Taraboulos, A., et al., *Synthesis and trafficking of prion proteins in cultured cells.* Mol Biol Cell, 1992. **3**(8): p. 851-63.

101. Supattapone, S., K. Nishina, and J.R. Rees, *Pharmacological approaches to prion research.* Biochem Pharmacol, 2002. **63**(8): p. 1383-8.

102. Krammer, C., et al., *Therapy in prion diseases: from molecular and cellular biology to therapeutic targets.* Infect Disord Drug Targets, 2009. **9**(1): p. 3-14.

103. Taraboulos, A., D. Serban, and S.B. Prusiner, *Scrapie prion proteins accumulate in the cytoplasm of persistently infected cultured cells.* J Cell Biol, 1990. **110**(6): p. 2117-32.

104. Beranger, F., et al., *Stimulation of PrP(C) retrograde transport toward the endoplasmic reticulum increases accumulation of PrP(Sc) in prion-infected cells.* J Biol Chem, 2002. **277**(41): p. 38972-7.

105. Lee, K.S., et al., *Hemin interactions and alterations of the subcellular localization of prion protein.* J Biol Chem, 2007. **282**(50): p. 36525-33.

106. Millhauser, G.L., *Copper and the prion protein: methods, structures, function, and disease.* Annu Rev Phys Chem, 2007. **58**: p. 299-320.

107. Muller, H., et al., *Separation of native prion protein (PrP) glycoforms by copper-binding using immobilized metal affinity chromatography (IMAC).* Biochem J, 2005. **388**(Pt 1): p. 371-8.

108. Todorova-Balvay, D., et al., *Copper binding to prion octarepeat peptides, a combined metal chelate affinity and immunochemical approaches.* J Chromatogr B Analyt Technol Biomed Life Sci, 2005. **818**(1): p. 75-82.

109. Aronoff-Spencer, E., et al., *Identification of the Cu2+ binding sites in the N-terminal domain of the prion protein by EPR and CD spectroscopy.* Biochemistry, 2000. **39**(45): p. 13760-71.

110. Hornshaw, M.P., J.R. McDermott, and J.M. Candy, *Copper binding to the N-terminal tandem repeat regions of mammalian and avian prion protein.* Biochem Biophys Res Commun, 1995. **207**(2): p. 621-9.

111. Viles, J.H., et al., *Local structural plasticity of the prion protein. Analysis of NMR relaxation dynamics.* Biochemistry, 2001. **40**(9): p. 2743-53.

112. O'Sullivan, D.B., et al., *Dynamics of a truncated prion protein, PrP(113-231), from (15)N NMR relaxation: order parameters calculated and slow conformational fluctuations localized to a distinct region.* Protein Sci, 2009. **18**(2): p. 410-23.

113. Klewpatinond, M., et al., *Deconvoluting the Cu2+ binding modes of full-length prion protein.* J Biol Chem, 2008. **283**(4): p. 1870-81.

114. Burns, C.S., et al., *Molecular features of the copper binding sites in the octarepeat domain of the prion protein.* Biochemistry, 2002. **41**(12): p. 3991-4001.

115. Viles, J.H., et al., *Copper binding to the prion protein: structural implications of four identical cooperative binding sites.* Proc Natl Acad Sci U S A, 1999. **96**(5): p. 2042-7.

116. Garnett, A.P. and J.H. Viles, *Copper binding to the octarepeats of the prion protein. Affinity, specificity, folding, and cooperativity: insights from circular dichroism.* J Biol Chem, 2003. **278**(9): p. 6795-802.

117. Valensin, D., et al., *The dimeric and tetrameric octarepeat fragments of prion protein behave differently to its monomeric unit.* Dalton Trans, 2004(9): p. 1284-93.

118. Walter, E.D., M. Chattopadhyay, and G.L. Millhauser, *The affinity of copper binding to the prion protein octarepeat domain: evidence for negative cooperativity.* Biochemistry, 2006. **45**(43): p. 13083-92.

119. Wells, M.A., et al., *Multiple forms of copper (II) co-ordination occur throughout the disordered N-terminal region of the prion protein at pH 7.4.* Biochem J, 2006. **400**(3): p. 501-10.

120. Davies, P. and D.R. Brown, *The chemistry of copper binding to PrP: is there sufficient evidence to elucidate a role for copper in protein function?* Biochem J, 2008. **410**(2): p. 237-44.

121. Hasnain, S.S., et al., *XAFS study of the high-affinity copper-binding site of human PrP(91-231) and its low-resolution structure in solution.* J Mol Biol, 2001. **311**(3): p. 467-73.

122. Burns, C.S., et al., *Copper coordination in the full-length, recombinant prion protein.* Biochemistry, 2003. **42**(22): p. 6794-803.

123. Jones, C.E., et al., *Preferential Cu2+ coordination by His96 and His111 induces beta-sheet formation in the unstructured amyloidogenic region of the prion protein.* J Biol Chem, 2004. **279**(31): p. 32018-27.

124. Jones, C.E., et al., *Probing copper2+ binding to the prion protein using diamagnetic nickel2+ and 1H NMR: the unstructured N terminus facilitates the coordination of six copper2+ ions at physiological concentrations.* J Mol Biol, 2005. **346**(5): p. 1393-407.

125. Brown, D.R., et al., *The cellular prion protein binds copper in vivo.* Nature, 1997. **390**(6661): p. 684-7.

126. Kramer, M.L., et al., *Prion protein binds copper within the physiological concentration range.* J Biol Chem, 2001. **276**(20): p. 16711-9.

127. Stockel, J., et al., *Prion protein selectively binds copper(II) ions.* Biochemistry, 1998. **37**(20): p. 7185-93.

128. Thompsett, A.R., et al., *High affinity binding between copper and full-length prion protein identified by two different techniques.* J Biol Chem, 2005. **280**(52): p. 42750-8.

129. Treiber, C., et al., *Real-time kinetics of discontinuous and highly conformational metal-ion binding sites of prion protein.* J Biol Inorg Chem, 2007. **12**(5): p. 711-20.

130. Nadal, R.C., et al., *Evaluation of copper2+ affinities for the prion protein.* Biochemistry, 2009. **48**(38): p. 8929-31.

131. Toni, M., et al., *Extracellular copper ions regulate cellular prion protein (PrPC) expression and metabolism in neuronal cells.* FEBS Lett, 2005. **579**(3): p. 741-4.

132. Varela-Nallar, L., et al., *Induction of cellular prion protein gene expression by copper in neurons.* Am J Physiol Cell Physiol, 2006. **290**(1): p. C271-81.

133. Herms, J., et al., *Evidence of presynaptic location and function of the prion protein.* J Neurosci, 1999. **19**(20): p. 8866-75.

134. Kretzschmar, H.A., et al., *Function of PrP(C) as a copper-binding protein at the synapse.* Arch Virol Suppl, 2000(16): p. 239-49.

135. Schmitt-Ulms, G., et al., *Evolutionary descent of prion genes from the ZIP family of metal ion transporters.* PLoS One, 2009. **4**(9): p. e7208.

136. Kralovicova, S., et al., *The effects of prion protein expression on metal metabolism.* Mol Cell Neurosci, 2009. **41**(2): p. 135-47.

137. Pauly, P.C. and D.A. Harris, *Copper stimulates endocytosis of the prion protein.* J Biol Chem, 1998. **273**(50): p. 33107-10.

138. Perera, W.S. and N.M. Hooper, *Ablation of the metal ion-induced endocytosis of the prion protein by disease-associated mutation of the octarepeat region.* Curr Biol, 2001. **11**(7): p. 519-23.

139. Brown, D.R., et al., *Prion protein-deficient cells show altered response to oxidative stress due to decreased SOD-1 activity.* Exp Neurol, 1997. **146**(1): p. 104-12.

140. Brown, D.R., et al., *Normal prion protein has an activity like that of superoxide dismutase.* Biochem J, 1999. **344 Pt 1**: p. 1-5.

141. Brown, D.R. and A. Besinger, *Prion protein expression and superoxide dismutase activity.* Biochem J, 1998. **334 (Pt 2)**: p. 423-9.

142. Wong, B.S., et al., *Differential contribution of superoxide dismutase activity by prion protein in vivo.* Biochem Biophys Res Commun, 2000. **273**(1): p. 136-9.

143. Hutter, G., F.L. Heppner, and A. Aguzzi, *No superoxide dismutase activity of cellular prion protein in vivo.* Biol Chem, 2003. **384**(9): p. 1279-85.

144. Jones, S., et al., *Recombinant prion protein does not possess SOD-1 activity.* Biochem J, 2005. **392**(Pt 2): p. 309-12.

145. Kim, B.H., et al., *The cellular prion protein (PrPC) prevents apoptotic neuronal cell death and mitochondrial dysfunction induced by serum deprivation.* Brain Res Mol Brain Res, 2004. **124**(1): p. 40-50.

146. Shyu, W.C., et al., *Overexpression of PrPC by adenovirus-mediated gene targeting reduces ischemic injury in a stroke rat model.* J Neurosci, 2005. **25**(39): p. 8967-77.

147. Rangel, A., et al., *Enhanced susceptibility of Prnp-deficient mice to kainate-induced seizures, neuronal apoptosis, and death: Role of AMPA/kainate receptors.* J Neurosci Res, 2007. **85**(12): p. 2741-55.

148. Spudich, A., et al., *Aggravation of ischemic brain injury by prion protein deficiency: role of ERK-1/-2 and STAT-1.* Neurobiol Dis, 2005. **20**(2): p. 442-9.

149. You, H., et al., *Abeta neurotoxicity depends on interactions between copper ions, prion protein, and N-methyl-D-aspartate receptors.* Proc Natl Acad Sci U S A, 2012. **109**(5): p. 1737-42.

150. Gasperini, L., et al., *Prion protein and copper cooperatively protect neurons by modulating NMDA receptor through S-nitrosylation.* Antioxid Redox Signal, 2015. **22**(9): p. 772-84.

151. Pattison, I.H. and J.N. Jebbett, *Histopathological similarities between scrapie and cuprizone toxicity in mice.* Nature, 1971. **230**(5289): p. 115-7.

152. Kimberlin, R.H. and G.C. Millson, *The effects of cuprizone toxicity on the incubation period of scrapie in mice.* J Comp Pathol, 1976. **86**(3): p. 489-96.

153. Qin, K., et al., *ATM-mediated transcriptional elevation of prion in response to copper-induced oxidative stress.* J Biol Chem, 2009. **284**(7): p. 4582-93.

154. Bellingham, S.A., et al., *Regulation of prion gene expression by transcription factors SP1 and metal transcription factor-1.* J Biol Chem, 2009. **284**(2): p. 1291-301.

155. Hijazi, N., et al., *Copper binding to PrPC may inhibit prion disease propagation.* Brain Res, 2003. **993**(1-2): p. 192-200.

156. Mitteregger, G., et al., *Role of copper and manganese in prion disease progression.* Brain Res, 2009. **1292**: p. 155-64.

157. Canello, T., et al., *Copper is toxic to PrP-ablated mice and exacerbates disease in a mouse model of E200K genetic prion disease.* Neurobiol Dis, 2012. **45**(3): p. 1010-7.

158. Sigurdsson, E.M., et al., *Copper chelation delays the onset of prion disease.* J Biol Chem, 2003. **278**(47): p. 46199-202.

159. Quaglio, E., et al., *Expression of mutant or cytosolic PrP in transgenic mice and cells is not associated with endoplasmic reticulum stress or proteasome dysfunction.* PLoS One, 2011. **6**(4): p. e19339.

160. Treiber, C., A. Simons, and G. Multhaup, *Effect of copper and manganese on the de novo generation of protease-resistant prion protein in yeast cells.* Biochemistry, 2006. **45**(21): p. 6674-80.

161. Nishina, K., et al., *In vitro prion protein conversion in detergent-solubilized membranes.* Biochemistry, 2004. **43**(9): p. 2613-21.

162. Orem, N.R., et al., *Copper (II) ions potently inhibit purified PrPres amplification.* J Neurochem, 2006. **96**(5): p. 1409-15.

163. Bocharova, O.V., et al., *Copper(II) inhibits in vitro conversion of prion protein into amyloid fibrils.* Biochemistry, 2005. **44**(18): p. 6776-87.

164. Flechsig, E., et al., *Prion protein devoid of the octapeptide repeat region restores susceptibility to scrapie in PrP knockout mice.* Neuron, 2000. **27**(2): p. 399-408.

165. Owen, F., et al., *Insertion in prion protein gene in familial Creutzfeldt-Jakob disease.* Lancet, 1989. **1**(8628): p. 51-2.

166. Beck, J.A., et al., *Two-octapeptide repeat deletion of prion protein associated with rapidly progressive dementia.* Neurology, 2001. **57**(2): p. 354-6.

167. Biljan, I., et al., *Structural rearrangements at physiological pH: nuclear magnetic resonance insights from the V210I human prion protein mutant.* Biochemistry, 2012. **51**(38): p. 7465-74.

168. Ilc, G., et al., *NMR structure of the human prion protein with the pathological Q212P mutation reveals unique structural features.* PLoS One, 2010. **5**(7): p. e11715.

169. van der Kamp, M.W. and V. Daggett, *The consequences of pathogenic mutations to the human prion protein.* Protein Eng Des Sel, 2009. **22**(8): p. 461-8.

170. Apetri, A.C., K. Surewicz, and W.K. Surewicz, *The effect of disease-associated mutations on the folding pathway of human prion protein.* J Biol Chem, 2004. **279**(17): p. 18008-14.

171. Liemann, S. and R. Glockshuber, *Influence of amino acid substitutions related to inherited human prion diseases on the thermodynamic stability of the cellular prion protein.* Biochemistry, 1999. **38**(11): p. 3258-67.

172. Swietnicki, W., et al., *Familial mutations and the thermodynamic stability of the recombinant human prion protein.* J Biol Chem, 1998. **273**(47): p. 31048-52.

173. Sigurdson, C.J., et al., *A molecular switch controls interspecies prion disease transmission in mice.* J Clin Invest, 2010. **120**(7): p. 2590-9.

174. Kurt, T.D., et al., *Prion transmission prevented by modifying the beta2-alpha2 loop structure of host PrPC.* J Neurosci, 2014. **34**(3): p. 1022-7.

175. Jones, E.M., K. Surewicz, and W.K. Surewicz, *Role of N-terminal familial mutations in prion protein fibrillization and prion amyloid propagation in vitro.* J Biol Chem, 2006. **281**(12): p. 8190-6.

176. Forloni, G., et al., *Influence of mutations associated with familial prion-related encephalopathies on biological activity of prion protein peptides.* Ann Neurol, 1999. **45**(4): p. 489-94.

177. Abskharon, R.N., et al., *Probing the N-terminal beta-sheet conversion in the crystal structure of the human prion protein bound to a nanobody.* J Am Chem Soc, 2014. **136**(3): p. 937-44.

178. Li, A., et al., *Neonatal lethality in transgenic mice expressing prion protein with a deletion of residues 105-125.* EMBO J, 2007. **26**(2): p. 548-58.

179. Baumann, F., et al., *Lethal recessive myelin toxicity of prion protein lacking its central domain.* EMBO J, 2007. **26**(2): p. 538-47.

180. Younan, N.D., et al., *Copper(II)-induced secondary structure changes and reduced folding stability of the prion protein.* J Mol Biol, 2011. **410**(3): p. 369-82.

181. Migliorini, C., et al., *Copper-induced structural propensities of the amyloidogenic region of human prion protein.* J Biol Inorg Chem, 2014. **19**(4-5): p. 635-45.

182. Borchelt, D.R., et al., *A vector for expressing foreign genes in the brains and hearts of transgenic mice.* Genet Anal, 1996. **13**(6): p. 159-63.

183. Mehrabian, M., et al., *CRISPR-Cas9-based knockout of the prion protein and its effect on the proteome.* PLoS One, 2014. **9**(12): p. e114594.

184. Westergard, L., J.A. Turnbaugh, and D.A. Harris, *A nine amino acid domain is essential for mutant prion protein toxicity.* J Neurosci, 2011. **31**(39): p. 14005-17.

185. Filipponi, A. and A. Di Cicco, *X-ray-absorption spectroscopy and n-body distribution functions in condensed matter. II. Data analysis and applications.* Phys Rev B Condens Matter, 1995. **52**(21): p. 15135-15149.

186. Colby, D.W., et al., *Prion detection by an amyloid seeding assay.* Proc Natl Acad Sci U S A, 2007. **104**(52): p. 20914-9.

187. Kaneko, K., et al., *Evidence for protein X binding to a discontinuous epitope on the cellular prion protein during scrapie prion propagation.* Proc Natl Acad Sci U S A, 1997. **94**(19): p. 10069-74.

188. Kascsak, R.J., et al., *Mouse polyclonal and monoclonal antibody to scrapie-associated fibril proteins.* J Virol, 1987. **61**(12): p. 3688-93.

189. Benetti, F., et al., *Cuprizone neurotoxicity, copper deficiency and neurodegeneration.* Neurotoxicology, 2010. **31**(5): p. 509-17.

190. McKinley, M.P., et al., *Ultrastructural localization of scrapie prion proteins in cytoplasmic vesicles of infected cultured cells.* Lab Invest, 1991. **65**(6): p. 622-30.

191. Negro, A., et al., *The metabolism and imaging in live cells of the bovine prion protein in its native form or carrying single amino acid substitutions.* Mol Cell Neurosci, 2001. **17**(3): p. 521-38.

192. Lee, K.S., et al., *Internalization of mammalian fluorescent cellular prion protein and N-terminal deletion mutants in living cells.* J Neurochem, 2001. **79**(1): p. 79-87.

193. Laine, J., et al., *Cellular and subcellular morphological localization of normal prion protein in rodent cerebellum.* Eur J Neurosci, 2001. **14**(1): p. 47-56.

194. Mironov, A., Jr., et al., *Cytosolic prion protein in neurons.* J Neurosci, 2003. **23**(18): p. 7183-93.

195. Gagescu, R., et al., *The recycling endosome of Madin-Darby canine kidney cells is a mildly acidic compartment rich in raft components.* Mol Biol Cell, 2000. **11**(8): p. 2775-91.

196. Geisow, M.J. and W.H. Evans, *pH in the endosome. Measurements during pinocytosis and receptor-mediated endocytosis.* Exp Cell Res, 1984. **150**(1): p. 36-46.

197. Cain, C.C., D.M. Sipe, and R.F. Murphy, *Regulation of endocytic pH by the Na+,K+-ATPase in living cells.* Proc Natl Acad Sci U S A, 1989. **86**(2): p. 544-8.

198. Hornemann, S. and R. Glockshuber, *A scrapie-like unfolding intermediate of the prion protein domain PrP(121-231) induced by acidic pH.* Proc Natl Acad Sci U S A, 1998. **95**(11): p. 6010-4.

199. Gerber, R., et al., *Conformational pH dependence of intermediate states during oligomerization of the human prion protein.* Protein Sci, 2008. **17**(3): p. 537-44.

200. Baskakov, I.V., et al., *Pathway complexity of prion protein assembly into amyloid.* J Biol Chem, 2002. **277**(24): p. 21140-8.

201. Marijanovic, Z., et al., *Identification of an intracellular site of prion conversion.* PLoS Pathog, 2009. **5**(5): p. e1000426.

202. Uchiyama, K., et al., *Prions disturb post-Golgi trafficking of membrane proteins.* Nat Commun, 2013. **4**: p. 1846.

203. Maley, F., et al., *Characterization of glycoproteins and their associated oligosaccharides through the use of endoglycosidases.* Anal Biochem, 1989. **180**(2): p. 195-204.

204. Chen, S.G., et al., *Truncated forms of the human prion protein in normal brain and in prion diseases.* J Biol Chem, 1995. **270**(32): p. 19173-80.

205. Jimenez-Huete, A., et al., *Endogenous proteolytic cleavage of normal and disease-associated isoforms of the human prion protein in neural and non-neural tissues.* Am J Pathol, 1998. **153**(5): p. 1561-72.

206. Harris, D.A., et al., *Processing of a cellular prion protein: identification of N- and C-terminal cleavage sites.* Biochemistry, 1993. **32**(4): p. 1009-16.

207. Caughey, B., et al., *Normal and scrapie-associated forms of prion protein differ in their sensitivities to phospholipase and proteases in intact neuroblastoma cells.* J Virol, 1990. **64**(3): p. 1093-101.

208. McKinley, M.P., D.C. Bolton, and S.B. Prusiner, *A protease-resistant protein is a structural component of the scrapie prion.* Cell, 1983. **35**(1): p. 57-62.

209. Polano, M., et al., *Structural insights into alternate aggregated prion protein forms.* J Mol Biol, 2009. **393**(5): p. 1033-42.

210. Rogers, D.R., *Screening for Amyloid with the Thioflavin-T Fluorescent Method.* Am J Clin Pathol, 1965. **44**: p. 59-61.

211. Colby, D.W., et al., *Protease-sensitive synthetic prions.* PLoS Pathog, 2010. **6**(1): p. e1000736.

212. Soto, C., G.P. Saborio, and L. Anderes, *Cyclic amplification of protein misfolding: application to prion-related disorders and beyond.* Trends Neurosci, 2002. **25**(8): p. 390-4.

213. Barria, M.A., D. Gonzalez-Romero, and C. Soto, *Cyclic amplification of prion protein misfolding.* Methods Mol Biol, 2012. **849**: p. 199-212.

214. Reichel, A., *The role of blood-brain barrier studies in the pharmaceutical industry.* Curr Drug Metab, 2006. **7**(2): p. 183-203.

215. Bonomo, R.P., et al., *Copper(II) binding modes in the prion octapeptide PHGGGWGQ: a spectroscopic and voltammetric study.* Chemistry, 2000. **6**(22): p. 4195-202.

216. Brown, D.R., *Copper and prion disease.* Brain Res Bull, 2001. **55**(2): p. 165-73.

217. Brown, D.R. and J. Sassoon, *Copper-dependent functions for the prion protein.* Mol Biotechnol, 2002. **22**(2): p. 165-78.

218. Brown, L.R. and D.A. Harris, *Copper and zinc cause delivery of the prion protein from the plasma membrane to a subset of early endosomes and the Golgi.* J Neurochem, 2003. **87**(2): p. 353-63.

219. Chattopadhyay, M., et al., *The octarepeat domain of the prion protein binds Cu(II) with three distinct coordination modes at pH 7.4.* J Am Chem Soc, 2005. **127**(36): p. 12647-56.

220. Qin, K., et al., *Copper(II)-induced conformational changes and protease resistance in recombinant and cellular PrP. Effect of protein age and deamidation.* J Biol Chem, 2000. **275**(25): p. 19121-31.

221. Quaglio, E., R. Chiesa, and D.A. Harris, *Copper converts the cellular prion protein into a protease-resistant species that is distinct from the scrapie isoform.* J Biol Chem, 2001. **276**(14): p. 11432-8.

222. Berti, F., et al., *Structural and dynamic characterization of copper(II) binding of the human prion protein outside the octarepeat region.* Chemistry, 2007. **13**(7): p. 1991-2001.

223. Emwas, A.H., et al., *Utilizing NMR and EPR spectroscopy to probe the role of copper in prion diseases.* Magn Reson Chem, 2013. **51**(5): p. 255-68.

224. Thakur, A.K., et al., *Copper alters aggregation behavior of prion protein and induces novel interactions between its N- and C-terminal regions.* J Biol Chem, 2011. **286**(44): p. 38533-45.

225. Watzlawik, J., et al., *Prion protein helix1 promotes aggregation but is not converted into beta-sheet.* J Biol Chem, 2006. **281**(40): p. 30242-50.

226. Solforosi, L., et al., *Toward molecular dissection of PrPC-PrPSc interactions.* J Biol Chem, 2007. **282**(10): p. 7465-71.

227. Ziegler, J., et al., *Putative aggregation initiation sites in prion protein.* FEBS Lett, 2006. **580**(8): p. 2033-40.

228. Norstrom, E.M. and J.A. Mastrianni, *The charge structure of helix 1 in the prion protein regulates conversion to pathogenic PrPSc.* J Virol, 2006. **80**(17): p. 8521-9.

229. Piccardo, P., et al., *Phenotypic variability of Gerstmann-Straussler-Scheinker disease is associated with prion protein heterogeneity.* J Neuropathol Exp Neurol, 1998. **57**(10): p. 979-88.

230. Wadsworth, J.D., et al., *Phenotypic heterogeneity in inherited prion disease (P102L) is associated with differential propagation of protease-resistant wild-type and mutant prion protein.* Brain, 2006. **129**(Pt 6): p. 1557-69.

231. Santini, S. and P. Derreumaux, *Helix H1 of the prion protein is rather stable against environmental perturbations: molecular dynamics of mutation and deletion variants of PrP(90-231).* Cell Mol Life Sci, 2004. **61**(7-8): p. 951-60.

232. Tsenkova, R.N., et al., *Prion protein fate governed by metal binding.* Biochem Biophys Res Commun, 2004. **325**(3): p. 1005-12.

233. Gaggelli, E., et al., *Interaction of the human prion PrP(106-126) sequence with copper(II), manganese(II), and zinc(II): NMR and EPR studies.* J Am Chem Soc, 2005. **127**(3): p. 996-1006.

234. Brown, D.R., et al., *Consequences of manganese replacement of copper for prion protein function and proteinase resistance.* EMBO J, 2000. **19**(6): p. 1180-6.

235. Abdelraheim, S.R., S. Kralovicova, and D.R. Brown, *Hydrogen peroxide cleavage of the prion protein generates a fragment able to initiate polymerisation of full length prion protein.* Int J Biochem Cell Biol, 2006. **38**(8): p. 1429-40.

236. Kim, N.H., et al., *Effect of transition metals (Mn, Cu, Fe) and deoxycholic acid (DA) on the conversion of PrPC to PrPres.* FASEB J, 2005. **19**(7): p. 783-5.

237. Giese, A., et al., *Effect of metal ions on de novo aggregation of full-length prion protein.* Biochem Biophys Res Commun, 2004. **320**(4): p. 1240-6.

238. Thackray, A.M., et al., *Metal imbalance and compromised antioxidant function are early changes in prion disease.* Biochem J, 2002. **362**(Pt 1): p. 253-8.

239. Brazier, M.W., et al., *Manganese binding to the prion protein.* J Biol Chem, 2008. **283**(19): p. 12831-9.

240. Lauren, J., et al., *Cellular prion protein mediates impairment of synaptic plasticity by amyloid-beta oligomers.* Nature, 2009. **457**(7233): p. 1128-32.